Spring 5-23-2019

Middle Miocene to Holocene History of the Delacroix Island Fault System

Jarrett Leigh Levesh
University of New Orleans, jllevesh@UNO.edu

Middle Miocene to Holocene History of the Delacroix Island Fault System

A Thesis

Submitted to the Graduate Faculty of the
University of New Orleans
in partial fulfillment of the
requirements for the degree of

Masters of Science
in
Earth and Environmental Sciences

by

Jarrett L Levesh

B.S. Juniata College, 2016

May, 2019

Acknowledgements

A countless number of people have helped me through this research journey. I first, and foremost, would like to thank my advisor, Dr. Mark Kulp, for providing me with the opportunity to achieve my goals as well as supporting and guiding me every step of the way. I would also like to thank Chris McLindon for his help and guidance, without him this work would have never been completed. My thanks also go to Brad Robison a mentor and motivator throughout my graduate career.

Furthermore I must thank the entire UNO Earth and Environmental Sciences department; professors, faculty, graduate and undergraduate students. You all have given me a second home here in New Orleans and allowed for me to have not only a successful graduate career, but one I greatly enjoyed. A special thanks to Ioannis Georgiou, head of the EES department, for his continued efforts helping and supporting not only me but the entire Department.

My thanks to Paleodata Inc. and Upstream Exploration LLC. who generously granted me access to data used throughout this study. I also would like to thank The New Orleans Geological Society, Chevron and Glen Hebert for graduate student awards and scholarships that helped fund this research.

Finally, I would like to thank my parents, who have always supported me in every endeavor I take on. To my mother, Terri Levesh, and my father, Craig Levesh, thank you for all your love and support.

Table of Contents

List of Figures

List of Tables

Glossary

Ma..... specific calendar year in millions of years before present

My.....duration of a period of time in millions of years

ka ..... specific calendar year in thousand of years before present

kyr.....duration of a period of time in thousands of years

bbl..... barrels of oil

API .....A unique, numeric identifyer for drilled wells

GOM ..... Gulf of Mexico

MRDP.....Mississippi River Delta Plain

Abstract

An in-depth field study of the Delacroix Island producing field illustrates the evolution of the east-trending Delacroix Island Fault during the last 13 My. Well log correlations and 3-D seismic interpretation of 22 subsurface bio-stratigraphic horizons across the fault reveal variable stratigraphic thicknesses and displacement. Wells, with well log curve data as shallow as 31 m (100 ft) below the surface, were used to calculate interval thicknesses, expansion indices, sediment accumulation rates, burial history and magnitudes of displacement. Through these analyses, a correlation was found between the positioning of ancient Miocene depocenters over Delacroix Island and a period of increased fault activity. Historic satellite imagery (last 34 yrs) of the field depicts a lineation on the modern marsh surface coincident with the upward projected fault plane. Continuous wetland loss on the downthrown side of the fault trace suggests that recent and continued fault movement may be contributing to marsh submergence.

Keywords; Faults, Geomorphology, Wetland Loss, Sediment Loading

Chapter 1. Introduction, Organization and Significance

1.1 *Introduction*

Land loss and inundation of wetlands is a historical and continuing problem for coastal Louisiana where approximately 90 % of the total costal wetland loss in the United States takes place (Couvillion et al., 2011). Between 1932 and 2010, Louisiana lost approximately 4,877 km^2 (1,883 mi^2) of land, a decrease of 25 % (Couvillion et al., 2011). Trend analyses have shown land loss increasing from 17.4 km^2 (6.7 mi^2) of total loss during 1913 to a rate of 42.7 km^2/yr (16.5 mi^2/yr) between 1985 and 2010 (Gagliano et al., 1981; Couvillion et al., 2011). More recently this rate has been decreasing (Couvillion et al. 2017) but continues to be prevalent across coastal Louisiana.

The majority of southern Louisiana land loss has occurred within the interior of the coastal plain, not along the Gulf of Mexico (GOM) shoreline (Penland et al., 2002). From 1932 to 1990, 69.91 % of land inundation took place within the interior of the coast (Penland et al., 2002). This loss of interior wetlands was due to submergence and not marsh edge erosion (Penland et al., 2002). Morton et al. (2005) confirmed this observation, suggesting that areas previously thought to be losing land to shoreline erosion were actually undergoing submergence through subsidence.

Subsidence is not a new process, it has occurred through the geologic history of the Mississippi River delta plain (MRDP) , ranging between 1 and 5 mm/yr during the past 5,000 years (Morton et al., 2005). More recently, for the period 1965 to 1993, subsidence rates were calculated to be on average between 8 and 12 mm/yr (Morton et al., 2005). These rates of subsidence vary spatially, reaching as much as 30 mm/yr between 1920 and 1995 as indicated by benchmark re-leveling studies, and generally increase towards the Gulf coast shoreline (Shinkle and Dokka, 2004).

Morton et al. (2005) found that although there have been variations in rates of subsidence through time, the geographic extent of high and low subsidence rates was consistent across the time frame of analysis (e.g. 1965-1993), which he suggested indicates a strong control by subsurface geologic processes that are spatially similar through time across the delta plain. Increasingly it has been recognized that one major geologic process potentially driving subsidence is surface and shallow sub-surface movement along deep-seated faults (10^2-10^3 m subsurface depth), which are common in the regional passive-margin deltaic setting (Armstrong et al., 2014; Cline et al., 2011; Dokka, 2006; Frank, 2017; Gagliano et al., 2003; Kuecher, 1995; Morton et al., 2003; Martin, 2006).

Armstrong et al. (2014) provided the first peer-reviewed study of how the presence of deep faults (e.g. formed in early Cenozoic) may have had a continuing effect on Late Miocene to Holocene depositional environments and modern surface geomorphology. Armstrong et al. (2014), using deep industry seismic data (<2,000 m (6,562 ft) penetration), identified a series of deep faults that may extend upward to the modern delta-plain surface but are unresolvable in the data at depths less than 500 m (1640 ft). One of these faults, the Delacroix Island Fault, is the focus of this investigation. Upward projection of the fault from depth by Armstrong et al. (2014) resulted in a surface fault trace, which coincides with an area of historic land loss. This is suggestive of a relationship between land loss and down-to-the-south motion along the fault that has contributed toward the conversion of land to open water in the area. The focus of this study is to examine: 1) the Cenozoic history of slip along the Delacroix fault, 2) the magnitude of fault throw along the fault, 3) the processes of fault motion within the Cenozoic, and 4) whether fault movement has impacted Holocene geomorphology. These efforts relied upon the correlation of

82 well logs, numerous biostratigraphic markers, interpretation of 3-D seismic data, examination of satellite imagery, and a consideration of regional geology within the study area (Fig. 1).

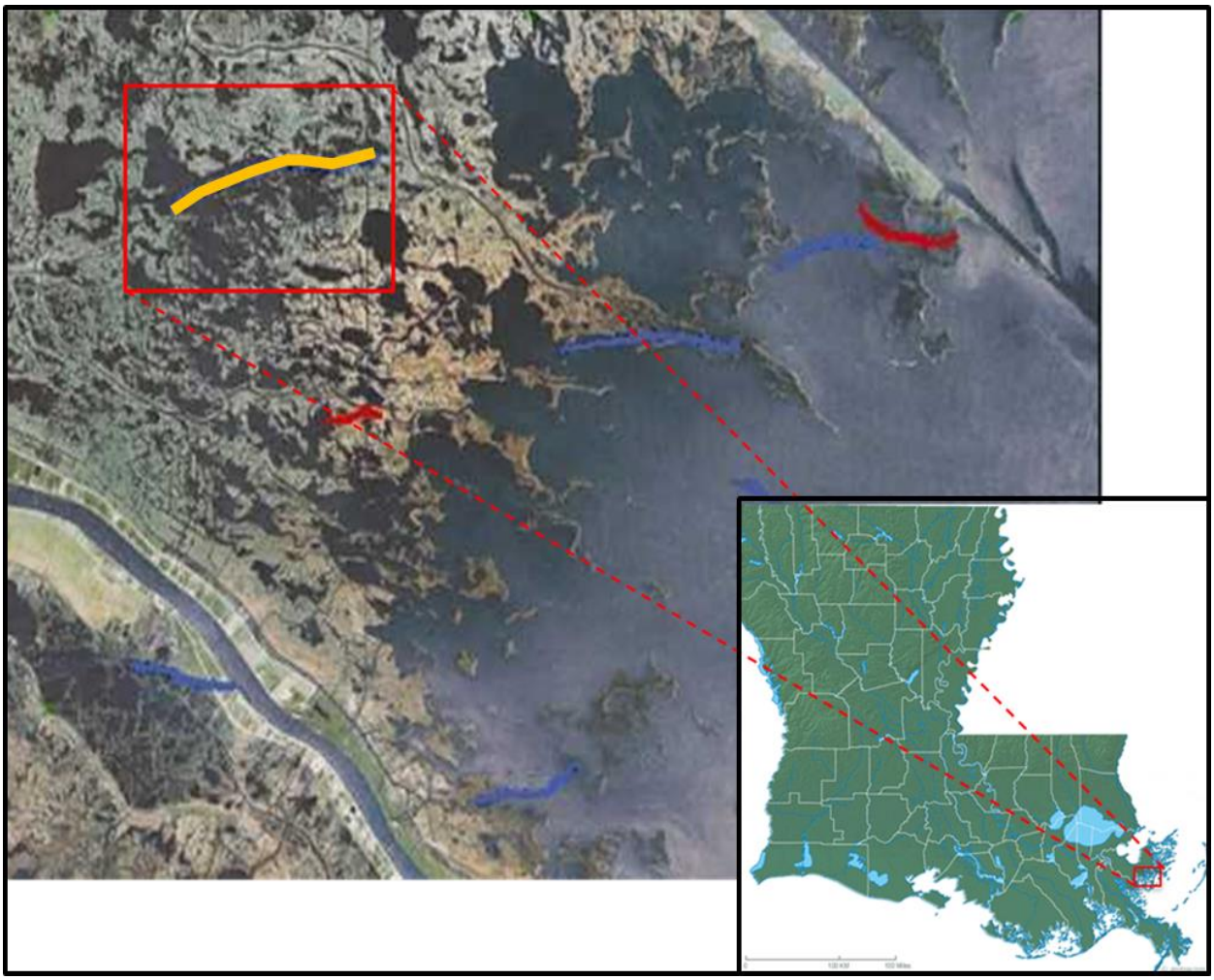

Figure 1. Study location of southeast Louisiana outlined by the red box. Delacroix Island fault shown in orange. Blue and red lines indicate surface expressions of faults identified by Armstrong et al. (2014). Blue lines designate down-to-the-south faults and red down- to- the- north faults. The Delacroix Island fault dips to the south (modified from Armstrong et al. 2014).

1.2 *Purpose and Hypothesis*

1.2.1 Purpose

The possibility of land surface subsidence created by motion along faults should be considered in the construction of all infrastructure. Fault movement can affect any structure that crosses an active fault, including levees protecting against riverine flooding and hurricane storm surges, transportation networks, real estate, and oil and gas infrastructure (Gagliano et al., 2003). For southern Louisiana, with metropolitan areas such as New Orleans with subsidence rates as much as 28 mm/yr (8 mm/yr mean) between 2002 and 2005 (Dixon et al., 2006), an understanding of whether faults are a contributor to the documented elevation changes is paramount.

The influence of fault motion on recent and modern geomorphology of southern Louisiana also needs to be considered in current and projected coastal sustainability efforts of the region. Past, present and future efforts to mitigate against coastal land loss have commonly targeted limiting or preventing erosion along the edges of coastal lands, a horizontal process with less consideration of the vertical process of land-surface submergence some of which has been suggested to be the result of movement of regional faults (Dokka et al. 2006; Dokka, 2006; Gagliano et al., 2003; e.g. Kuecher, 1995). Inasmuch that fault-induced elevation changes may be contributing to widespread land loss of the MRDP (e.g. Penland et al., 2002) coastal land loss mitigation efforts will only be successful if a more complete understanding of subsidence processes, such as faults, is established.

1.2.2 Hypothesis

The hypotheses of this effort are that: 1) deep-seated faults in Plaquemines Parish, Louisiana can be accurately identified and mapped through an analysis of well logs and seismic data, 2) sediment loading is a mechanism that can drive fault slip, 3) the Delacroix Island Fault can be traced to the shallow subsurface of the modern MRDP, and 4) Holocene fault slip is responsible for marsh submergence on the downthrown side of the fault.

1.3 *Importance*

1.3.1 Land Loss in the Gulf

Gagliano et al. (1981) studied land loss across an 29,785 km^2 (11,500 mi^2) area of southern Louisiana using maps, black-and-white aerial photographs, and color infrared imagery taken during five periods spanning 1890 to 1978. Gagliano et al. (1981) determined that during the last two centuries the amount of land loss has increased at a geometric rate. In the year 1913 total land loss amounted to 17.4 km^2 (6.7 mi^2), this number rose to 72.8 km^2 (28.1 mi^2) in the year 1967 (Gagliano et al., 1981). The study projected that Plaquemine Parish was on the verge of losing as much as 8,831 acres/yr (35.7 km^2/yr or 13.8 mi^2/yr) over the next few decades and had a life expectancy of approximately 50 years (Gagliano et al., 1981).

1.3.2 Fault Induced Land Loss

Yuill et al. (2009) summarized the work of many previous researchers and noted that subsidence, and subsequent land loss, in coastal Louisiana is due to a combination of factors including faulting, sediment compaction, sediment loading, glacial isostatic adjustment, and surface water drainage and management. During the last two decades there has been a growing consensus that fault motion is a larger contributor to the land loss in southern Louisiana than

previously recognized (Dokka et al. 2006; Dokka, 2006; Gagliano et al., 2003; e.g. Kuecher, 1995).

Multiple studies conducted in southeast Louisiana have contributed to the suggestion that a primary driver of regional subsidence is fault movement (Gagliano, 2005; Gagliano et al. 2003; Gagliano & Wiltenmuth, 2003). Each of these studies suggested that near surface motion, along listric faults that merge into a Oligocene-Miocene detachment surface at depths of 6,096 to 9,144 m (20,000 to 30,000 ft), was creating surface land loss (Gagliano et al., 2003) (Fig. 2). Gagliano (2003) identified more than 100 surface fault traces and fault-line scarps across the central coastal zone with a 61 % correlation to known sub-surface faults (Gagliano et al., 2003). Some of these regional faults have been periodically active for 100 My or more and are likely to remain active indefinitely (Gagliano et al., 2003).

On the basis of global positioning system (GPS) vertical and horizontal motion measurements Dokka et al. (2006) suggested that there exists a south Louisiana allochthon, a 7-10 km (4.3-6.2 mi) thick block that is detached from stable North America to the north and incrementally moving south toward the GOM. The work by Dokka et al. (2006) suggested the presence of a "breakaway zone" at the location of the faulted, updip portion of the allochthon, at the Tepate-Baton Rouge fault system (Fig. 2), which experiences higher rates of subsidence than other areas of the allochthon. Study sites south of these faulted zones subsided at an average 5.2 mm/yr, whereas the sites north of the fault systems displayed no significant vertical motion (Dokka et al. 2006).

Kuecher (1995) studied wetland loss in Terrebonne and Lafourche parishes of southern Louisiana and concluded that one of the main subsurface processes driving wetland loss was

active growth faulting. Kuecher (1995) found a correlation between areas of interior wetland loss and subsurface growth faults, suggesting that the faults may still be active. Despite the many previous studies that have suggested fault induced subsidence is significant across southern Louisiana, faults remain an underestimated natural hazard across the region.

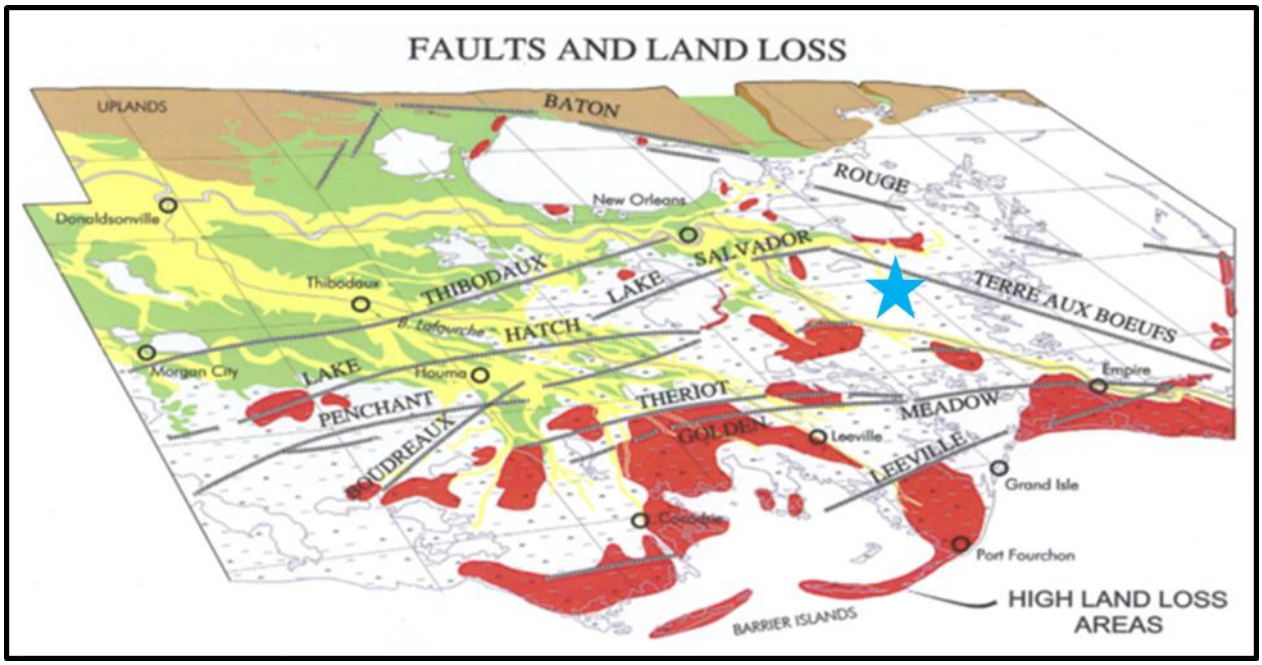

Figure 2. Map showing the major fault trends of southeastern Louisiana and their relationship with areas of high land loss. Areas of high land loss are shown in red, major faults are depicted as gray lines. The blue star approximately indicates the study area. (from Gagliano et al., 2003).

Chapter 2. Geologic Framework and Study Area

2.1 Geologic History of the Gulf of Mexico

2.1.1 Triassic

The formation of the GOM began in the Late Triassic with fragmentation of Pangaea along the southern margin of Laurentia (Salvador, 1991). Rifting lasted 50 My, through the Early to Middle Jurassic creating a series of grabens on the North American cratonic margin (Salvador, 1991).

Salt deposition within the rift basin resulted in 1,000 to 3,000 m (3,280 to 9,843 ft) of halite, referred to as the Middle Jurassic Louann Salt (Salvador, 1991). This is the first indication of seawater reaching the GOM Basin, wherein marine water filled the depressed areas and evaporation exceeded the inflow of marine water (Salvador, 1991). The salt deposits are found in the northern and southern GOM, and absent in the central Gulf Basin (Salvador, 1991).

2.1.2 Jurassic

Following deposition, the Louann Salt began to undergo deformation and evacuation, which happened during multiple stages. An array of salt structures formed as a result and the salt deformation influenced sediment accumulation patterns of the basin (Wu and Galloway, 2002). The basic stratigraphic, tectonic, and geographic framework of the GOM was established by the end of the Jurassic (Salvador, 1987). The deep central Gulf was surrounded by the stable terrains of the Yucatan and Florida Peninsula and there were open marine conditions shared with the central Atlantic and, likely, the Pacific Ocean (Worrall and Snelson, 1989).

2.1.3 Cretaceous

By the Cretaceous, the GOM was stable, with tectonism restricted to the deformation of the Middle Jurassic salt, and a series of listric normal faults formed around the rims of the Cretaceous depocenters (Salvador, 1991). Deposition was dominated by sedimentation across relatively shallow-water carbonate platforms and within time equivalent deep-water environments. The main influx of terrigenous sediment during this time came from the Ouachita and Appalachian Mountains to the north and northeast (Salvador, 1991; Bentley, 2015). Sediment influx diminished into the Late Cretaceous. During the Late Cretaceous, the tectonic stability of the GOM was interrupted as the Laramide orogeny began (Salvador, 1991). The Laramide orogeny was the result of the nearly horizontal subduction of the Farallon oceanic plate beneath the Pacific margin of the North American plate. Clastic sediment influx into the basin from the Laramide uplifts to the northwest increased throughout the Late Cretaceous (Salvador, 1991).

2.1.4 Cenozoic

Deposition of terrigenous sediments from the Laramide orogeny increased significantly during the Early Cenozoic, specifically the Paleocene and Eocene, as uplift and orogenic deformation progressed eastward (Salvador, 1991). As the Laramide orogeny ended, the influx of sediments to the GOM continued intermittently causing progradation of the GOM shorelines (Galloway et al., 1991). Sedimentation also had an effect on the underlying Jurassic salt bodies, resulting in the creation of numerous features such as salt diapirs and massifs as well as the initial formation of an allochthonous salt massif at the down-dip toe of the system (Salvador, 1991) (Fig. 3). Around the perimeter of the active depocenters listric normal faulting was

common (Salvador, 1991) and the evolution of these growth faults across the Louisiana continental shelf and slope has been dependent on concomitant evacuation of deep salt (Galloway et al., 1991; Salvador, 1991).

The Cenozoic depositional history of the northern and northwestern area of the GOM is distinguished by the abundant supply of terrigenous clastic sediments provided by multiple tectonic events including the Laramide orogeny and uplift of the Colorado Plateau and Appalachian Mountains (Galloway et al., 1991). Delivery of this sediment caused progradation of the clastic shelf margin toward the deep Cenozoic GOM, and accumulation of a thick clastic section across the continental slope (Galloway et al., 1991; Coleman, et al. 1998) (Fig. 3). Throughout this time growth faulting was common at the prograding shelf margin as unstable sedimentary packages failed and subsided (Ewing, 1991).

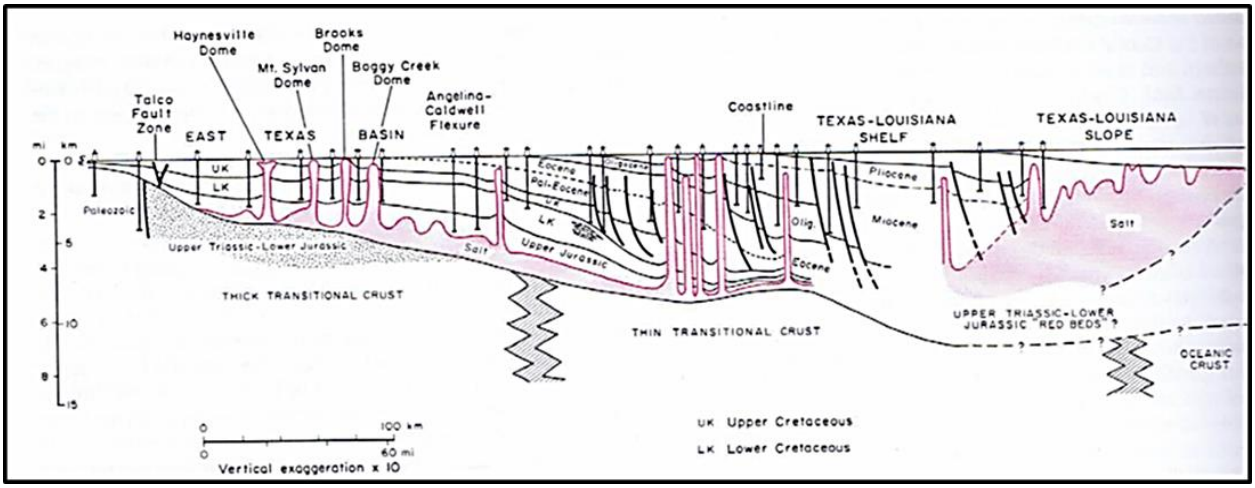

Figure 3. Cross section through the northern Gulf of Mexico basin, from the East Texas Basin to the Texas-Louisiana Slope, depicting the prograded and overlapped depositional pattern of the Cenozoic strata. The influx of terrigenous sediment contributed to the formation of salt diapirs as well as the early development of a large allochthonous salt mass at the down-dip end of the system (shown in pink) (from Salvador, 1991).

2.1.4.1 Paleocene / Eocene

During the Late Paleocene and Early Eocene, large volumes of terrigenous sediment entered the GOM basin fluvial networks that evolved toward the large-scale drainage template that persists today (Galloway et al., 1991; Bentley, 2016). Through the Paleocene and Early Eocene, the GOM was fed by the ancestral Tennessee River with the ancestral Mississippi system flowing through the Mississippi embayment (Bentley, 2015). This fluvial deposition resulted in large progradational deltaic complexes focused in the northwest GOM (Salvador, 1991). The sediment loading caused by these complexes initiated the first of a series of growth faulting events during the Cenozoic, as well as the mobilization of the Terrebonne salt sheet, which generated the Wilcox fault zone (Salvador, 1991; Wu and Galloway, 2002).

2.1.4.2 Oligocene

Massive sediment influx continued through the Oligocene, sourced primarily from Mexico and the southwest United States (Galloway et al., 2000). This influx resulted in the deposition of one of the most substantial progradational wedges of the northwest GOM basin. During this time as much as 4,500 m (14,763 ft) of sediment was deposited and prograded the shelf margin as much as 80 km (50 mi) (Galloway et al., 1991; Salvador, 1991). Sediment loading from this deltaic complex resulted in the Vicksburg and Frio fault zones, developing much in the same way as the Wilcox fault zone (Salvador, 1991).

2.1.4.3 Miocene

During the Miocene large growth fault zones with horizontal slips of as much as 30 to 40 km (18 to 25 mi) and rollover folding developed along the gulfward margin of the deltaic systems (Salvador, 1991). This development of complex faulted structures was due to the rapid

deposition that triggered the mobilization of underlying salt bodies, the growth faults were initiated and remained active during deltaic deposition (Curtis, 1970; Galloway et al., 1991; Salvador, 1991).

Miocene uplift along the east flank of the Rocky Mountains, accompanied by uplift of the southern Appalachian Plateau, rejuvenated sediment delivery from upland Wyoming, the central Rocky Mountains and Appalachians (Wu and Galloway, 2002). This shifted sediment depocenters eastward to the east-central Gulf basin and caused the Mississippi system to become one of the dominant sources of sediment to the GOM basin (Wu and Galloway, 2002; Bentley, 2015). Loading from these prograding depocenters evacuated the Terrebonne salt sheet, eventually forming what is known as the Terrebonne Trough (Wu and Galloway, 2002) (Fig. 4).

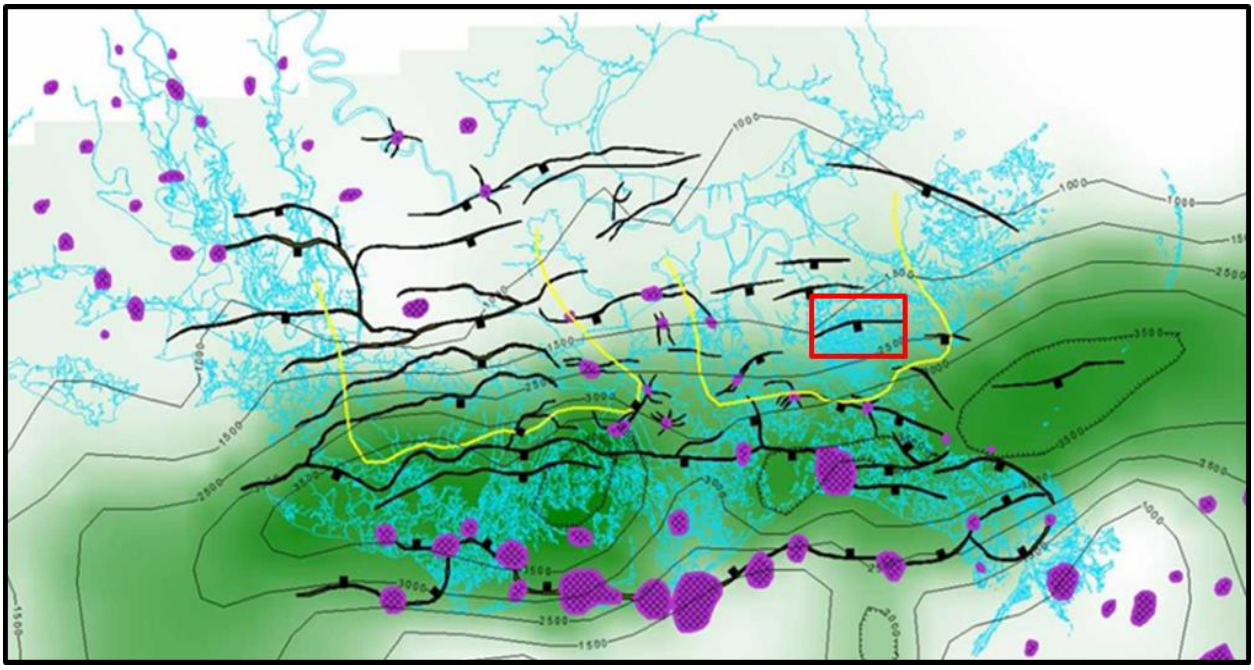

Figure 4. A regional map of southeast Louisiana displaying faults (in black), salt domes (in purple) (NOGS, 2015), isopach contours from the *Bigenerina 2* (10.8 Ma) to *Textularia W* (12.0 Ma) biostratigraphic tops (Galloway and Wu, 2002) and the Late Miocene delta outlines in yellow (Curtis, 1970). The study location is outlined in red (from McLindon, 2017).

2.1.4.5 Pliocene / Pleistocene

The Pliocene-Pleistocene was the shortest and last major depositional episode in the GOM basin (Galloway et al., 1991). Progradation of successive shelf-margin deltas advanced the central GOM continental margin as much as 80 km (50 mi) to its present day position (Galloway et al., 2000; Galloway et al., 1991). This fast accumulation of sediments was accompanied by growth faulting and triggered the mobilization of the underlying Middle Jurassic salt (Salvador, 1991). The present day continental slope of the northern GOM is representative of the relict Pleistocene depositional surface of the latest Pleistocene glacial stage (Galloway et al., 1991).

2.1.4.6 Quaternary

Quaternary deposits are as much as 3,000 to 3,600 m (9,842 to 11,811 ft) thick across the present shelf and in the deep basin of the GOM (Coleman, et al., 1991). These deposits show a complex depositional pattern that was strongly influenced by climatically driven sea level fluctuations. Lowering of sea level caused incised river beds, progradation of river deltas and ultimately rapid sediment deposition on the continental margin (Blum, 2009; Coleman et al., 1991). Rising sea levels caused submergence of vast areas of the coastal plain, raised base level of streams and ultimately aggraded river valleys (Blum, 2009; Coleman et al., 1991). These rapid fluctuations controlled the depocenter of the primary fluvial source, the Mississippi River.

The Wisconsin glacial maximum at 18 ka (Curray, 1960) created the most recent glacial lowstand, which was followed by an initially rapid rise of sea level, resulting in the deposition of sediment across large parts of the continental shelf in the GOM (Andel, 1960). Subsequent Mississippi River deposition resulted in the development of the Holocene delta plain through

fluvial avulsions creating a complex stratigraphy of fluvial and marine sediments above the existing latest Quaternary strata (e.g. Curray, 1960).

Salt deformation, growth faulting, and gravity slumping is still active in the GOM today, particularly across the northern slope (Coleman et al., 1991). Numerous small basins have formed between salt massifs and ridges throughout the Quaternary and subsidence rates in these basins are among some of the highest in the world (Coleman et al., 1991).

2.2 Louisiana Faults

The fault systems of south Louisiana became known primarily during the 20th century through the exploration for hydrocarbons in the deep subsurface (McCulloh et al., 2012). One of the major fault systems, the Baton Rouge, was first mapped by Fisk (1945) and introduced by Durham and Peeples (1956) as a deep subsurface fault distinguished by conspicuous surface expression and geologically recent activity (McCulloh & Heinrich, 2012). Durham and Peeples (1956) noted that Fisk (1945) mapped displacement on Pleistocene stratigraphy, indicating activity during the late Pleistocene and a potential for modern activity (McCulloh et al., 2012).

Murray (1961) summarized the subsurface fault systems in southern Louisiana, consisting mainly of listric normal faults with down-to-the-south displacements (Bradshaw and Zoback, 1988). Listric normal faults are extensional features characterized by a decreasing dip with depth (Bradshaw and Zoback, 1988). The faults are mainly growth faults, which are distinguished from other normal faults by differential thickening, or expansion, of displaced strata on the down-thrown blocks compared to time equivalent units on the up-thrown blocks (McCulloh et al., 2012; Thorsen, 1963). Dokka et al. (2006) suggests that this large system of listric normal faults form the northern boundary of a 7 to 10 km (4.3 to 6.2 mi) thick allochthon

that is detached from stable North America, causing southeast Louisiana to subside and move southward along a detachment rooted in a weak layer of salt or shale (Dokka et al., 2006).

Murray (1961) accepted that the Baton Rouge faults reflected the Quaternary reactivation of Cenozoic growth faults originally active in the Oligocene (McCulloh et al., 2012). Additionally, Hanor (1982) investigated the movement history across the Tepetate-Baton Rouge system fault and confirmed geologically recent reactivation of a subsurface growth faults that had been inactive since the Oligocene. Modern rates of fault movement were found to be between 5 to 10 mm/yr, whereas geologically historic rates were approximately 0.003 to 0.1 mm/yr (McCulloh et al., 2012).

2.3 Delacroix Island Study Area

The Delacroix Island field is located in northeastern Plaquemines Parish, Louisiana, approximately 48 km (30 mi) southeast of New Orleans. Delacroix Island was first drilled by Texaco, Inc. in May of 1941. By January 1st, 1965 43 wells had been drilled, with 31 oil wells, producing 3,555,720 bbl of oil in total (Keller, 1965). Production was almost entirely on the downthrown side of the Delacroix Island Fault but several wells were drilled upthrown to the fault. Apache Corporation later took over the field production and acquired 3D seismic data across the entire field to facilitate continued development and production. Hydrocarbon recovery continued until Hurricane Katrina destroyed much of the field infrastructure in 2005, making it economically unreasonable for field production (Fig. 5).

The Delacroix Island Fault is a basin ward (southeast) dipping growth fault. The arcuate surface trace covers a linear distance of approximately 12.8 km (8 mi) trending west across the upper Carnarvon basin. Data, such as well logs, biostratigraphic markers, and seismic, enabled

an analysis of the fault from approximately 122 m to 3048 m (400 ft to 10,000 ft) depth and a time period approximately spanning 12.85 Ma to 0.60 Ma. From the surface to 1,981 m (6,500 ft) the fault dips at an approximate angle of 82°. From 1,981 m (6,500 ft) to 3,048 m (10,000 ft) the dip angle decreases to approximately 78°.

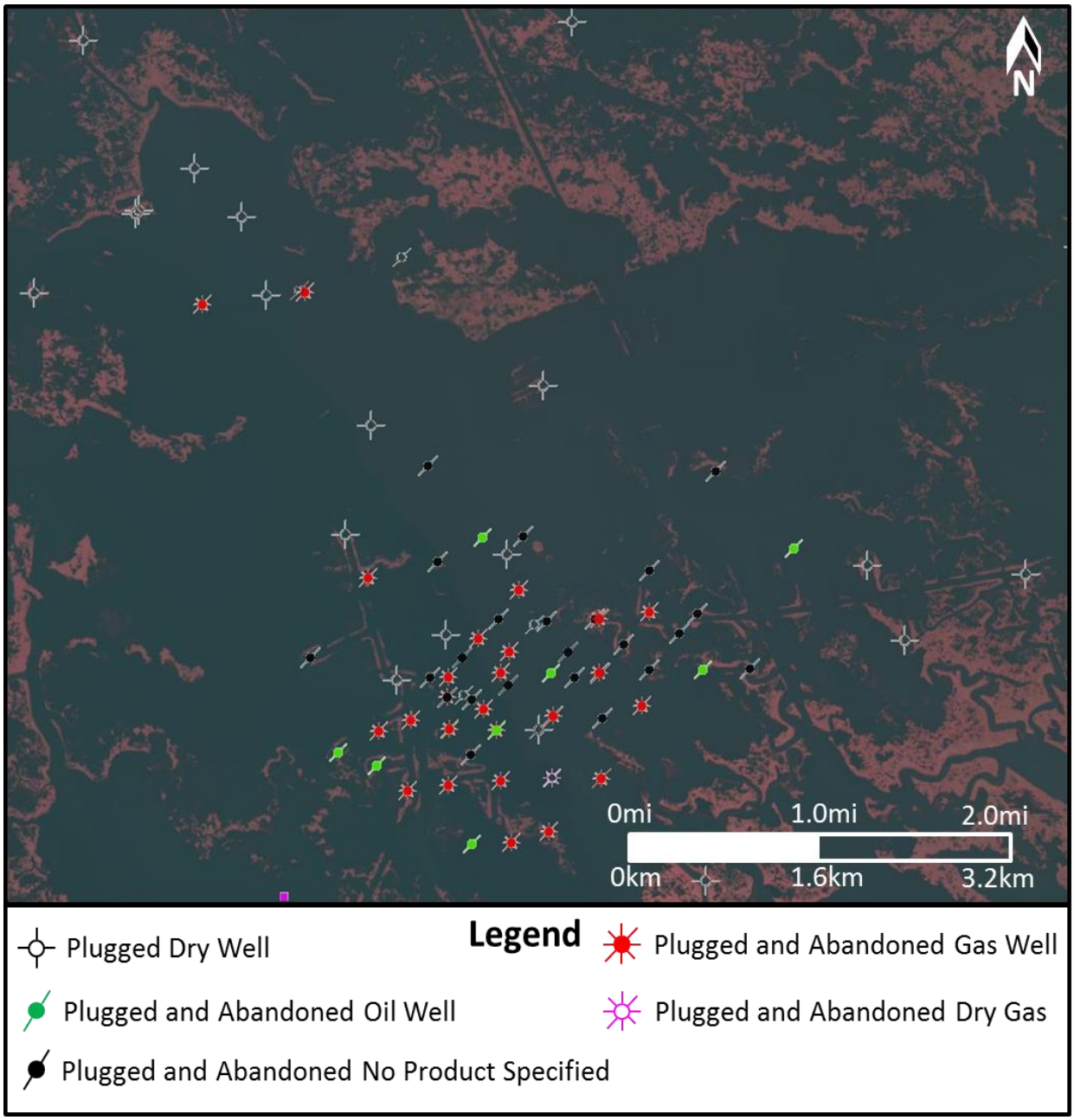

Figure 5. Base map of the Delacroix Island hydrocarbon field, located approximately 48 km (30 mi) southeast of New Orleans, Louisiana. There are 70 total wells; 16 plugged dry wells, 8 plugged and abandoned oil wells, 23 plugged and abandoned wells with no product specified, 23 plugged and abandoned gas wells, and 1 plugged and abandoned dry gas well. The productive interval of the field ranges from 2,134 m (7,000 ft) to 3,505 m (11,500 ft) with the deepest well at 4,008 m (13,150 ft). The field is owned and operated by Texaco, Inc. (well locations from LA Department of Natural Resources website SONRIS).

Chapter 3. Methods

3.1 Well Logs

3.1.1 Well Log Acquisition

As a result of the exploration and production of hydrocarbons, well logs are abundant in the Delacroix Island area and are publicly available (Fig. 5) through the Louisiana Department of Natural Resources Website SONRIS (Strategic Online Natural Resources Information System) (SONRIS, 2018). The majority of well logs used recorded spontaneous potential (SP), resistivity at shallow and deep intervals, and conductivity. Gamma ray logs are not present because it was not a method of subsurface stratigraphic logging that was widely utilized at the time that these wells were initially drilled.

Spontaneous potential measures (in millivolts) the electrical potential difference between the voltage in the wellbore and a surface electrode to identify permeable strata, distinguishing porous zones, such as sand, from non-porous zones, such as shales or salts. The resistivity tool passes a current through the formation and measures the resistance of pore fluids, which distinguishes brine (saltwater) filled strata from hydrocarbon zones. The vertical profile of specific log intervals indicated by these tools provides an opportunity to distinguish lithologic intervals, which can be correlated across the field.

3.1.2 Well Log Correlation

Well log correlations were completed by hand using paper copies of the logs. Biostratigraphic foraminifera (PaleoData, 2018), combined with well log signatures, were used to correlate stratigraphic packages across the Delacroix Island field. A total of 18 biostratigraphic formation tops were correlated, ranging from Middle Miocene to middle Pliocene. Four shallow

formation tops, from the top of the Pliocene to early Pleistocene, were correlated where shallow well data was available. No absolute biostratigraphic dates exist for biomarkers younger than the middle Pliocene, for the purposes of this study however inferred ages were used to study Miocene through latest Quaternary Delacroix Island Fault evolution (PaleoData, 2018).

The Delacroix Island Fault was identified in as many well logs as possible by identifying stratigraphic omissions. Well log correlations across the fault enabled the identification of fault displacement, recognized by stratigraphic thickening and offsets.

3.2 Industry 3-D Seismic Data

3.2.1 Seismic Acquisition and Synthetic Seismogram

The 1,375 km^2 (854 mi^2) seismic volume of this study was acquired by WesternGeco in 1998 and 1999 and is currently held by Upstream Exploration LLC. Only the portion of the seismic data set immediately proximal to the Delacroix Island field was utilized for this study. The volume was uploaded into the *IHS Kingdom* interpretive software where all seismic data interpretation and manipulation was completed.

Time-depth data was not available for this survey so a time-depth curve for the field had to be created in order to accurately correlate the wells to the 3-D seismic data. For this study, the *IHS Kingdom* program *Synpack* was used to construct a synthetic seismogram using digitized sonic and density well logs. A well located immediately outside the Delacroix Island field (BOPCO 41) contained the necessary logs and was used to create the synthetic trace (Fig. 6). The synthetic seismogram was then aligned to the actual seismic trace, connecting peaks and troughs and pinning the synthetic in properly correlated sections. Once the synthetic seismogram was

tied to the actual seismic, a time-depth chart was created and applied to all the wells in the Delacroix Island field (Table 1) allowing the wells to be hung accurately inside the seismic data.

In order to check that the seismic synthetic was accurate a time-depth chart was created using fault cuts in the well logs. Eight well logs were utilized and fault cut depths were recorded. The two-way time contoured fault-plane map was then used to identify at what time the fault crossed those wells and the depth was plotted against the time. Points from the time-depth chart were then plotted onto the same graph to display the correlation between the two, showing that the seismic synthetic was accurate (Fig. 7).

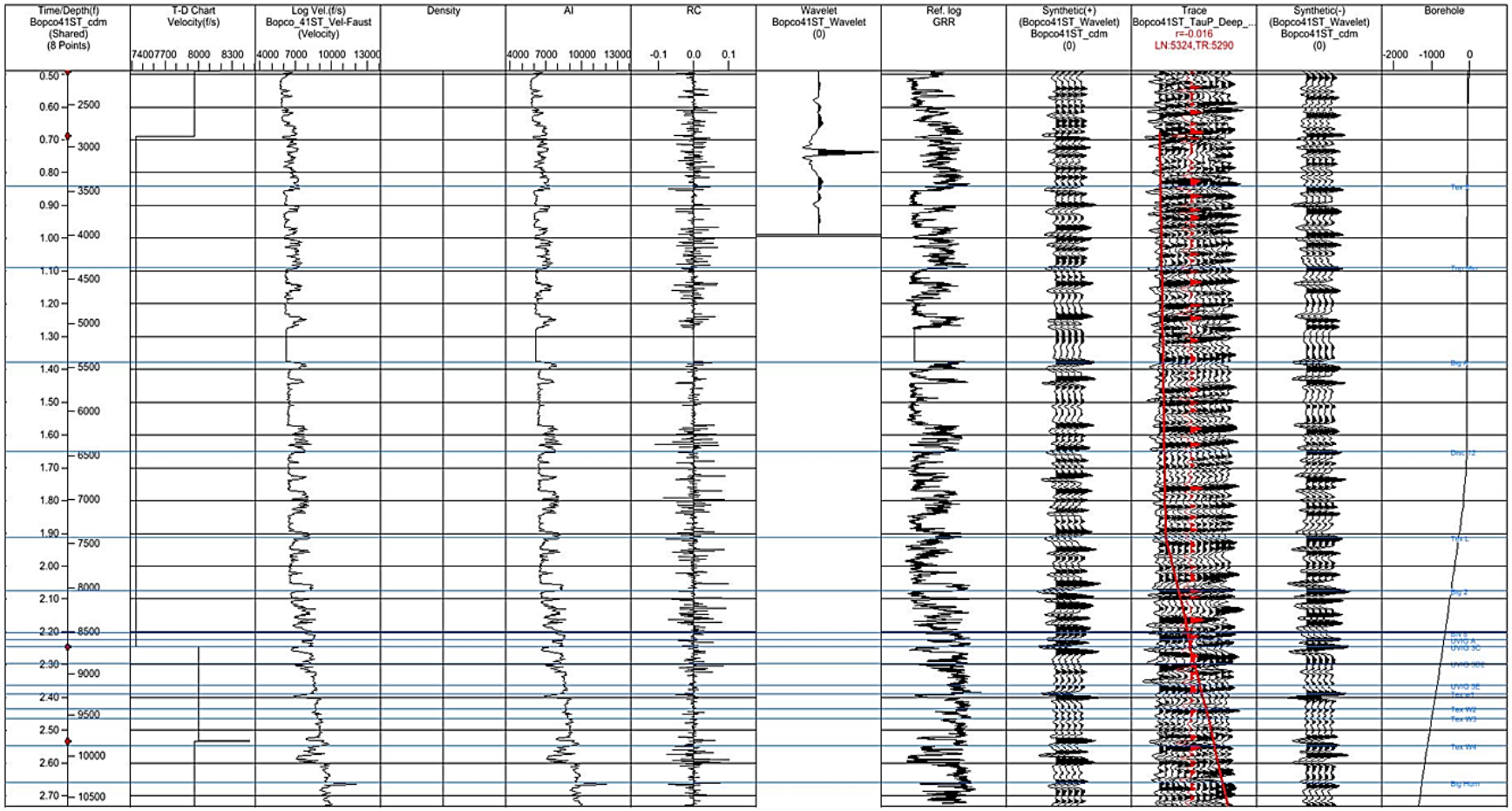

Figure 6. Seismic Synthetic created using the BOPCO 41 well, located outside the Delacroix Island field. This synthetic allowed for wells to be hung accurately inside the 3D seismic data.

Formation Top	Formation Depth (ft)	TVD (ft)	Avg Velocity (ft/sec)	Time to Formation Top (sec)	Time Thickness (sec)	Interval Velocity (ft/sec)	Formation Thickness (ft)
Tex X	3481.2	3446.2	8189.3	0.84169			
Top Mio	4403.0	4368.0	8019.3	1.08937	0.24773	7441.8	921.8
Big A	5473.5	5438.5	7898.7	1.37706	0.2877	7441.8	1070.5
Disc 12	6492.5	6457.5	7822.9	1.65092	0.27386	7441.8	1019
Tex L	7463.3	7428.3	7770.6	1.91318	0.26226	7441.8	975.8
Big 2	8073.2	8038.2	7744.9	2.07575	0.16257	7441.8	604.2
BN 8	8550.2	8515.2	7727.3	2.20394	0.12819	7441.8	477.0
Uvig A	8630.6	8595.6	7724.5	2.22554	0.02160	7441.8	80.4
Uvig 3C	8706.3	8671.3	7721.9	2.24589	0.02036	7441.7	75.7
Uvig 3D2	8909.4	8874.4	7728	2.29668	0.05078	7997.9	203.1
Uvig 3E	9177.8	9142.8	7735.7	2.36377	0.06710	8080.0	263.4
Tex W1	9276.2	9241.2	7738.5	2.38836	0.02459	7999.9	98.4
Tex W2	9459.2	9424.2	7743.4	2.93411	0.04575	8080.0	183
Tex W3	9576.6	9541.6	7748.4	2.46347	0.02935	8080.0	117.4
Tex W4	9914.8	9879.8	7755.1	2.54795	0.08448	8088.1	338.3
Big hum	10361.4	10326.4	7763.4	2.66015	0.1122	7961.0	446.6

Table 1. Time-depth chart created from the seismic synthetic and applied to all wells in the Delacroix Island field.

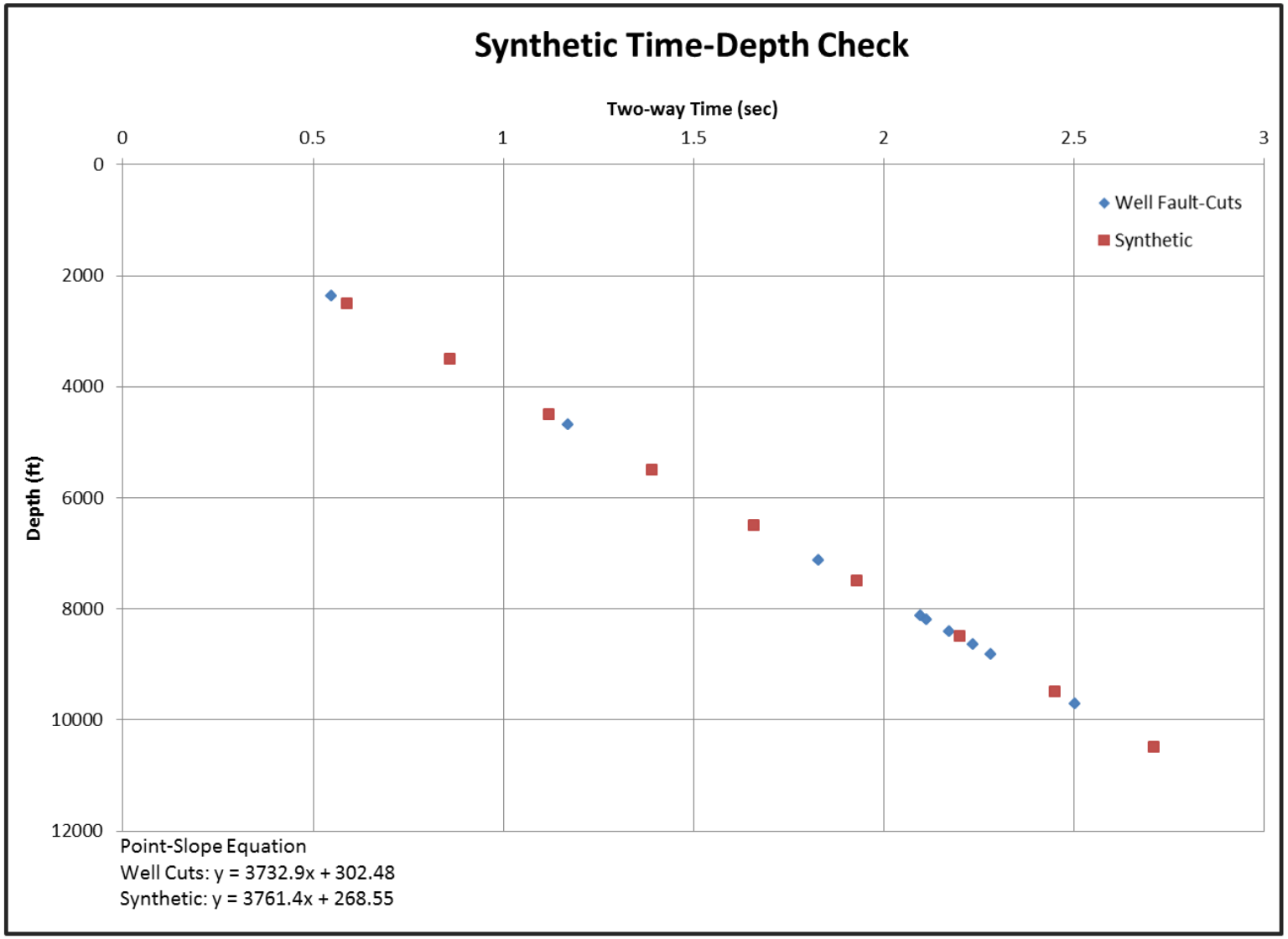

Figure 7. Plot displaying the correlation between the time-depth plot from the synthetic seismogram and from fault-cuts in well logs.

3.2.2 Structure and Isopach Maps

Structure and isopach maps were created to better understand the structural and stratigraphic variability of the field. These maps also enabled the identification of displacement and stratigraphic thickening across the fault (see appendices A & B).

3.3 Analyses of Biostratigraphic Data and Burial History

Ages along with biostratigraphic interval thicknesses were used to create plots depicting fault evolution. Comparison of the thickness of biostratigraphic intervals from the upthrown and downthrown sides of the fault allowed for the calculation of expansion indices. The expansion index expresses the amount that a stratigraphic interval has thickened across the fault, and the amount of interval thickening across a fault is a reflection of the amount of fault movement (Thorsen, 1963). Any expansion index greater than 1 quantitatively illustrates fault movement. Expansion indices were plotted against depth and time to display change in stratigraphic thicknesses throughout the time range covered and as a function of depth.

Magnitudes of fault displacement were identified at each biostratigraphic horizon. A culture line was created across the fault and upthrown and downthrown biostratigraphic formation tops were recorded, providing an amount of displacement. Displacement at each horizon was plotted against depth, creating a depth versus displacement diagram.

A plot of sediment accumulation for the downthrown side of the field was produced using a well with the most shallow well log curve data (well #3). Accumulation rates were obtained by finding the age midpoint of each biostratigraphic interval and dividing that time by the stratigraphic thickness of the interval, producing an approximate rate of sedimentation. The

accumulation rate was plotted against time to show a rate of change during the development of the Delacroix Island Fault.

To further assess stratigraphic variability of the field a burial history diagram was created using biostratigraphic thicknesses and lithologies from the #3 well. A burial history diagram plots the history of sedimentation throughout time and it can be used to study the rate of sediment burial, or subsidence, throughout the history of that area. A correlation of the sediment accumulation graph with the burial history diagram was used to highlight the connection between rates of sedimentation and intervals of increased fault activity.

3.4 Modern Geomorphologic Fault Signatures

The final component of this investigation was to evaluate whether Delacroix Island Fault motion has had an effect on modern geomorphology. The USGS website *LandsatLookviewer* was used to obtain historic satellite images of the area and examine patterns of land loss in the study area. Satellite images were available from August 1972 through April 2018 and selected at 10-year intervals, based on clarity and cloud cover, to study the geomorphologic change proximal to the fault.

Chapter 4. Results

4.1 Seismic and Well Log Correlations

Seismic data and well logs, correlated with biostratigraphic foraminifera and geophysical signatures, reveal the fault-slip history in the Delacroix Island field. Vertically displaced stratigraphic horizons as well as stratigraphic thickening of intervals are evident in fault-perpendicular cross sections (Figs. 8 & 9). Offset of biostratigraphic markers is evident as shallow as approximately 130 m (427 ft) and as deep as approximately 3,000 m (9,843 ft) indicating displacement across the entire fault plane. Magnitudes of displacement increase with depth, varying from 32 m (105 ft) at the shallowest horizon to 168 m (551 ft) at the deepest (Fig. 9). Each biostratigraphic interval analyzed demonstrates some level of stratigraphic thickening, ranging from an increase of 6 m (20 ft) to 100 m (328 ft), indicating variable levels of fault activation during each of the biostratigraphic time intervals.

A correlation restricted to the hanging wall block (trending east-west) has no visible stratigraphic displacement or thickening (Fig. 10). Biostratigraphic intervals show little to no offset remaining at a moderately consistent depth and thickness from east to west.

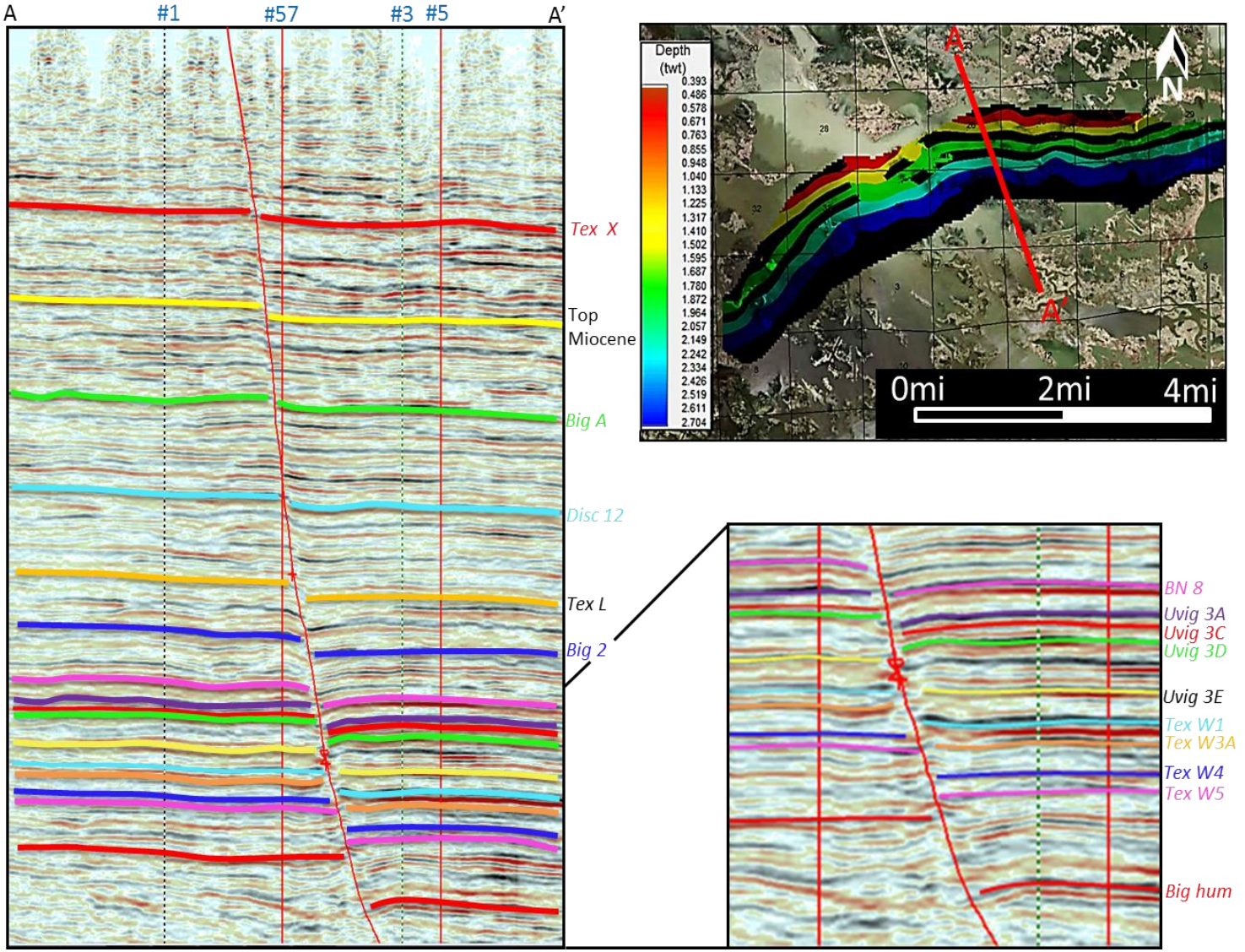

Figure 8. Seismic line (A-A') across the Delacroix Island fault, displaying displacement as well as stratigraphic thickening on the downthrown side of the fault. Horizontal colored lines and labels indicate biostratigraphic markers. Also displayed on the basemap is a depth-contoured map of the fault plane, where cooler colors indicate greater depths or two-way travel times.

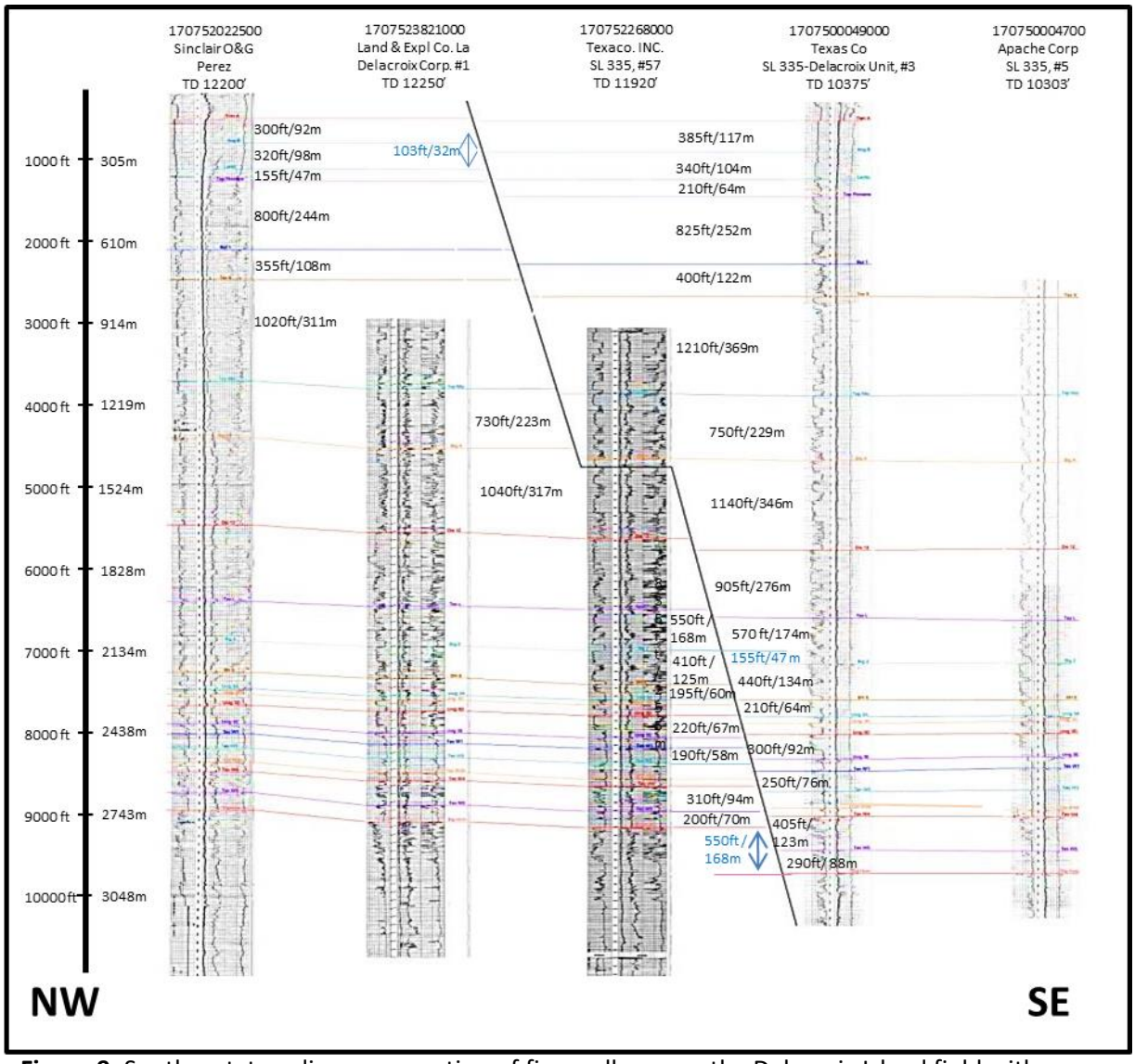

Figure 9. Southeast trending cross section of five wells across the Delacroix Island field with correlated biostratigraphic formation top markers. Displacement of horizons and stratigraphic thickening can be seen and has been recorded based on the well logs. The fault cut in well #57 was identified through omitted stratigraphy in the well log.

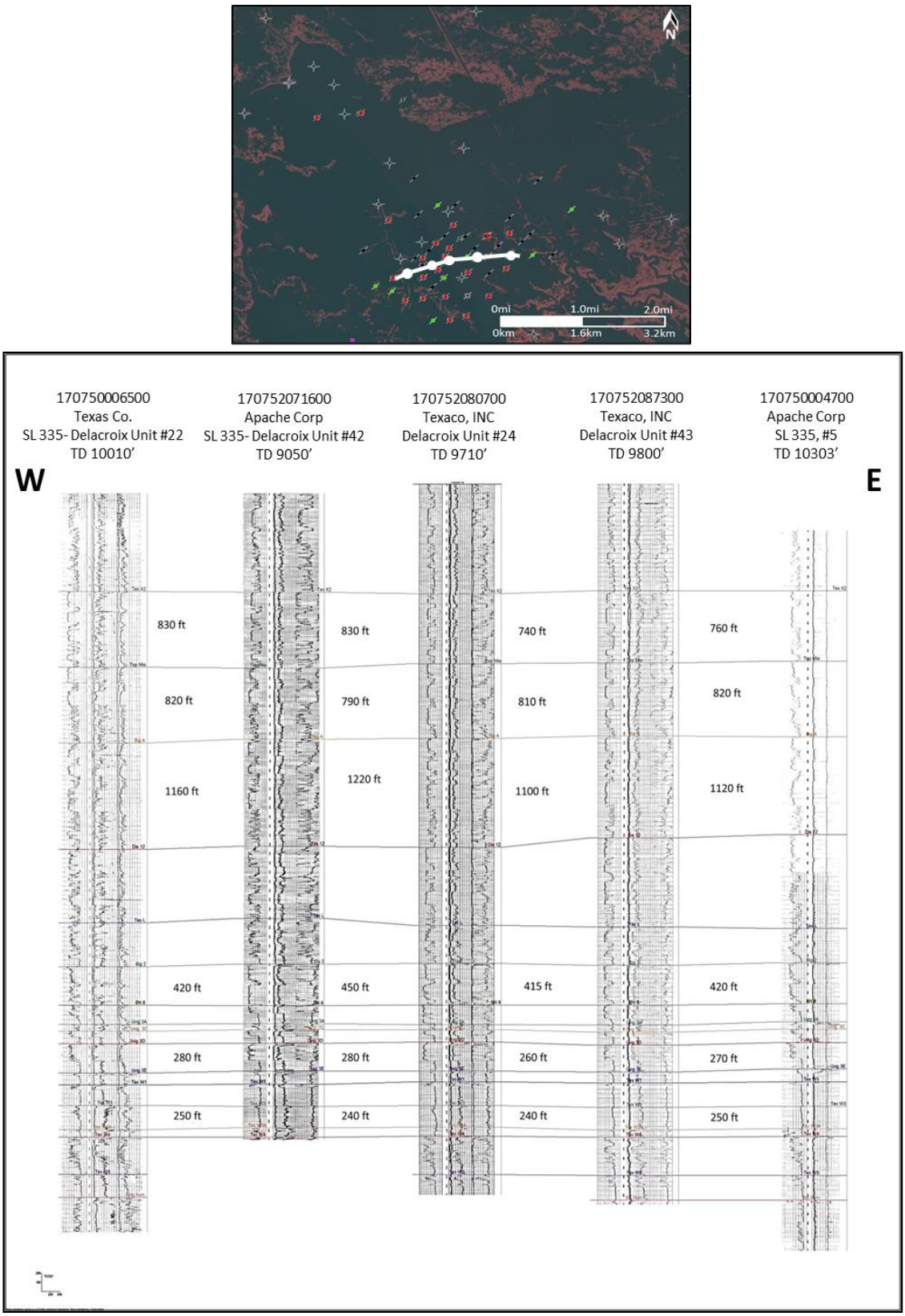

Figure 10. East-trending cross section, on the downthrown block and parallel to the fault trace showing minimal change in depth to correlated horizons and in stratigraphic interval thickness.

4.2 Structure and Isopach Maps

In addition to displaying the geologic structure of an area, structural contour maps can be utilized to study fault movement. Each structure map is contoured and the contours terminate against the fault on both the upthrown and downthrown side. If a contour is followed on the upthrown side to termination then the relative difference in value of the contour directly across the fault (on the downthrown side) provides the vertical displacement at that stratigraphic level. The *Bigenerina humblei* contoured horizon is a good example of this form of displacement identification, depicting an average difference of approximately 52 m (500 ft) between the upthrown and downthrown contours (Fig. 11).

Isopach maps provide an understanding of sedimentary response to fault movement. Isopach maps reveal two distinct forms of fault movement in the Delacroix Island field, regional fault-slip events and local fault-slip events. During regional fault-slip events most of, or the entire, downthrown block is completely displaced. These events cause the entire downthrown stratigraphic interval to be thicker than the temporally similar upthrown interval. The *Textularia W5* to *Bigenerina humblei* stratigraphic interval displays this relationship (Fig. 12) as indicated by isopachs that depict interval thickening, hence displacement, of the entire downthrown block. Similar conditions are depicted in isopach maps *Uvigerina 3D* to *Uvigerina 3E* and *Textularia W4* to *Textularia W5* (Appendix B).

Local fault-slip events create accommodation more proximal to the fault resulting in thicker stratigraphic intervals. The *Textularia L* to *Bigenerina 2* stratigraphic section exhibits a local fault-slip event (Fig. 13). In this case, although the upthrown and downthrown sides of the fault are relatively the same thickness, there is a much thicker section proximal to the fault on the

downthrown side. A similar example can be seen in isopach map *BN8* to *Uvigerina 3A* (Appendix B).

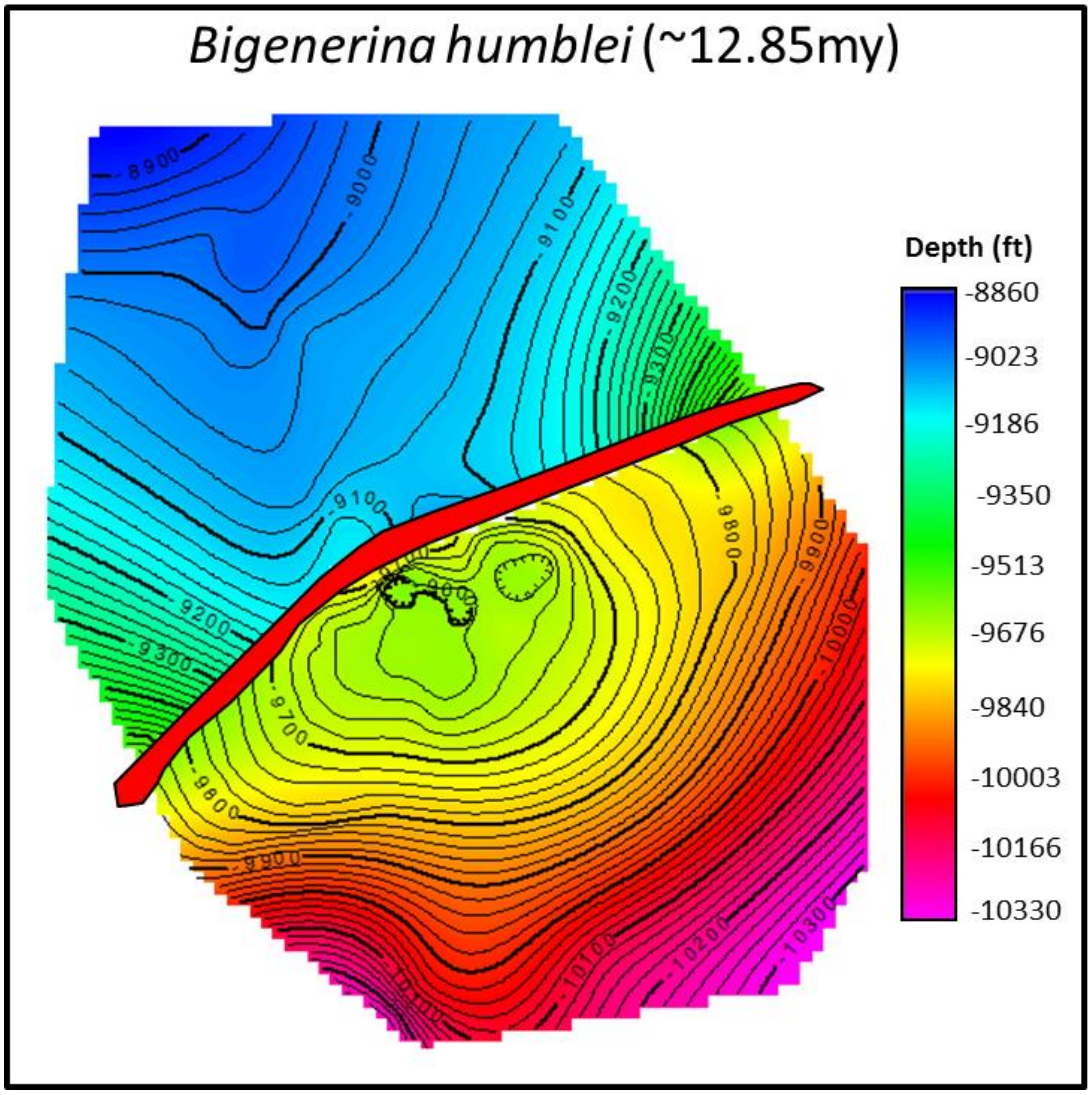

Figure 11. Contoured structure map of the *Bigenerina humblei* biostratigraphic horizon. Structure maps can be used to identify fault displacement by following depth contours from the upthrown side of the fault to the downthrown side; the difference in depth is the amount of vertical displacement. Hotter colors on the entire downthrown block, compared to the upthrown, depict displacement of the entire downthrown block at this biostratigraphic interval.

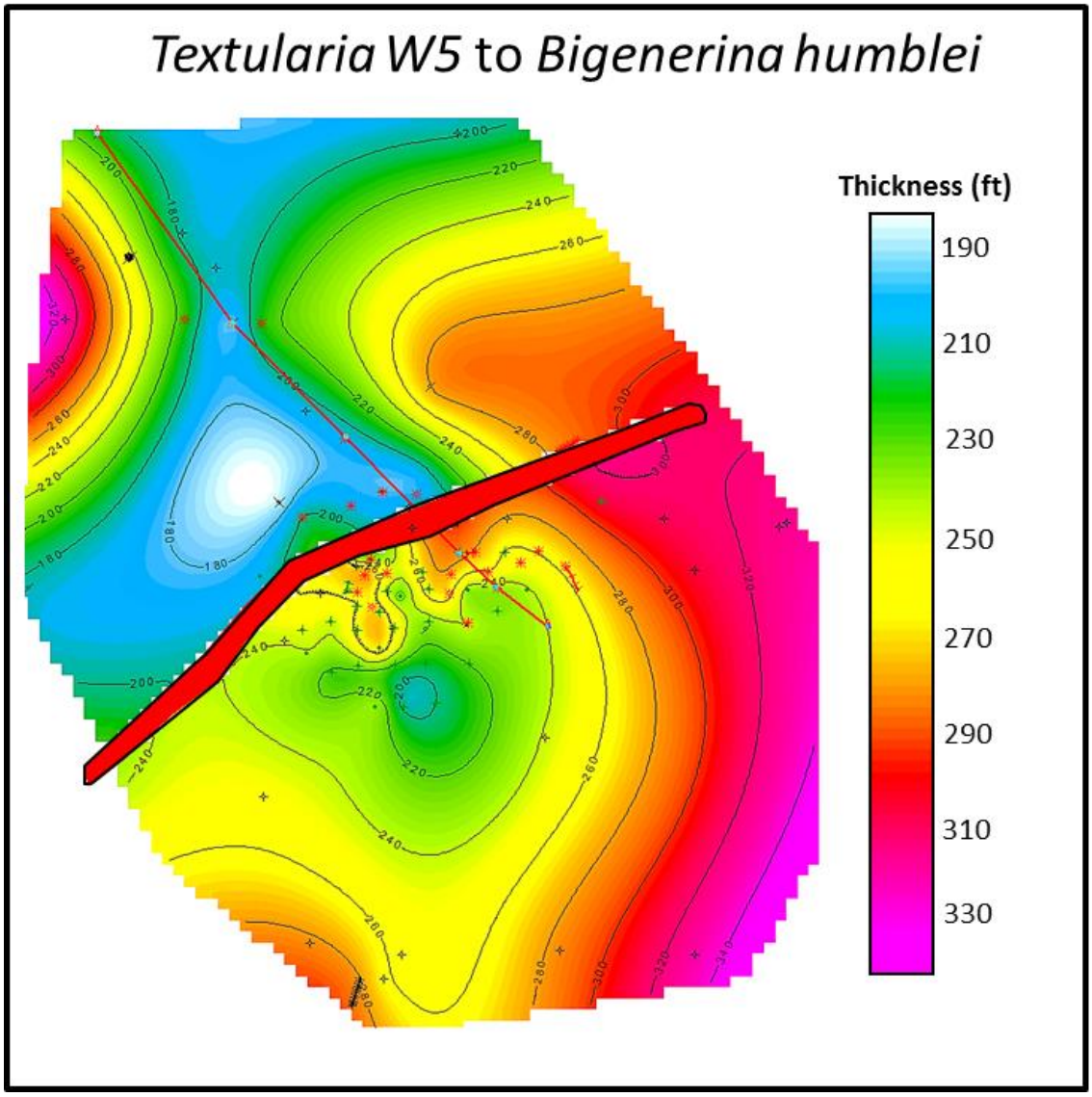

Figure 12. Contoured isopach map of the *Textularia W5* to *Bigenerina humblei* biostratigraphic interval. The upthrown block interval is almost completely thinner than the downthrown block interval, representing a period of regional-fault slip. The red line is representative of the cross section in figure 9.

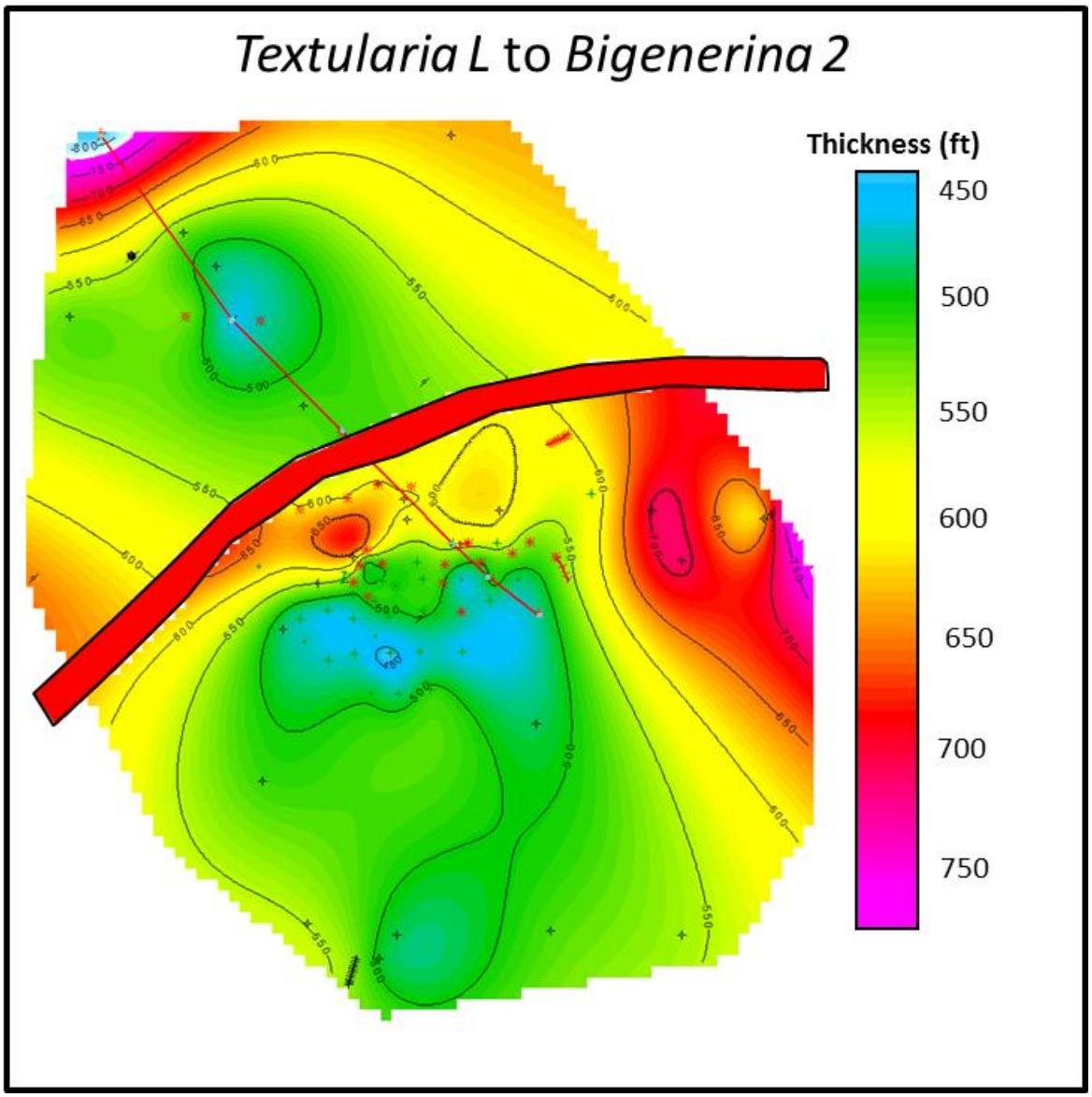

Figure 13. Contoured isopach map of the *Textularia L* to *Bigenerina 2* biostratigraphic interval. The upthrown and downthrown blocks contain similarly thick intervals (color), but there is increasing thickness locally against the fault on the downthrown side. This represents an interval of local fault-slip. The red line is representative of the cross section in figure 9.

4.3 Analyses of Biostratigraphic Data and Burial History

The analysis of biostratigraphic foraminifera markers provides evidence for episodic movement of the Delacroix Island Fault since its inception. The majority of biostratigraphic intervals indicate some level of expansion across the fault, with indices ranging from 0.98 to 2.05 (Fig. 14). This indicates that during approximately the past 13 My there has been variation in the magnitude of fault activity, which created accommodation and allowed for the accumulation of thicker stratigraphic packages on the downthrown side of the fault. For the two intervals where the expansion indices are slightly less than 1.0 it is possible that this records a period of minor erosion on the downthrown block and is stratigraphically thinner than the equivalent upthrown block strata. Alternatively, it could represent an error in the equivalent biostratigraphic picks.

A depth versus displacement diagram also depicts fault movement. As documented in well log cross section, fault-slip causes displacement of stratigraphic intervals and displacement increases with depth along the fault plane (Fig. 15). This is to be expected as the fault moves throughout its time frame of existence, and consequently deep strata become more offset then shallow strata.

The sediment accumulation analyses measure a range of accumulation from approximately 0.06 mm/yr (during a period of 1.12 My) to as much as 0.89 mm/yr (during a period of 0.15 My) (Fig. 16). Although this is a wide range, there is accumulation through time, all the way to the upper limit of the biostratigraphic data (0.74 Ma). This means that there has been continuous subsidence at the location of the #3 well with a long-term trend of higher to lower rates of sediment accumulation and large short-term variation.

The Delacroix Island burial history plot depicts the history of continuous subsidence within the field. Increased subsidence rates are identifiable on the plot during time frames when the slope of the lines increases. A comparison with the sediment accumulation diagram reveals a correlation between periods of higher sediment accumulation and relatively high rates of subsidence on the downthrown block (Fig. 17).

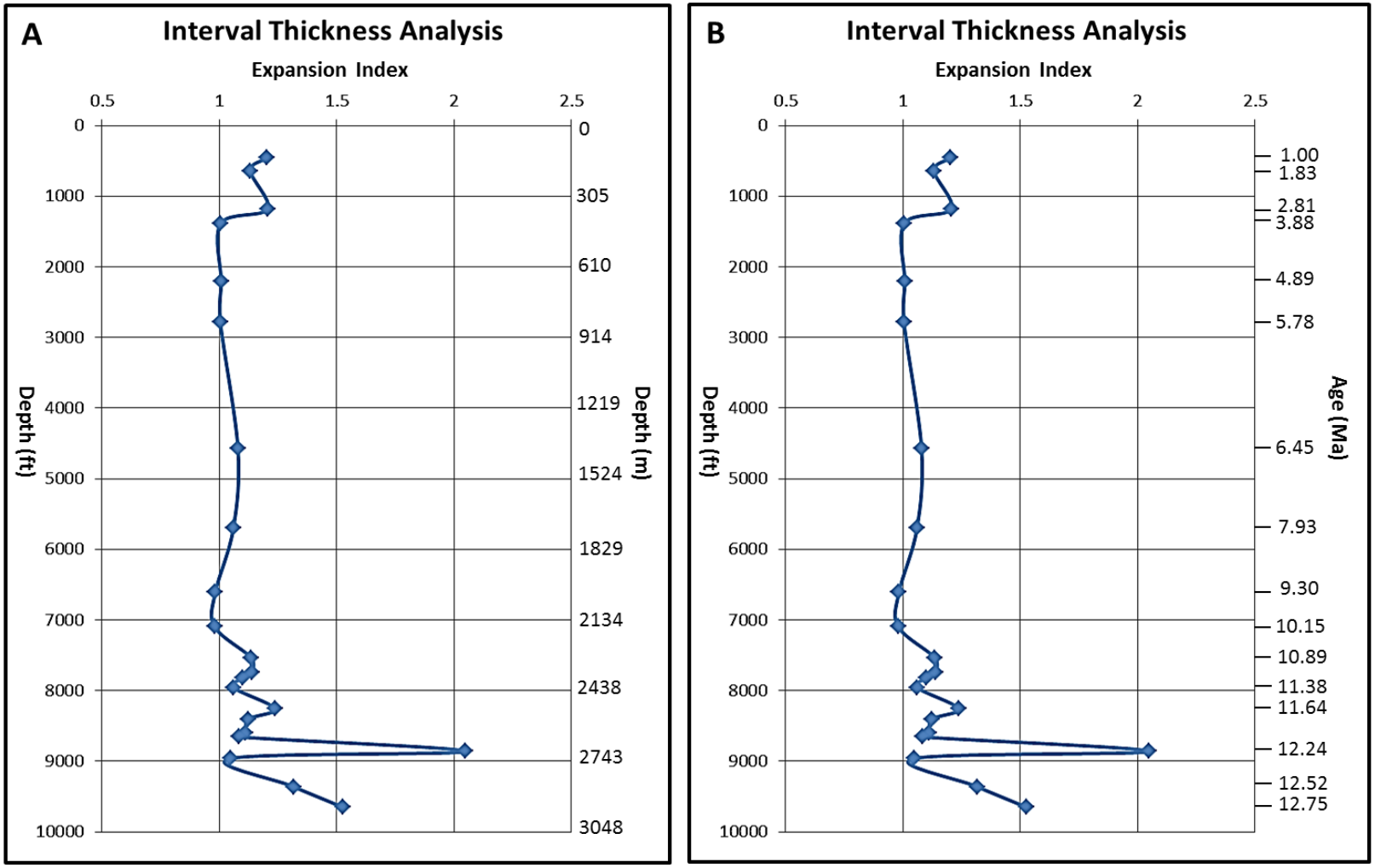

Figure 14. Plot of expansion index versus depth (A) and time (B). Ages were obtained from biostratigraphic formation tops (Paleodata, 2018). These plots depict the amount of expansion for a stratigraphic interval across the fault. An expansion index greater than one indicates a thicker interval on the downthrown side. Note that the largest expansion corresponds to approximately 2650 m (8694 ft) depth and 12.24 Ma.

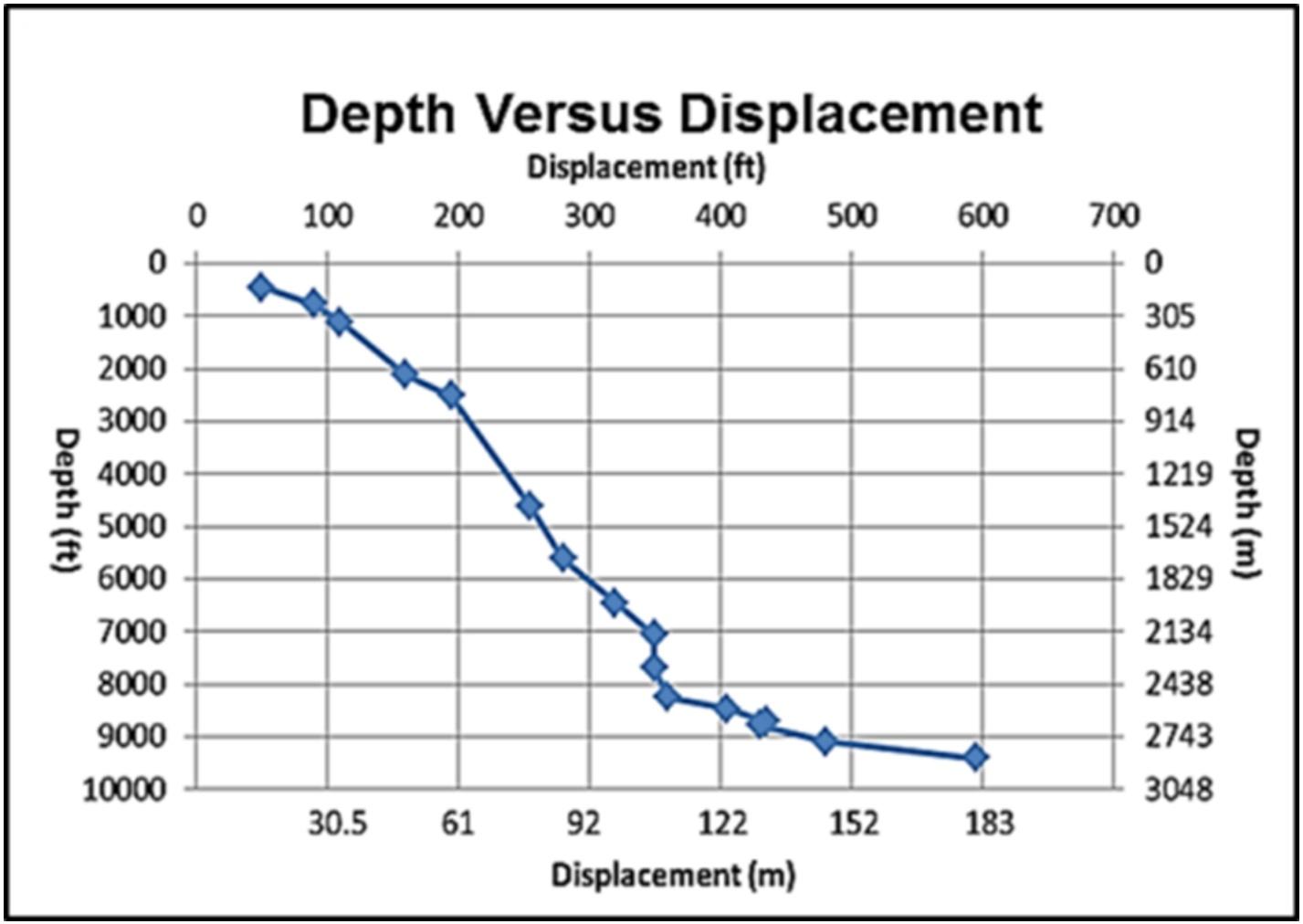

Figure 15. Plot of amount of fault displacement with depth, recorded using the #3 well (API 170750004900). An increase of displacement with depth is the result of intermittent fault movement throughout time. As the fault continues to slip the deeper intervals become more displaced. Fault displacement increases substantially below 2500 m (8202 ft) (approximately 12 Ma and older)

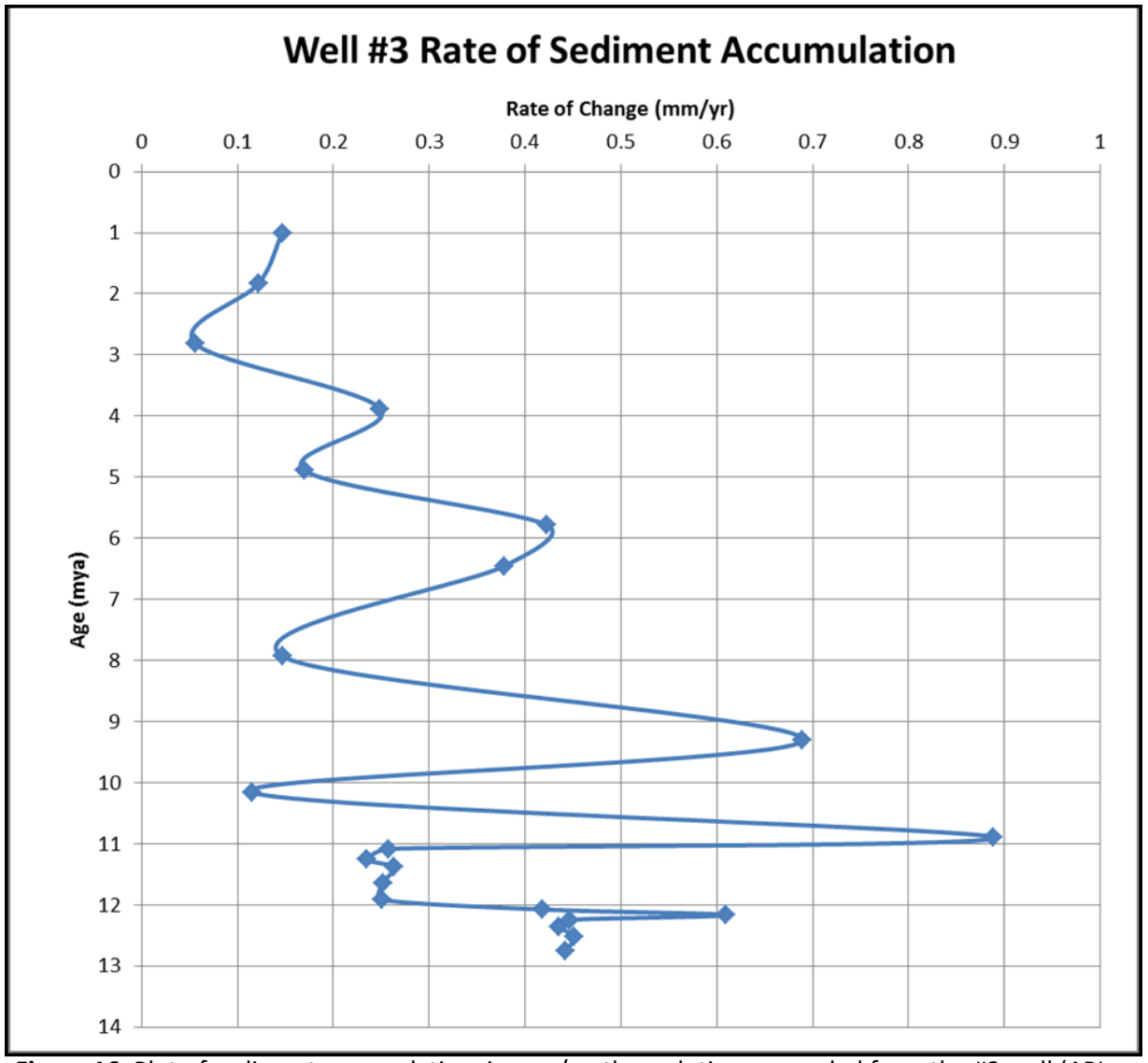

Figure 16. Plot of sediment accumulation, in mm/yr, through time, recorded from the #3 well (API 170750004900). This plot depicts a long-term trend from higher to lower rates of sediment accumulation with large short-term variation.

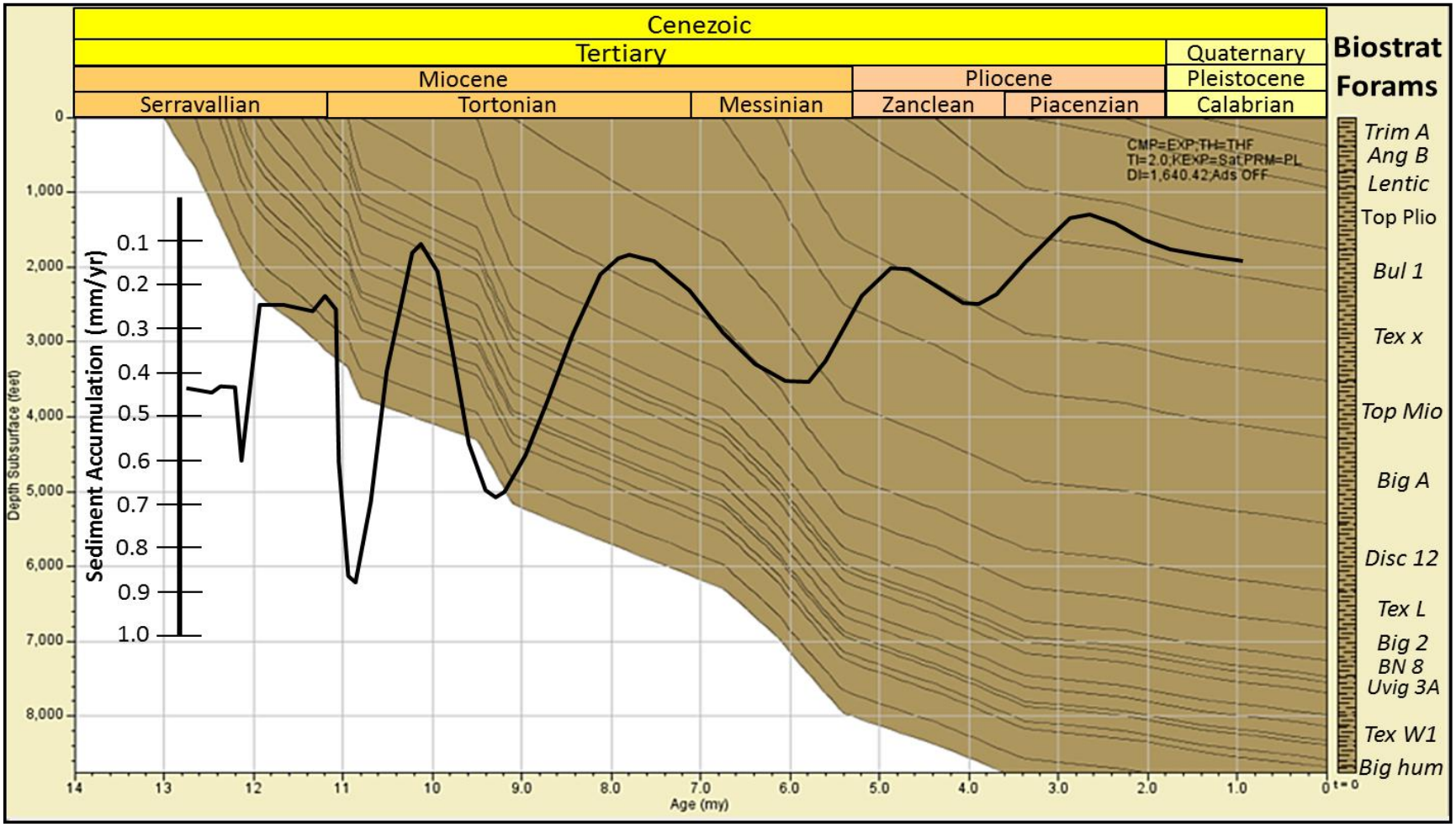

Figure 17. Sediment accumulation graph overlain on burial history diagram of the #3 well (API 170750004900). Burial history depicts the rate of burial, or subsidence in the Delacroix Island field. Steeper slopes indicate periods of greater subsidence. Comparison of sediment accumulation displays a correlation between periods of increased sedimentation and higher rates of subsidence/burial.

Chapter 5. Discussion

5.1 Delacroix Island Fault Activity

The analyses such as the burial history, sediment accumulation, and interval thickness analysis indicate that the Delacroix Island Fault has been active at variable rates since its inception. Although, of the 22 biostratigraphic intervals examined the *Textularia W3* to *Textularia W3A* interval, with an age midpoint of approximately 12.24 Ma, stood out as having the largest expansion index and highest sediment accumulation rate. All of these analyses indicate that the largest magnitude of slip along the fault took place during the Middle Miocene, but the cause of the fault-slip remains to be understood.

5.2 Miocene Delta Progradation and Sediment Loading

During the Miocene, sediment supply from the Rockies and Appalachians shifted depocenters eastward to the east-central Gulf basin (Wu and Galloway, 2002). Loading from this sedimentation caused evacuation of the Terrebonne salt sheet, creating accommodation which was filled in by the progradation of the Mississippi River delta lobes (Wu and Galloway, 2002).

Sediment loading is a proposed mechanism of fault-slip motion (Bishop, 1973; Brandes et al., 2011; Gagliano, 2003; Galloway, 1986; Thorsen, 1963), which prompted additional research to identify the size and distribution of Miocene delta lobes that may have had an effect on the Delacroix Island field and fault. The ancient Mississippi river delta lobes during the Miocene have been extensively studied to date (Combellas-Bigott and Galloway, 2005; Curtis, 1970; Wu and Galloway, 2002) and each of these studies provides insight into how Cenozoic deltaic deposition likely affected the Delacroix Island field.

5.2.1 Early Miocene: the Creation of the Delacroix Island Fault

In the Early Miocene the area that would become the Delacroix Island field was located on the lower continental slope, with the Mississippi River deltaic depocenter positioned to the northwest (Curtis, 1970) (Fig. 18). Large amounts of sediment were deposited across the area, some of which was transported onto the slope. As sediment from a prograding delta is deposited and accumulates on the delta front, the overburden on the slope can cause slumping events and peripheral faulting (Coleman et al., 1974). The initiation of the Delacroix Island Fault likely occurred in this way during the Early Miocene.

5.2.2 Middle Miocene: Largest Fault Movement

The Mississippi River delta, as well as the continental slope, continued to prograde through the Middle Miocene, eventually the Delacroix Island Fault was located on the upper continental slope and under the edge of the Middle Miocene depocenter (Curtis, 1970) (Fig. 19). Deposition of hundreds of meters of sediment would cause fault-slip, displacement and subsequent interval thickening. This interval of time represents the initiation of the largest magnitude of Delacroix Island Fault movement, for the span of data available, on the basis of the largest expansion index (2.05) and periods of increased sediment accumulation (as much as 0.88 mm/yr) (Fig. 14 & 16).

Deltaic sedimentation (*sensu* Curtis 1970) continued through the Middle Miocene, prograding the continental shelf such that the Delacroix Island Fault was located in the center of the depocenter (Fig 20). This time interval correlates with the lower portion of the UM1 depositional episode (10.8 to 12.0 Ma) of Wu and Galloway (2004) and also includes Genetic Cycle 4 (12.8 Ma to 12.2 Ma) identified by Cambellas-Bigott and Galloway (2005). During this

depositional episode large quantities of sediment, approximately 762 to 1317 m (2500 to 4500 ft), was deposited proximal to the Delacroix Island area (Combellas-Bigott and Galloway, 2005). This increase in sedimentation at the shelf edge and slope caused the formation of a more complex fault system, with an increasing number of faults. Furthermore, the increased sediment loading on these faults, specifically the Delacroix Island Fault, apparently increased the rate of fault-slip rate and consequently stratigraphic displacement and thickening as indicated by the well log, seismic, and biostratigraphic data.

Additionally, this time of abundant sedimentation throughout the Middle Miocene correlates with a marked increase in expansion index (to 2.05) and sediment accumulation (as much as 0.88 mm/yr) (Figs. 14 & 15). Wu and Galloway (2004) identified deposition of approximately 914 m (3,000 ft) of sediment throughout the UM-1 episode (approximately 1.20 My), equating to a time-averaged accumulation rate of approximately 0.76 mm/yr (Fig. 3.13 from Wu and Galloway, 2004). That value correlates with the values during the same time frame on the sediment accumulation graph created for the Delacroix Island field (0.23 mm/yr to 0.89 mm/yr) (Fig. 16).

Genetic cycle 4 (GC4) from Combellas-Bigott and Galloway (2005) represents the upper portion of the Middle Miocene and spans a time frame of approximately 12.80 Ma to 12.20 Ma. This sequence, characterized by regional continental-margin outbuilding resulted in prominent offlap and slope aprons with a depocenter located in the immediate area of the Delacroix Island field (Combellas-Bigott and Galloway, 2005) (Fig. 21). This influx of sediment during GC4 (12.80 Ma to 12.20 Ma) also correlates with the anomalous spike in the expansion index of the Delacroix Island field at the time frame of 12.24 Ma (Fig. 14).

Studies analyzing Miocene delta progradation and sedimentation (Curtis, 1970; Wu and Galloway, 2002; Combellas-Bigott and Galloway, 2005) identify increased sediment during Miocene deltaic sedimentation, which correlates with a large fault-slip of the Delacroix Island Fault at approximately 12.24 Ma.

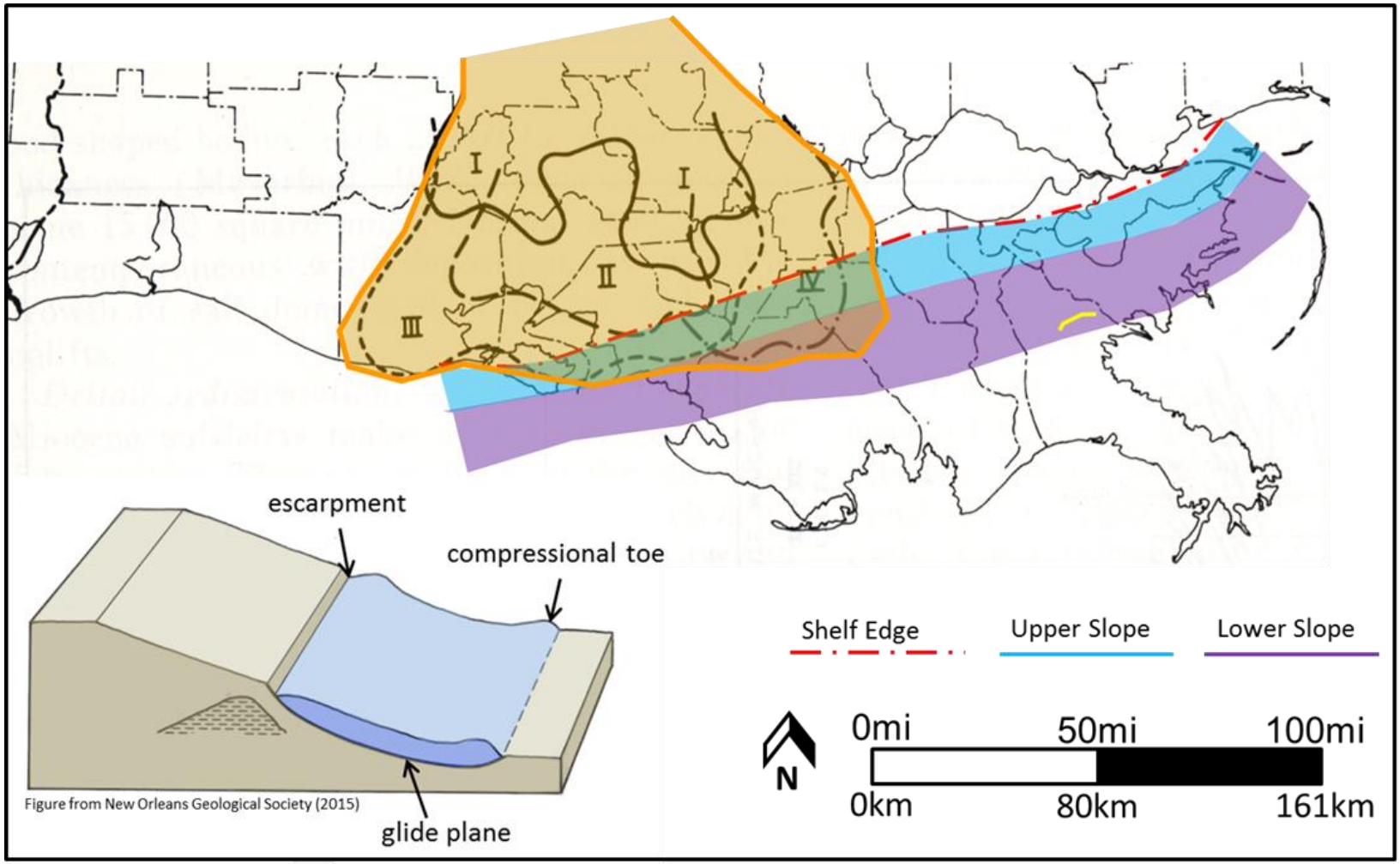

Figure 18. Early Miocene delta lobe, as defined by Curtis (1970), along with the shelf edge (red), upper slope (blue) and lower slope (purple) during that time frame as defined by biostratigraphic data from PaleoData Inc. (2018). The location of the Delacroix Island fault is displayed in yellow. A highly conceptualized 3D block model from the NOGS (2015) shows approximately how the Delacroix Island fault formed as a massif of strata was translated basinward.

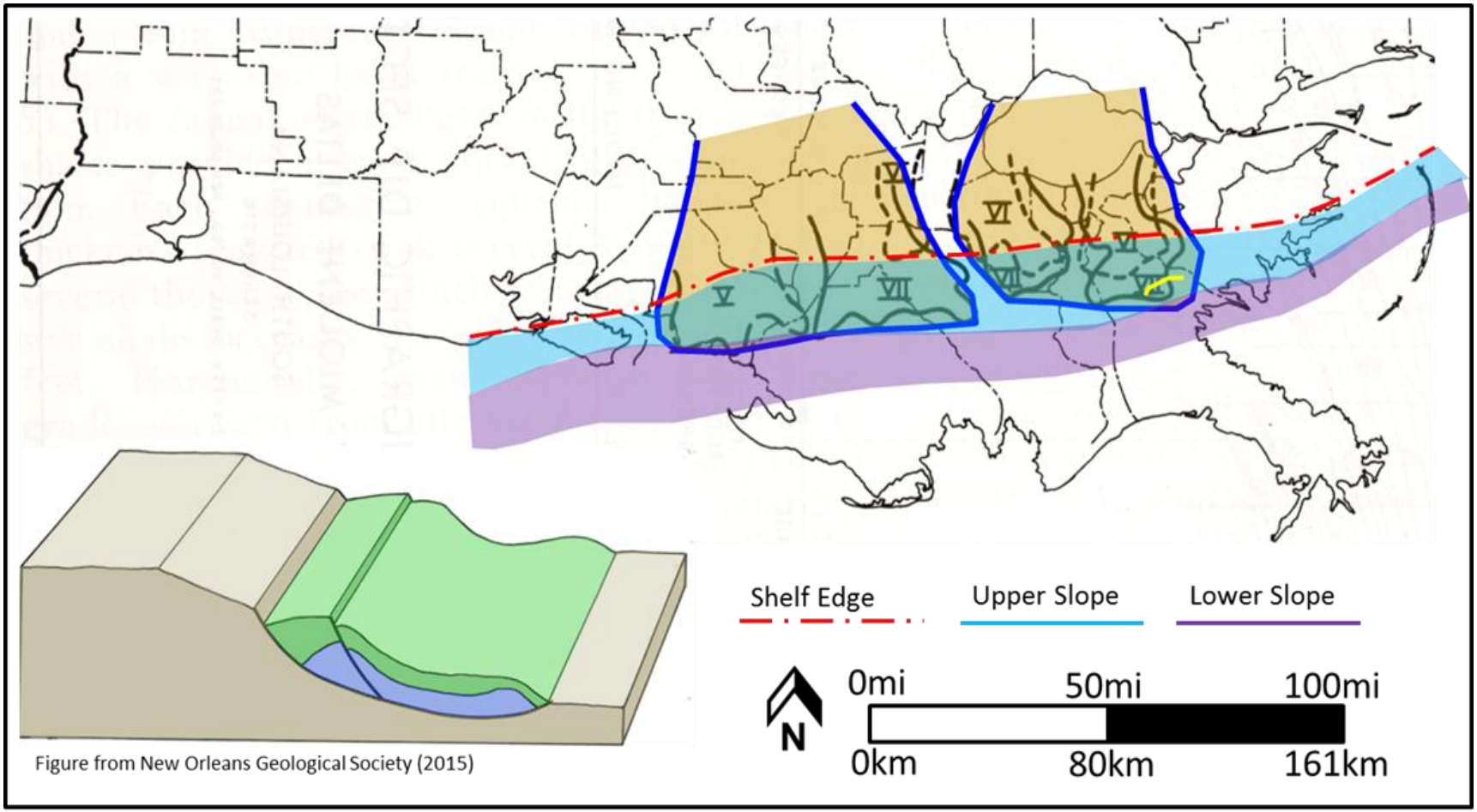

Figure 19. Middle Miocene I delta lobes, as defined by Curtis (1970), along with the shelf edge (red), upper slope (blue) and lower slope (purple) during that time frame defined by biostratigraphic data from PaleoData Inc. (2018). The Delacroix Island fault is displayed in yellow. A highly conceptualized 3D block model from the NOGS (2015) displays approximately how the Delacroix Island fault and surrounding area would react to the prograding delta.

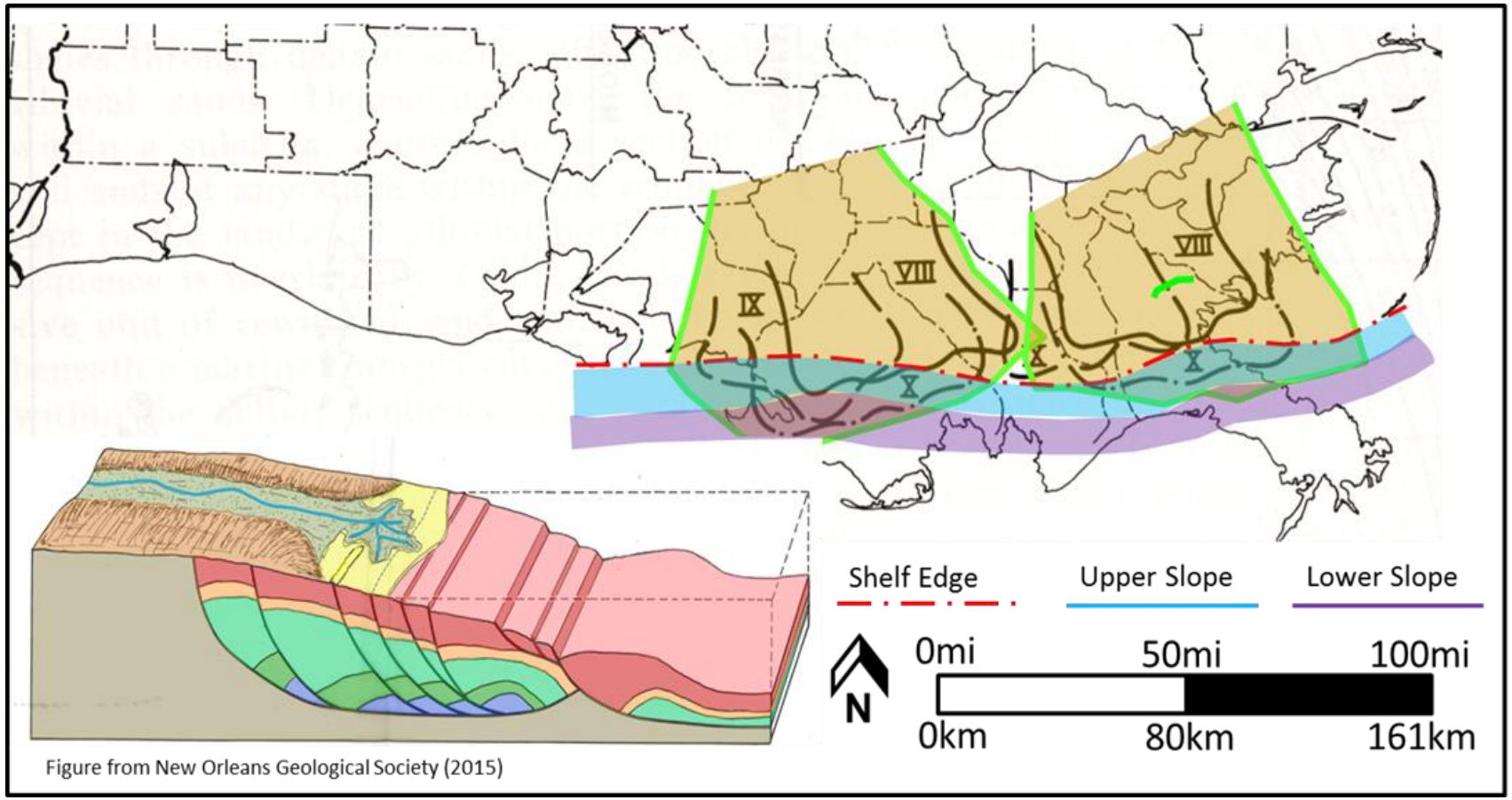

Figure 20. Second episode of Middle Miocene delta progradation (Curtis, 1970). By this time the Delacroix Island fault (green) is located near the shelf edge as the deltas continue to prograde over the shelf edge (red), upper slope (blue) and onto the lower slope (purple) (based on biostratigraphic data from by PaleoData Inc., 2018). A highly conceptualized 3D block model from NOGS (2015) displays approximately how the Delacroix Island fault and surrounding area would have reacted to the continuing progradation delta.

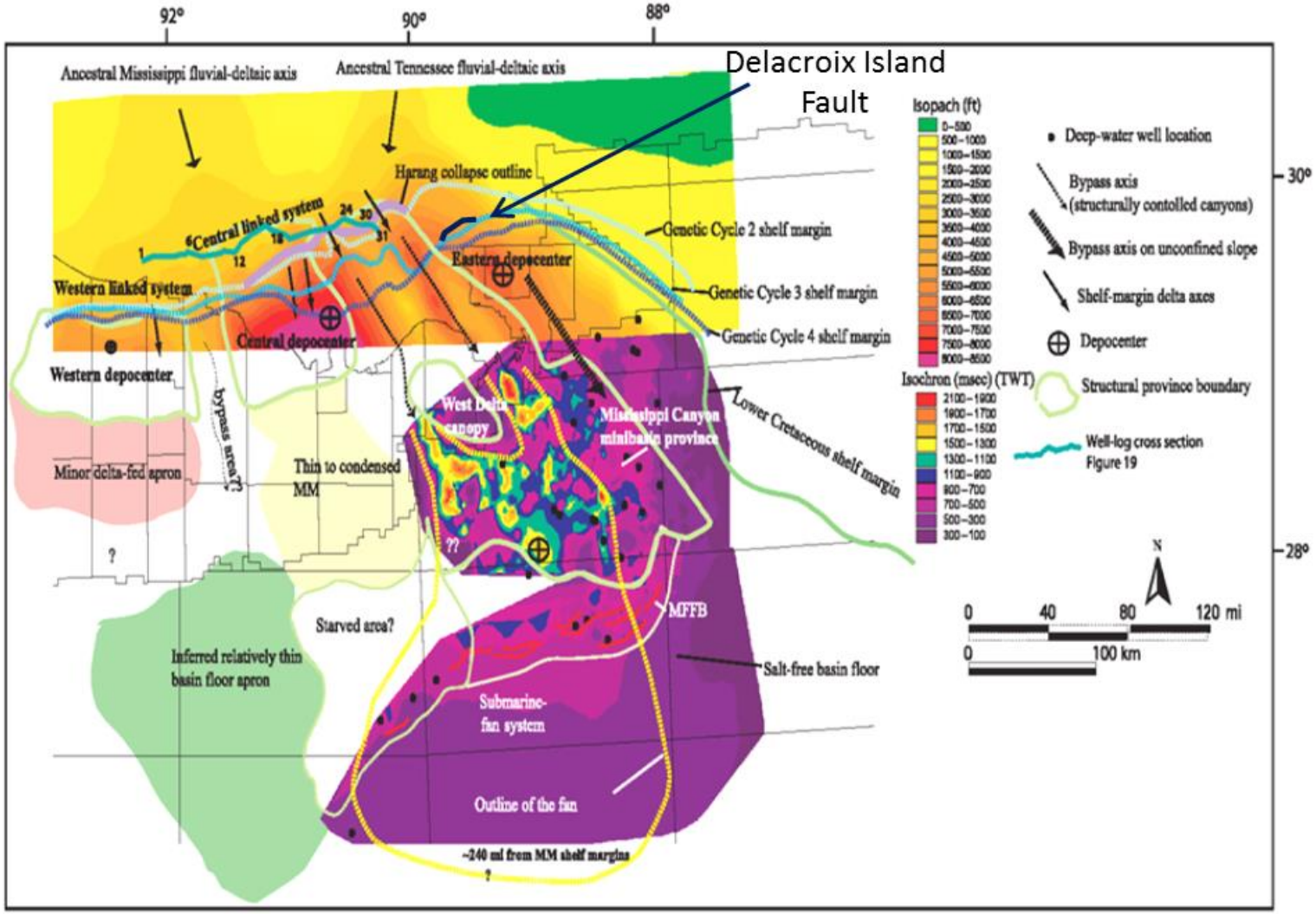

Figure 21. Middle Miocene major depocenters as defined by Combellas-Bigott and Galloway (2005), showing geographic loci of deposition during the Miocene. This is also depicted by color-coded isopachs (ft) with yellows indicating thinner sections and reds indicating thicker sections. The "Eastern Depocenter" is situated in the vicinity of the Delacroix Island fault (black), showing that approximately 1372 to 1676 m (4500 to 5500 ft) of sediment was deposited in the area during the Middle Miocene.

5.3 Geomorphologic Evidence of Modern Fault Movement

There is evidence of fault movement from the lower to upper limits of the data available for this study. This investigation reveals sediment accumulation rates on the order of 0.8 mm/yr (Fig. 16), expansion indices ranging from 1.06 to 1.36 (Fig. 14) and displacement ranging from 15 m to 30 m (49 to 98 ft) throughout the Pliocene and Pleistocene (Fig. 15). Although there are no quantitative data available to identify Delacroix Island Fault movement more recently than the Pleistocene, modern (approximately last 100 yrs) movement can be observed qualitatively.

Several studies have identified modern fault movement across the Mississippi River delta plain in the form of geomorphologic signatures (Gagliano, 2003; Goswami, 2012; Koch, 1933; Verbeek, 1979). Gagliano et al. (2003) identified multiple surficial expressions of fault movement including fault-line scarps, associated marsh breakup, fault-stream alignment and ballooned channels (Fig. 22). In the Delacroix Island field the geomorphology of the land and water configuration suggests that two of these signatures may be present: marsh edge breaks and fault-stream alignment.

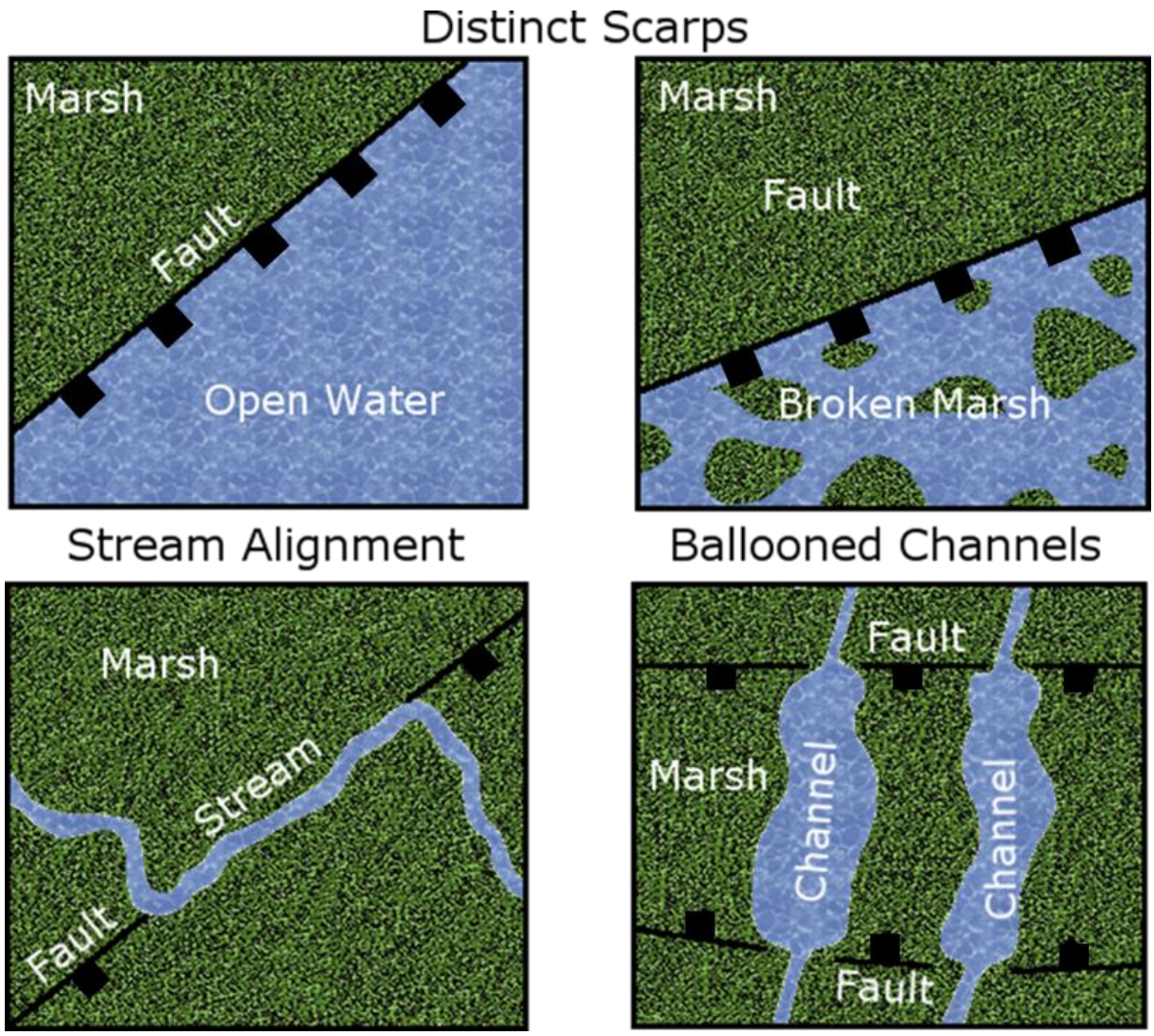

Figure 22. Conceptual models of how fault movement can be identified through geomorphologic characteristics based on field observations by Gagliano et al. (2003). Distinct scarps (top left and right) are created as fault-slip motion causes marshlands on the downthrown block to become submerged, leaving a scarp coincident with the surface fault trace. Stream alignment (bottom left) occurs when a stream follows the path of a fault trace at the surface. Faults can also cause channels to "balloon", or become wider, as they cross the fault trace.

5.3.1 Distinct Marsh Scarps

A land change map created by Couvillion et al. (2017) displays areas of persistent land loss dating back to 1932 (Fig. 23) and provides a record of land loss in the Delacroix Island study area. Interestingly, the projected surface trace of the Delacroix Island Fault is located at the boundary between stable marshlands and an area of persistent land loss. Stable marsh is located on the upthrown side of the fault, retaining much of the marshland in 2015 that was present in 1932. Alternatively the downthrown side is characterized by persistent land loss during this time frame, with nearly all of the 1932 marsh converted to open water by 2015.

In figure 23 the Lake Campo Fault trace, mapped by Armstrong et al. (2014), forms a boundary between stable wetlands on the upthrown side and completely open water on the downthrown side of the fault. The oldest topographic map available of the area (1893) shows minor amounts of wetlands on the downthrown block, suggesting that persistent marsh loss has occurred on the downthrown side of the Lake Campo Fault, just as in Delacroix Island. If the Delacroix Island area is undergoing the same processes as Lake Campo there will be no marshlands on the downthrown side of the fault in the future.

Historic satellite images provide additional evidence of modern fault movement. Satellite images from the United States Geological Survey database *Landsat Look* were available from August 1972 through March 2018. Selections of these images in 10 year intervals, based on clarity and cloud cover, were used to document the geomorphologic evolution in the study area (Fig. 24). In 1985 wetland cover is quite dense on both the upthrown and downthrown side of the fault. In subsequent years, such as 1995 and 2005, wetland coverage on the downthrown fault block decreases, exposing a larger area to open water. By March of 2018, the downthrown side

of the Delacroix Island Fault is almost entirely open water. Although not a focus of this work, the increase in open water coverage for the upthrown and downthrown blocks was measured using *Google Earth*. Between 1985 and 2018 open water coverage in the downthrown block of the Delacroix Island Fault approximately doubled, from 30 % to 60 %, whereas upthrown open water coverage increased only 1.5 times, from 27 % to 42 %. It is important to note that the 2005 image was taken on October 25th, two months after hurricane Katrina passed through the area followed by the passage of hurricane Rita along western Louisiana. Although these major storms caused the erosion and fragmentation of 527 km^2 (327 mi^2) of wetlands (Barras et al., 2008), it is plausible that reduced elevation induced by fault slip caused the marsh on the downthrown side to be more susceptible to erosion and subsequent marsh failure.

As mentioned, Gagliano et al. (2003) identified fault-line scarps and associated marsh breakup as a geomorphologic sign of fault induced land loss and that is very likely what is occurring in the Delacroix Island field. A distinct difference in the amount of marsh converted to open water is present between the areas upthrown and downthrown to the marsh edge that is coincident with the fault surface trace. Gagliano (2003) described this type of geomorphologic feature as a “D-shaped lake”, referring to the D-shaped marsh trace created as the downthrown fault block continues to subside.

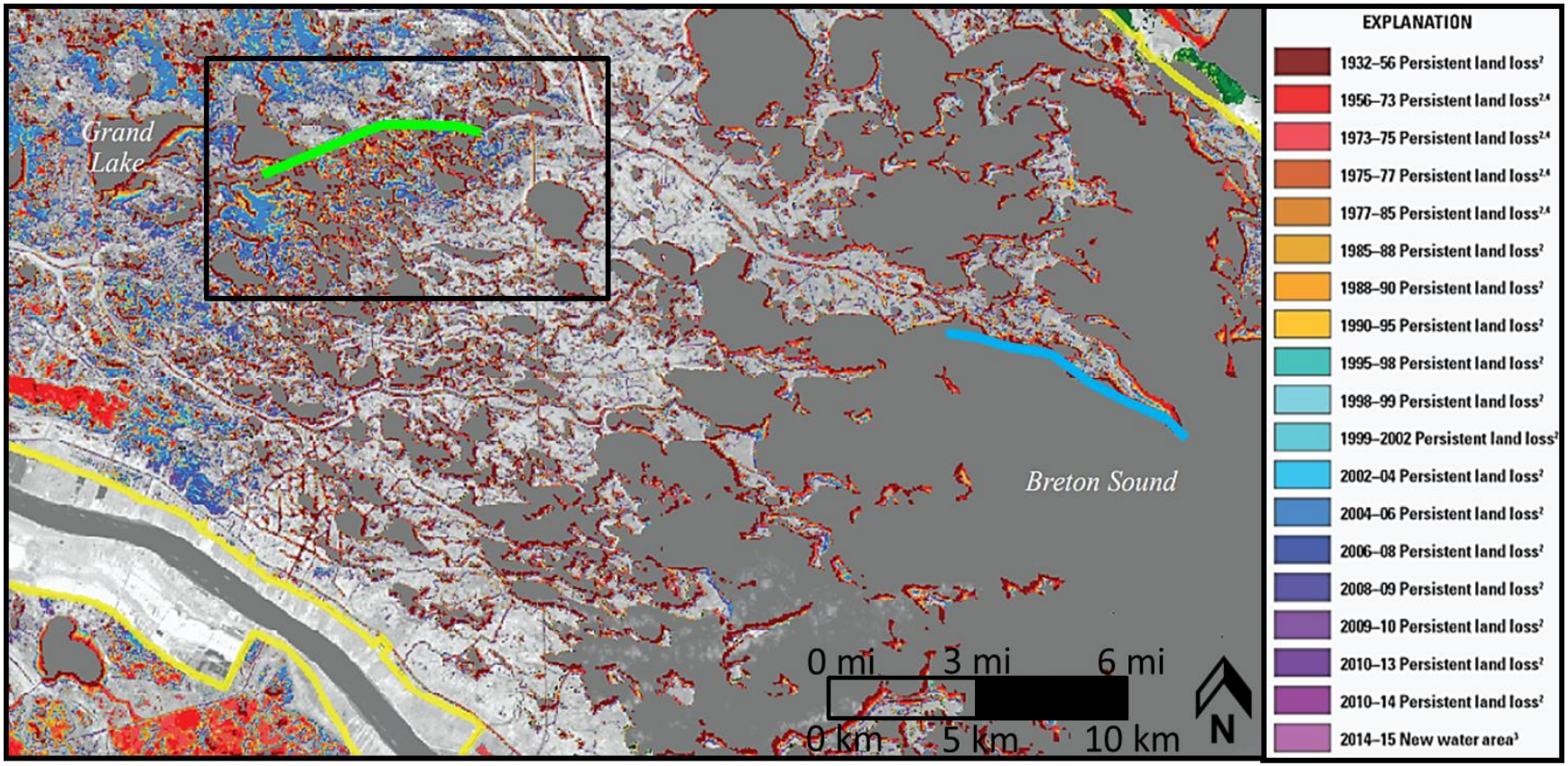

Figure 23. Land change map from 1932 through 2015 from Couvillion et al. (2017). Each color represents land loss during a specific interval of time. Highlighted in blue is the Lake Campo Fault and highlighted in green is the Delacroix Island fault. The Lake Campo Fault is another down-to-the-south growth fault that currently represents a boundary between stable marshlands on the upthrown side and open water on the downthrown side. The Delacroix Island Fault is following this trend, with the downthrown side consistently losing land since 1932. The black box represents the approximate study area and also the boundaries of the satellite images in figure 24.

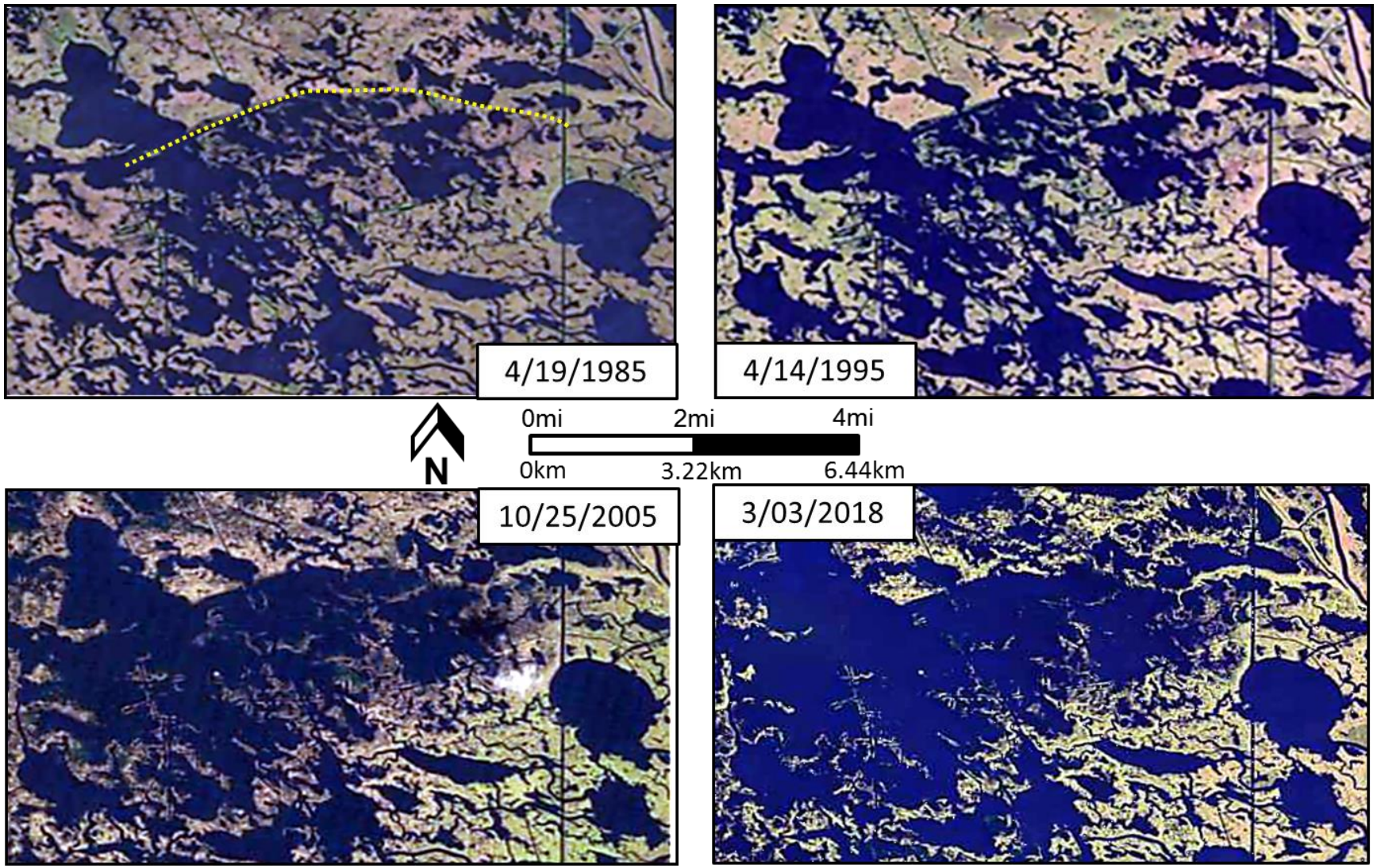

Figure 24. Historical satellite images from USGS Landsatlook Viewer dating back to 1985. These images depict a pattern of wetland loss in the Delacroix Island field that is coincident with the downthrown block of the fault. This spatial relationship suggests that fault-slip movement may be a process contributing to land loss and relative sea-level rise. The yellow dotted line in the 1985 image represents that approximate surface trace of the fault.

5.3.2 Stream Alignment

Topographic maps dating back to the 1935 indicate the presence of a bayou named "Bayou Long", an arcuate, concave to the south, generally east trending feature (Fig. 24). This same bayou is observed in historical satellite imagery as far back as 1973. The bayou is coincident with the surficial trace of the Delacroix Island Fault, which has become more defined as marsh inundation increases (Fig. 25).

The spatial coincidence of the bayou with the surface trace of the fault is an example of what Gagliano (2003) called fault-stream alignment. Fault movement is known to influence elevation and slope of the surface and also creates conditions that impact fluvial channel pathways (Armstrong et al., 2014; Gagliano, 2003). Armstrong et al. (2014) concluded that individual channels can be directed along the hanging wall of a fault and subsequently follow its surface trace. Evidence of this is seen in Delacroix Island, as Bayou Long directly follows the faults surface trace. All available topographic maps provide supplementary evidence that the Delacroix Island Fault has been influencing the geomorphology of the Delacroix Island field during modern history.

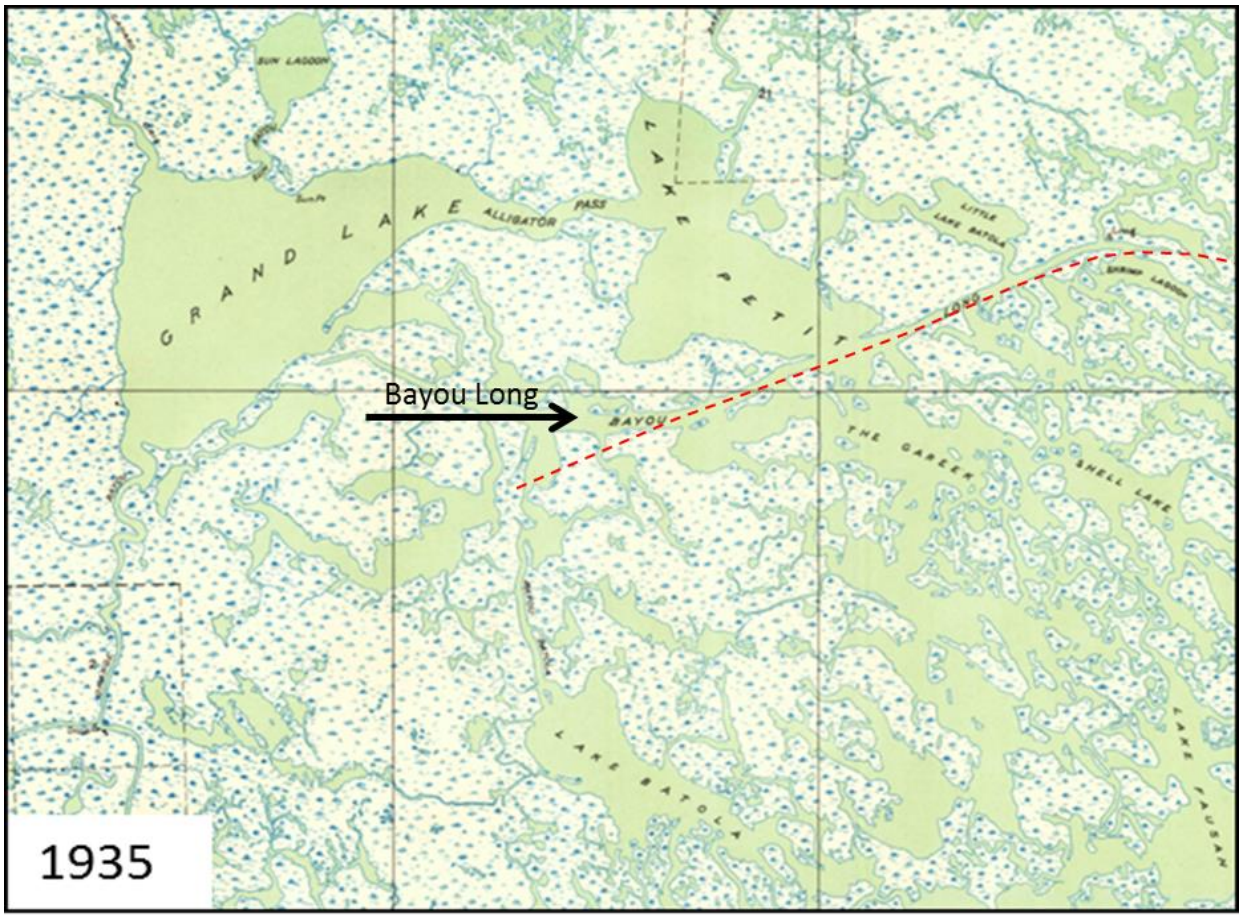

Figure 24. Topographic map of the Delacroix island area from 1935. Shown in this map is Bayou Long, which coincides with the fault trace (dashed red line).

5.4 Fault induced Subsidence and Marsh Edge Retreat

Field observations reveal the Delacroix Island marsh edge, located at the surface fault trace, is not as well defined as it appears in satellite imagery. This is due to the Delacroix Island marsh undergoing wetland loss in both the vertical and horizontal dimensions (elevation change versus lateral retreat). Wetland loss is a factor of many processes including the erosive power of wave attack on the marsh edge adjacent to open-water bodies (Wilson and Allison, 2008). Wilson and Allison (2008) studied a selection of southern Louisiana marsh and found that wave erosion accounted for 60 to 70 % of marsh loss, the remainder due to subsidence. Penland (2002) studied the entirety of coastal Louisiana and found that lateral retreat of gulf environments accounted for approximately 25 % of overall wetland loss between 1932 and 1990. It can be inferred that Delacroix Island is also undergoing changes due to lateral retreat.

The Delacroix Island marsh is undergoing a combination of processes causing wetland loss including marsh edge erosion and inundation due to fault movement. Episodes of fault movement combined with periods of marsh edge erosion cause a rough, preferentially eroded, lineation in the marsh. Although this wetland area is experiencing differential subsidence due to fault movement, it is still affected by the shoreline erosion and retreat that all of coastal Louisiana is undergoing.

5.5 Evidence of these Processes in Other Deltas of the World

Evidence from studies completed on deltas around the world provides support for recent fault movement causing increased rates of subsidence and subsequent land loss. The northeastern margin of the Nile delta has subsided at rates of as much as 5 mm/yr during the last 7.5 kyr (Stanley, 1988). Stanley (1988) reported that several stratigraphic and tectonic processes may be

causing this rapid subsidence, including listric, down-to-basin faults of the Nile delta that have been recently slipping and, as a result, affecting the Holocene geomorphology.

The Ganges-Brahmaputra delta in India is an additional area where sediment supply and tectonics strongly affect sedimentation patterns (Goodbred and Kuehl, 1999). Throughout the late Quaternary, subsidence in the Ganges-Brahmaputra basin has not been dominated by shallow sediment compaction, but rather tectonic processes that generate rates as much as 4 mm/yr (Goodbred and Kuehl, 2000). Accommodation throughout the Ganges-Brahmaputra flood plains is continuously generated by fault movement as well as isostatic loading (Goodbred and Kuehl, 1999). Several geophysical studies of the area have identified a fault system in the region (Agarwal and Mitra, 1991; Khan 1991; Khandoker, 1978) that coincides with significant, spatially variable, rates of subsidence (Goodbred and Kuehl, 2000).

Neotectonic movements have also caused differential subsidence of Quaternary deposits in the Rhine-Meuse delta of the Netherlands. Results from seismographic backstripping, subsidence analysis, and historic and paleo-seismologic studies indicate that the major faults of the Roer Valley Graben have been active during the late Quaternary and continue to be active today (Cohen et al., 2002). Houtgast and Van Balen (2000) found minimum displacement rates along the Peel Boundary Fault Zone of the Rhine-Meuse delta to range from .05 mm/yr in the middle Quaternary to .08 mm/yr in the late Quaternary. Furthermore, Stouthamer and Berendsen (2002) studied the distribution of avulsion sites throughout the Holocene and identified a correlation between avulsion locations and fault zones. The study found that 83 % of avulsion locations, between 5.6 ka and 1.6 ka, were located coincident with the Peel Boundary and Tegelen fault zones. It was also found that active faulting promoted downstream migration of braided rivers in favor of lateral migration, aligning the rivers to the faults (Miller, 2006).

Chapter 6. Conclusions

An in-depth analysis of the Delacroix Island Fault using well logs, industry seismic data, regional geology, and satellite imagery suggests a long-lived history of episodic motion (approximately 13 My). Fault movement has been identified qualitatively by correlating horizons in seismic data and well logs as well as quantitatively through the use of biostratigraphic foraminifera.

Recognizing that delta progradation, and ultimately sediment loading, during the Miocene caused the creation and largest movement event of the Delacroix Island Fault supports the suggestion that faults are an integral part of deltas and that sediment loading plays a large factor in fault movement. Furthermore, numerous lines of evidence such as historical satellite imagery, topographic and land loss maps suggest that the Delacroix Island Fault continues to move through modern time frames (last approximately 100 years). In order to achieve some level of coastal sustainability or at least to help mitigate against future land loss an understanding of fault influence on modern geomorphology will be a necessity.

Although data are currently scarce other evidence suggests that fault-slip, likely caused by sediment loading, occurred throughout the Holocene just as it did during the Miocene. Frazier (1967) identified the progradation of the Mississippi River delta lobes throughout the Holocene and although sufficient data is not available to test whether these events caused fault movement, this would be a topic that could be investigated in the future.

References

Agarwal, R. P., & Mitra, D. S. (1991). Paleogeographic reconstruction of Bengal delta during Quaternary period. Quaternary deltas of India. Mem Geol Soc India, *22*, p. 13-24.

Armstrong, C., Mohrig, D., Hess, T., George, T., & Straub, K. M. (2014). Influence of growth faults on coastal fluvial systems: examples from the Late Miocene to Recent Mississippi River Delta. Sedimentary Geology, 301, p. 120-132.

Barras J.A., Bernier J.C., Morton R.A. (2008) Land area changes in coastal Louisiana— A multi decadal perspective (from 1956 to 2006). US Geological Survey Scientific Investigations Map 3019, 14 scale 1:250;000.

Bentley, S. J., Blum, M. D., Maloney, J., Pond, L., & Paulsell, R. (2016). The Mississippi River source-to-sink system: Perspectives on tectonic, climatic, and anthropogenic influences, Miocene to Anthropocene. Earth-Science Reviews, 153, p. 139-174.

Bishop, W. F. (1973). Late Jurassic contemporaneous faults in north Louisiana and south Arkansas. AAPG Bulletin, v. 57(5), p. 858-877.

Blum, M. (2009). High Frequency Cyclical Isostatic Adjustments: Significance for Incised Valleys. Oral Presentation at the AAPG International Conference, Cape Town, South Africa.

Bradshaw, G. A., & Zoback, M. D. (1988). Listric normal faulting, stress refraction, and the state of stress in the Gulf Coast basin. Geology, v. 16 no. 3, p. 271-274.

Brandes, C., Polom, U., & Winsemann, J. (2011). Reactivation of basement faults: interplay of ice-sheet advance, glacial lake formation and sediment loading. Basin Research, v. *23*(1), p. 53-64.

Cline, M. D., Feagin, R. A., Yeager, K. M., & Van Alstyne, J. M. (2011). Fault-induced wetland loss at Matagorda, Texas, USA: land cover changes from 1943 to 2008. Geocarto International, v. 26, no.8, p. 633-645.

Cohen, K. M., Stouthamer, E., & Berendsen, H. J. A. (2002). Fluvial deposits as a record for Late Quaternary neotectonic activity in the Rhine-Meuse delta, The Netherlands. Netherlands Journal of Geosciences/Geologie en Mijnbouw, v. 81 p. 3-4.

Coleman, J. M., Roberts, H. H., & Bryant, W. R. (1991). Late quaternary sedimentation. The Gulf of Mexico Basin: Boulder, Colorado, Geological Society of America, The Geology of North America, v. J, p. 325-352.

Coleman, J. M., Roberts, H. H., & Stone, G. W. (1998). Mississippi River delta: an overview. Journal of Coastal Research, p. 699-716.

Coleman, J. M., Suhayda, J. N., Whelan, T., & Wright, L. D. (1974). Mass movement of

Mississippi River delta sediments. Gulf Coast Association of Geological Societies Transactions, v. 24, p. 49-68.

Combellas-Bigott, R.I. and Galloway, W.E. (2006). Depositional and Structural Evolution of the Middle Miocene Depositional Episode, East-Central Gulf of Mexico. AAPG bulletin, v. 90, no. 3, p. 335-362.

Couvillion, B. R., Barras, J. A., Steyer, G. D., Sleavin, W., Fischer, M., Beck, H. & Heckman, D. (2011). Land area change in coastal Louisiana from 1932 to 2010.

Couvillion, B. R., Beck, H., Schoolmaster, D., & Fischer, M. (2017). Land area change in coastal Louisiana 1932 to 2016: US Geological Survey Scientific Investigations Map 3381: p 16. Pamphlet.

Curray, J. R. (1960). Sediments and History of Holocene Transgression, Continental Shelf, Northwest Gulf of Mexico. p. 1-46.

Curtis, D. M. (1970). Miocene deltaic sedimentation, Louisiana Gulf Coast. Society of Economic Paleontologists and Mineralogists. p. 293-308.

Dokka, R. K. (2006). Modern-day subsidence in coastal Louisiana. Geology. v.34 p. 281-284.

Dokka, R. K., Sella, G. F., & Dixon, T. H. (2006). Tectonic control of subsidence and southward displacement of southeast Louisiana with respect to stable North America. Geophysical Research Letters, v. 23, p. 33

Durham Jr, C. O., & Peeples III, E. M. (1956). Pleistocene fault zone in southeastern Louisiana, Gulf Coast Association Geological Society, Transactions, v. 6, p. 65-66.

Dixon, T. H., Amelung, F., Ferretti, A., Novali, F., Rocca, F., Dokka, R., & Whitman, D. (2006). Space geodesy: Subsidence and flooding in New Orleans. Nature, 441 (7093), p. 587.

Ewing, T. E. (1991). “Structural Framework.” The Gulf of Mexico Basin: Geological Society of America, The Geology of North America, v. J p. 31-52.

Fisk, H. N. (1945). Geological investigation of the alluvial valley of the Lower Mississippi River. War Department, Corps of Engineers, p. 1-78.

Flocks, J., Kulp, M., Smith, J., & Williams, S. J. (2009). Review of the geologic history of the Pontchartrain Basin, Northern Gulf of Mexico. Journal of Coastal Research, p. 12-22.

Frank, J.P. (2017). Evidence of Fault Movement During the Holocene in Southern Louisiana:

Integrating 3d Seismic Data with High resolution Seismic Data. [M.S. Thesis]: New Orleans, University of New Orleans. p. 1-90.

Frazier, D. E. (1967). Recent deltaic deposits of the Mississippi River: their development and chronology. Gulf Coast Association of Geological Societies Transactions, v. 17, p. 287-315.

Gagliano, S. M., Meyer-Arendt, K. J., & Wicker, K. M. (1981). Land loss in the Mississippi River deltaic plain. Gulf Coast Association of Geologic Societies, p. 295-300.

Gagliano, S.M., Kemp III, E.B., Wicker, K.M., Wiltenmuth, K.S., & Sabate, R.W. (2003). Neo-tectonic framework of southeast Louisiana and applications to coastal restoration. Gulf Coast Association of Geological Societies Transaction, v. LIII p. 262-272.

Galloway, W. E., Ganey-Curry, P. E., Li, X., & Buffler, R. T. (2000). Cenozoic depositional history of the Gulf of Mexico basin. *AAPG bulletin*, *84*(11), p. 1743-1774.

Galloway, W.E., (1986). Growth Faults and Fault-Related Structures of Prograding Terrigenous Clastic Continental Margins. Transactions of the Gulf Coast Association of Geological Societies, v. 36, p. 121-128.

Galloway, W. E., Bebout, D. G., Fisher, W. L., Dunlap Jr, J. B., Cabrera-Castro, R., Lugo-Rivera, J. E., & Scott, T. M. (1991). Cenozoic. *In* Salvador, A., ed., The Gulf of Mexico Basin: Boulder, Colorado, Geological Society of America, The Geology of North America, v. J, p. 245-324.

Goodbred Jr, S. L., & Kuehl, S. A. (1999). Holocene and modern sediment budgets for the Ganges-Brahmaputra river system: Evidence for highstand dispersal to flood-plain, shelf, and deep-sea depocenters. Geology, v. 27, no. 6, p. 559-562.

Goodbred Jr, S. L., & Kuehl, S. A. (2000). The significance of large sediment supply, active tectonism, and eustasy on margin sequence development: Late Quaternary stratigraphy and evolution of the Ganges–Brahmaputra delta. Sedimentary Geology, v.133, no. 3-4, p. 227-248.

Goswami, P. K. (2012). Geomorphic evidences of active faulting in the northwestern Ganga Plain, India: implications for the impact of basement structures. Geosciences Journal, v. 16, no.3, p. 289-299.

Houtgast, R.F. and Van Balen, R.T., (2000). Neotectonics of the Roer Valley Rift System, the Netherlands. Global and Planetary Change. v. 27. p. 131-146.

Kazmann, R. G. and Heath, M. M. Land Subsidence Related to Ground-Water offtake in the New Orleans Area. Gulf Coast Association of Geological Societies Transactions. v 18, p. 108-113.

Keller, R. (1965). Delacroix Island Field. Pan American Petroleum Corporation. p. 58-61.

Khan, F. H. (1991). *Geology of Bangladesh*. Wiley Eastern. p. 207.

Khandoker, R. A. (1987). Origin of elevated Barind-Madhupur areas, Bengal basin: result of neotectonic activities. Bangladesh Journal of Geology, v. 6, no.2, p. 1-9.

Koch, T. W. (1933). Analysis and effects of current movement on an active fault in Buena Vista Hills oil field, Kern County, California. AAPG Bulletin, v. 17, no. 6, p. 694-712.

Kuecher, G. J. (1995). The dominant processes responsible for subsidence of coastal wetlands in South Louisiana (No. ANL/ES/CP-85829; CONF-951098-2). Argonne National Lab., IL (United States).

Martin, E. (2006) Fault Induced Subsidence Near Empire and Bastian Bay, Louisiana. [M.S. Thesis]: New Orleans, Tulane University. p. 1-71.

McCulloh, R. P., and Heinrich, P. R. (2012). Surface faults of the south Louisiana growth-fault province. Geological Society of America Special Papers. v. 493, p. 37-49.

McLindon, C. (2017). History of fault slip and interaction with deltaic deposition from the Middle Miocene to present – Barataria fault, coastal Louisiana. American Geophysical Union annual meeting, New Orleans, Louisiana.

Miller, B. (2006). Hydrocarbon Production, Surface Subsidence, and Land Loss in Louisiana. Gulf Coast Association of Geological Societies Transactions. v. 56, p. 579-589.

Morton, R. A., Bernier, J. C., Barras, J. A., & Ferina, N. F. (2005). Rapid subsidence and historical wetland loss in the Mississippi delta plain: likely causes and future implications. U. S. Geological Survey. Open-file report 2005-1216.

New Orleans Geological Society (2015). Oil and Gas Industry Infrastructure in Coastal Louisiana. www.nogs.org

Paleodata (2018). Unpublished Biostratigraphic Formation tops and Paleobathymetry Maps. Paleodata Inc., Metairie, Louisiana

Penland, S., Beall, A. D., & Britsch III, L. D. (2002). Geologic classification of coastal land loss between 1932 and 1990 in the Mississippi River Delta Plain, southeastern Louisiana. Gulf Coast Association of Geological Societies. Transaction, v. 52, p. 799-807.

Salvador, A. 1987, Late Triassic-Jurassic paleogeography and origin of the Gulf of Mexico Basin. American Association of Petroleum Geologists Bulletin. v. 71, p. 419-451.

Salvador, A. (1991). Origin and development of the Gulf of Mexico basin. *In* Salvador, A., ed.,

The Gulf of Mexico Basin: Boulder, Colorado, Geological Society of America, The Geology of North America, v. J, p. 389-444.

Salvador, A. (1991). Triassic-Jurassic. *In* Salvador, A., ed., The Gulf of Mexico Basin: Boulder, Colorado, Geological Society of America, The Geology of North America, v. J, p. 131-180.

Shinkle, K. D., & Dokka, R. K. (2004). Rates of vertical displacement at benchmarks in the lower Mississippi Valley and the northern Gulf Coast (Vol. 50). US Department of Commerce, National Oceanic and Atmospheric Administration, National Ocean Service, National Geodetic Survey.

Stanley, D. J. (1988) Subsidence in the Northeastern Nile Delta: Rapid Rates, Possible Causes, and Consequences. Science. v. 240, p. 497-500.

Stouthamer, E., & Berendsen, H. J. (2000). Factors controlling the Holocene avulsion history of the Rhine-Meuse delta (The Netherlands). *Journal of Sedimentary Research*, v. *70*, no.5, p.1051-1064.

Stoyanoff, J. & Purinton, S. (2010). Black Bay Complex Update. Oil and Gas Fields of South Louisiana. p.55-59.

Thorsen, C. E. (1963). Age of growth faulting in southeast Louisiana. Gulf Coast Association of Geological Societies Transactions, v.13, p. 103-107.

Van Andel, T. H. (1960). Sources and dispersion of Holocene sediments, northern Gulf of Mexico. p. 34-55.

Verbeek, E. R. (1979). Quaternary Fault Activity in Texas Gulf Coast. AAPG Bulletin, v. 63, no.3 p. 545-545.

Wilson, C. A., & Allison, M. A. (2008). An equilibrium profile model for retreating marsh shorelines in southeast Louisiana. Estuarine, Coastal and Shelf Science, v. 80, no.4, p. 483-494.

Worrall, D. M., & Snelson, S. (1989). Evolution of the northern Gulf of Mexico, with emphasis on Cenozoic growth faulting and the role of salt. The geology of North America; an overview: Geological Society of America, v. A, p. 97-138.

Wu, X., & Galloway, W. E. (2002). Upper Miocene depositional history of the central Gulf of Mexico basin. Gulf Coast Association of Geological Societies transactions. v.52, p. 1019-1030.

Yuill, B., Lavoie, D., & Reed, D. J. (2009). Understanding subsidence processes in coastal Louisiana. Journal of Coastal Research, v. 23-3

Appendix A Geologic Structure Maps

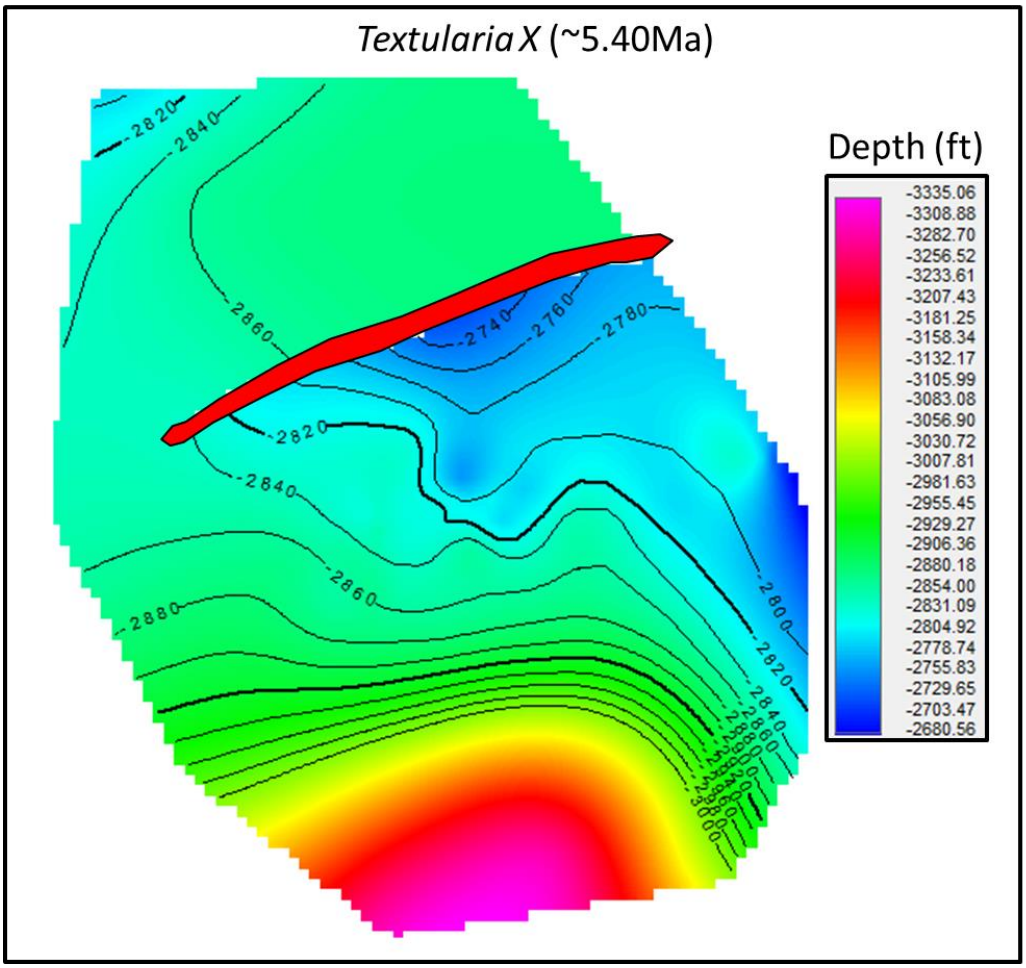

Appendix A Figure 1. Depth contoured structure map of the *Textularia X* horizon.

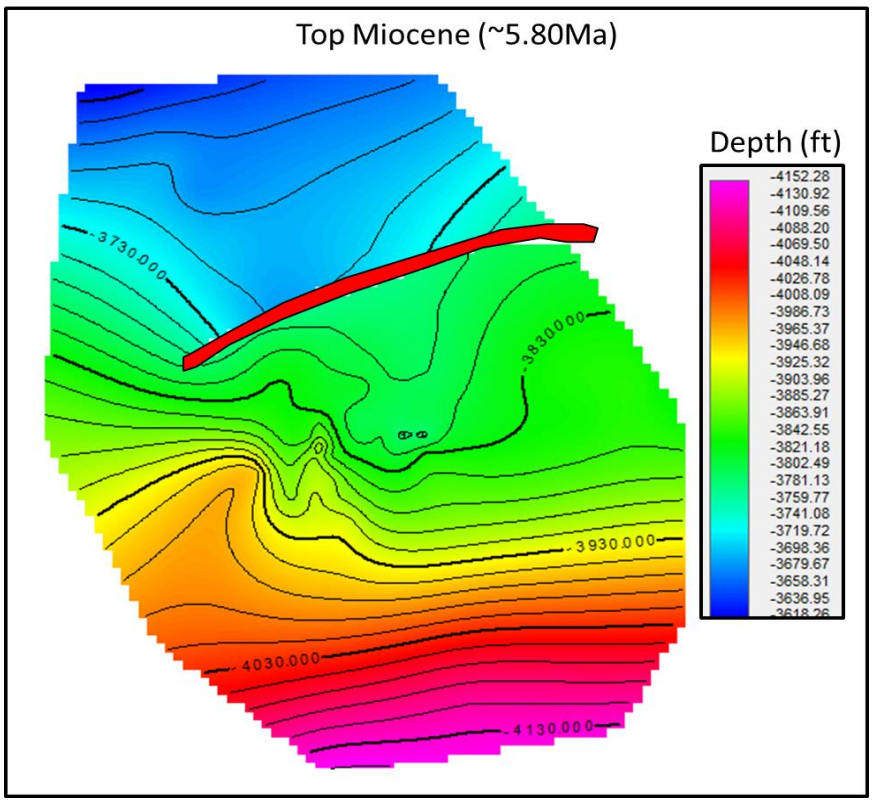

Appendix A Figure 2. Depth contoured structure map of the *Top Miocene* horizon.

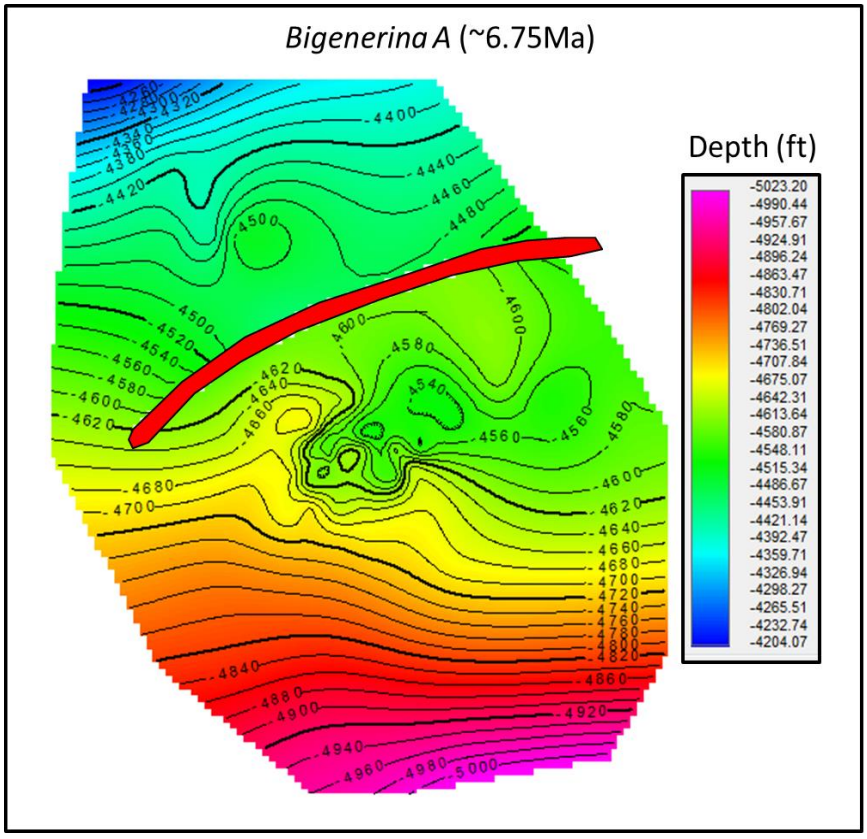

Appendix A Figure 3. Depth contoured structure map of the *Bigenerina A* horizon.

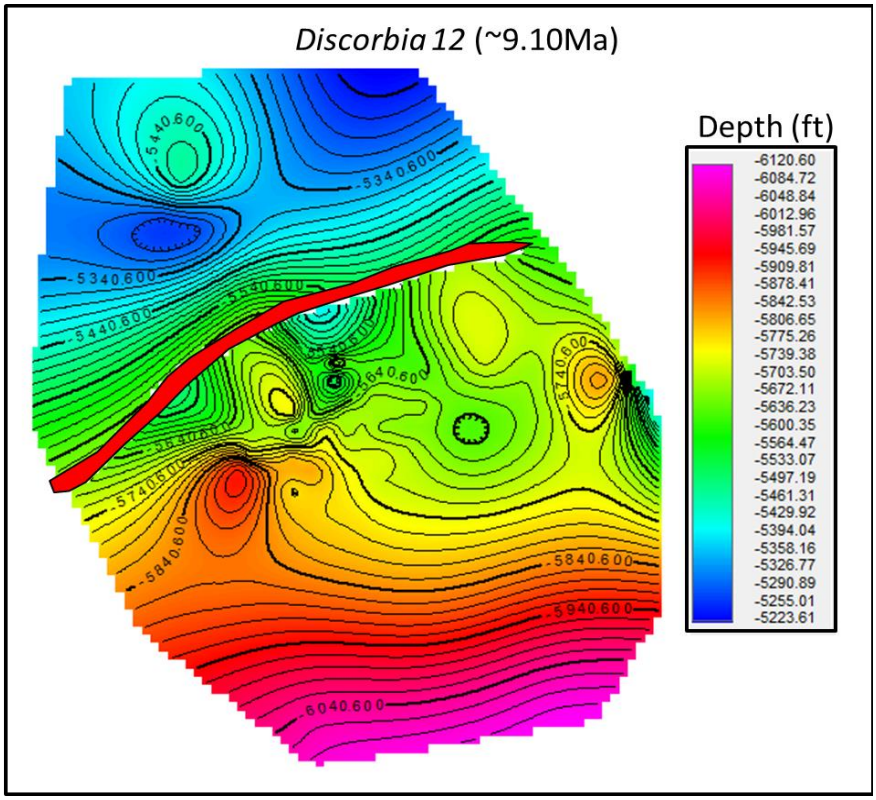

Appendix A Figure 4. Depth contoured structure map of the *Discorbia 12* horizon.

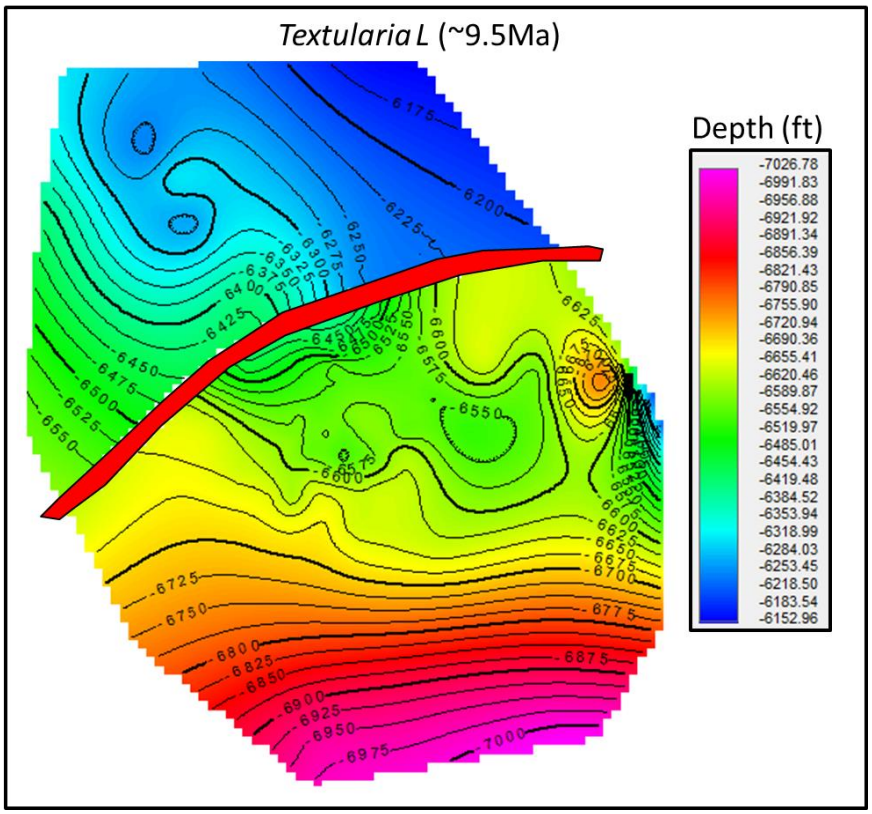

Appendix A Figure 5. Depth contoured structure map of the *Textularia L* horizon.

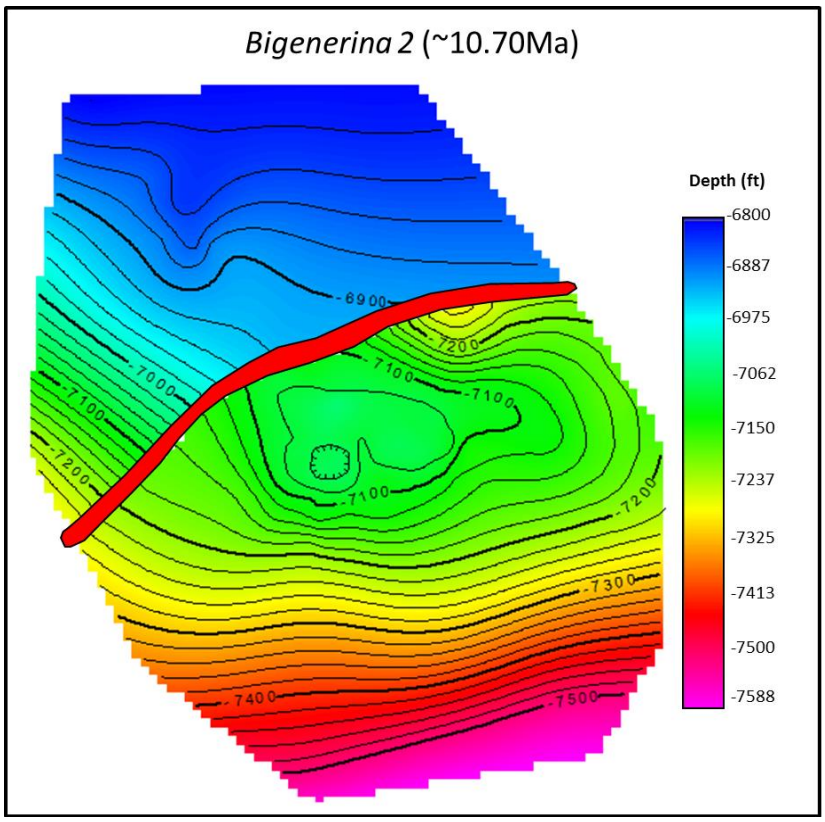

Appendix A Figure 6. Depth contoured structure map of the *Bigenerina 2* horizon.

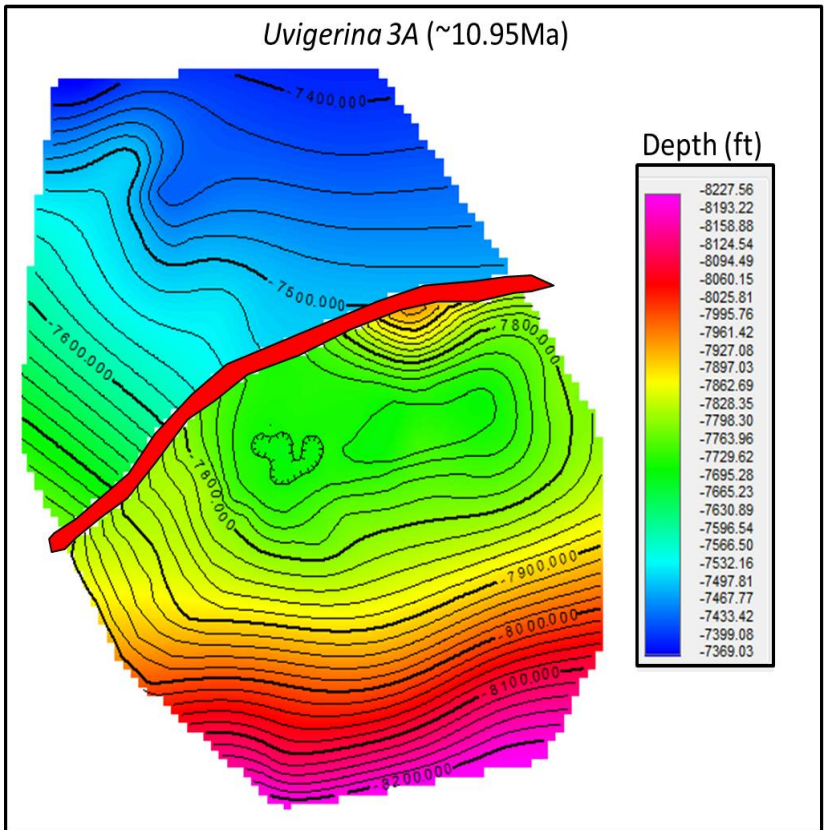

Appendix A Figure 7. Depth contoured structure map of the *Uvigerina 3A* horizon.

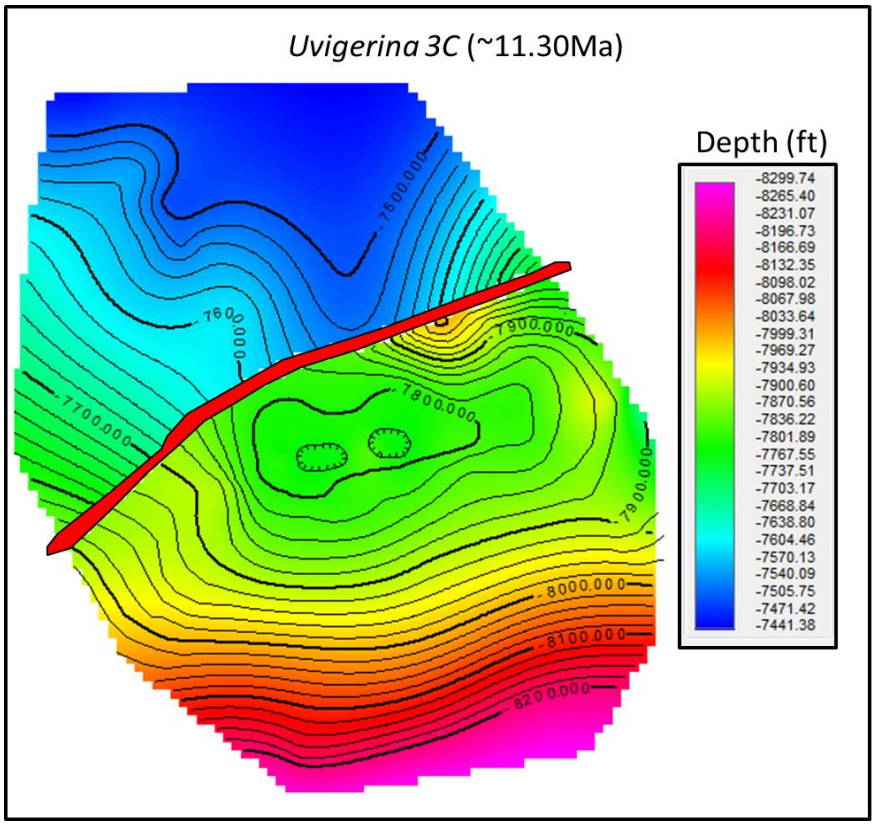

Appendix A Figure 8. Depth contoured structure map of the *Uvigerina 3C* horizon.

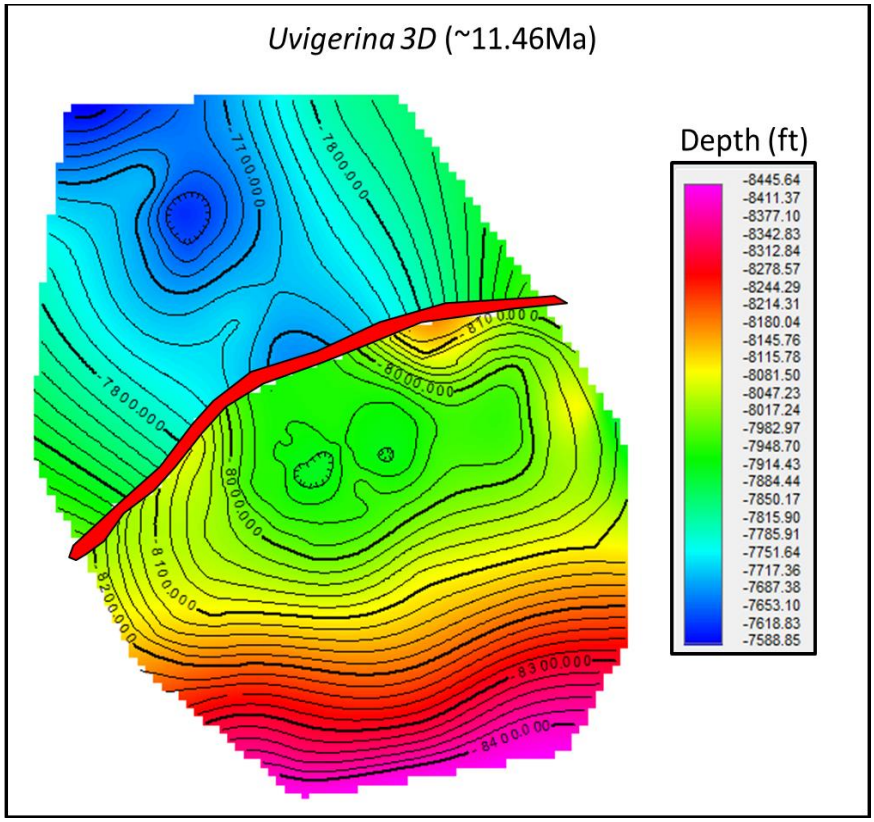

Appendix A Figure 9. Depth contoured structure map of the *Uvigerina 3D* horizon.

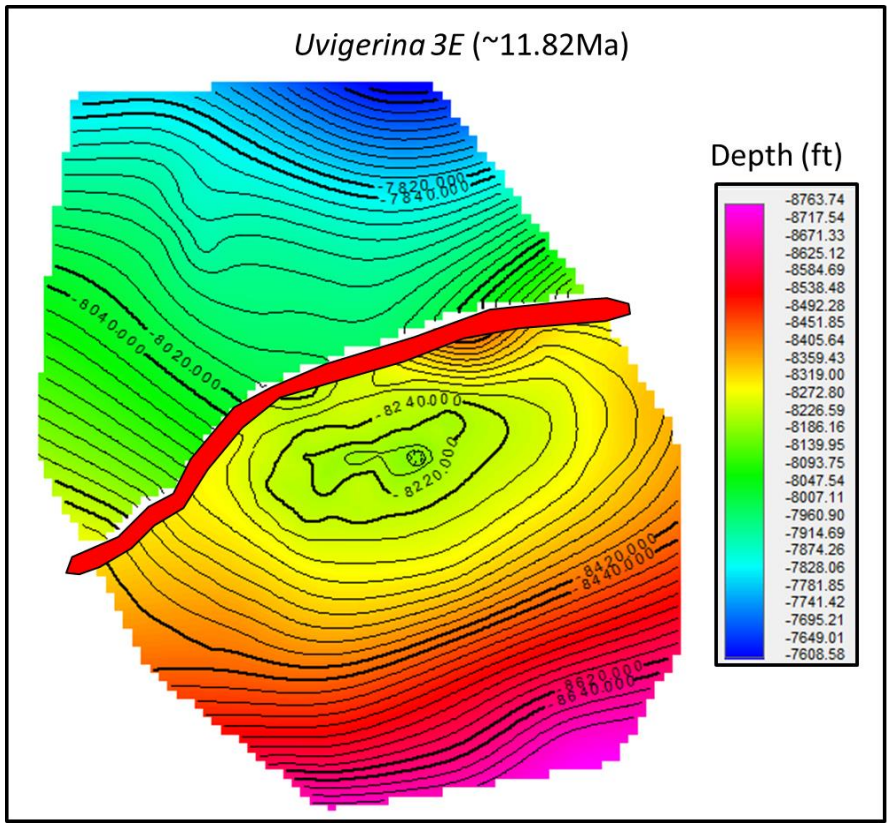

Appendix A Figure 10. Depth contoured structure map of the *Uvigerina 3E*

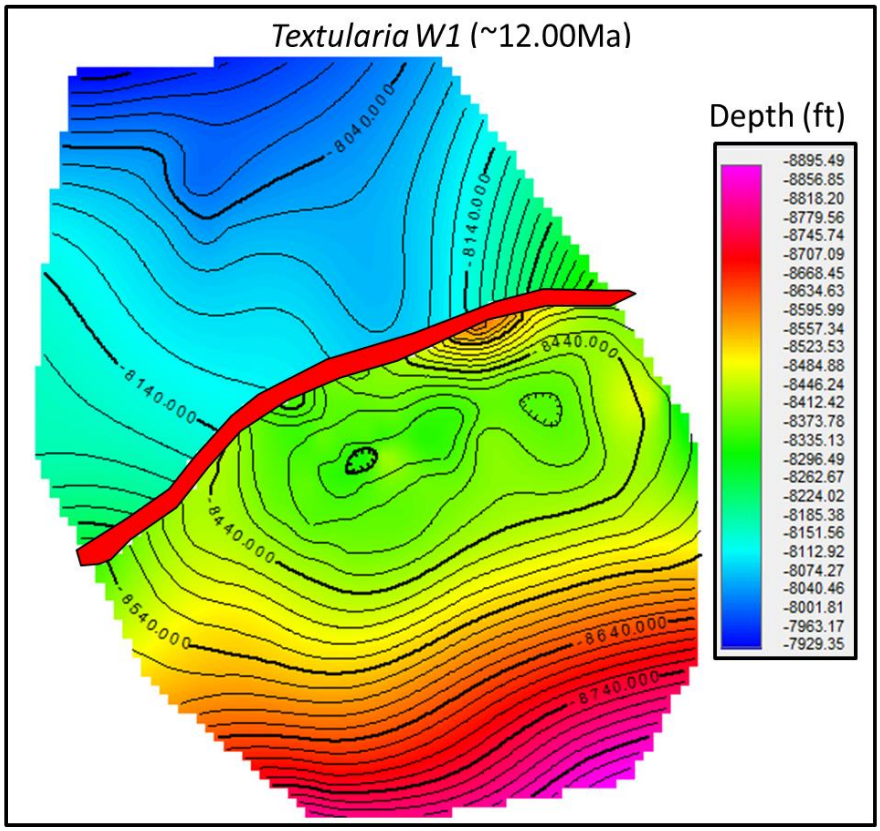

Appendix A Figure 11. Depth contoured structure map of the *Textularia W1* horizon.

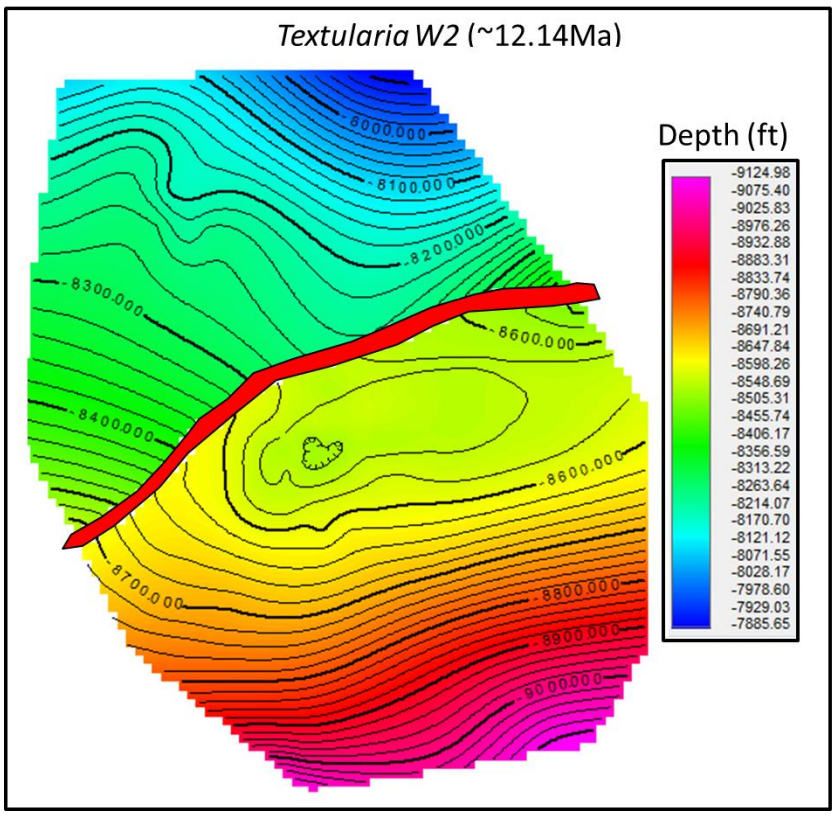

Appendix A Figure 12. Depth contoured structure map of the *Textularia W2* horizon.

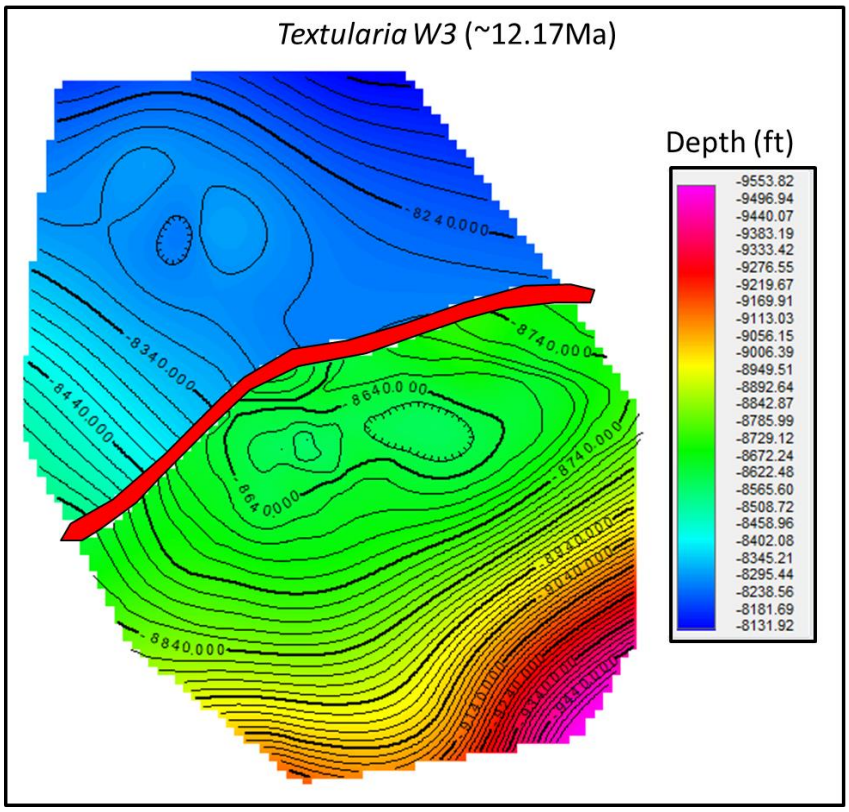

Appendix A Figure 13. Depth contoured structure map of the *Textularia W3* horizon.

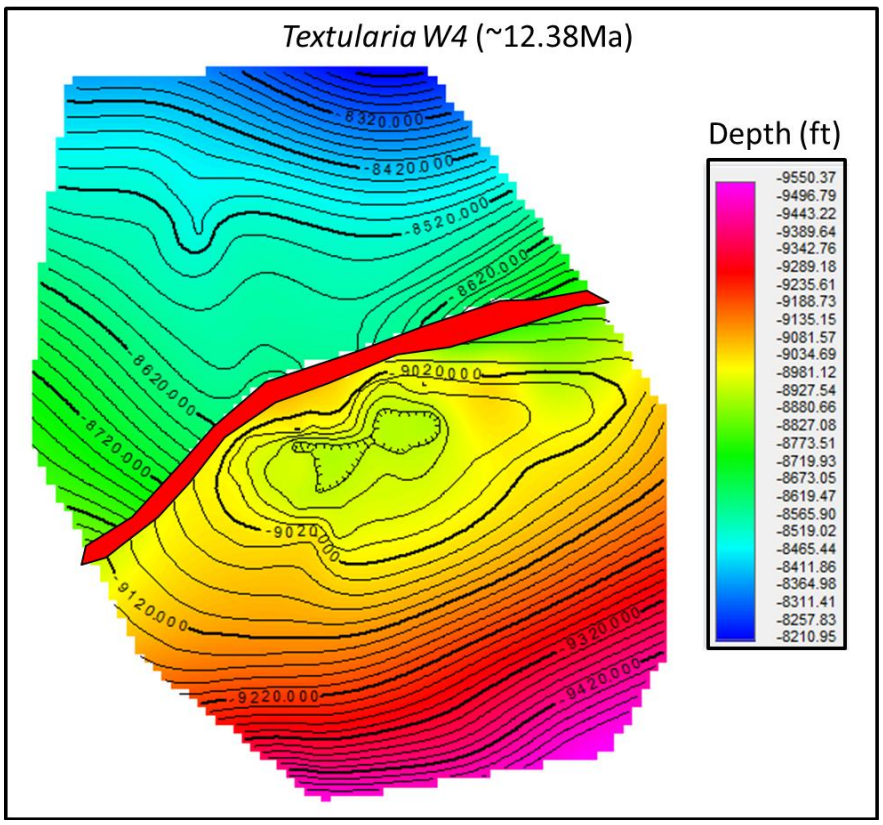

Appendix A Figure 14. Depth contoured structure map of the *Textularia W4* horizon.

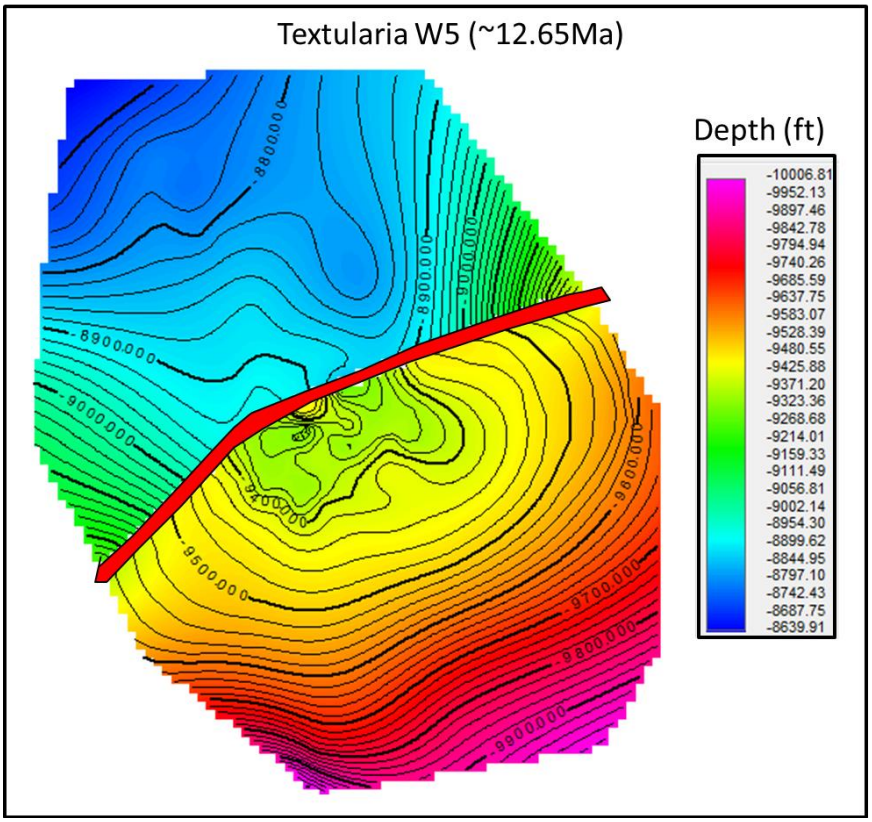

Appendix A Figure 15. Depth contoured structure map of the *Textularia W5* horizon.

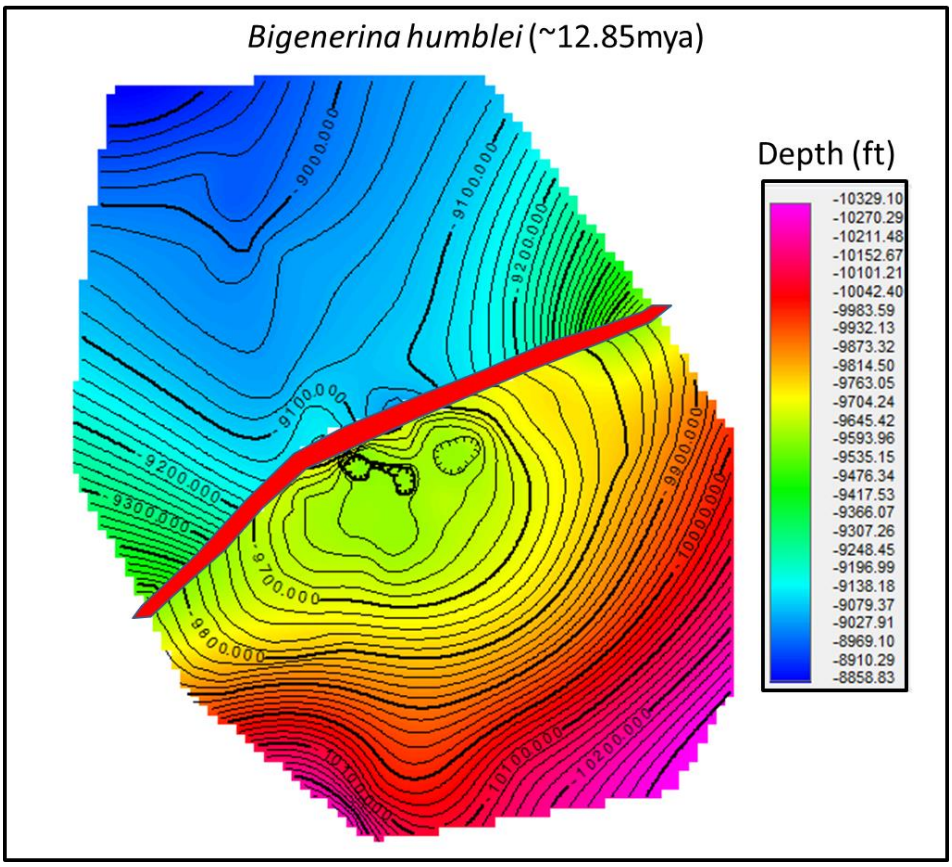

Appendix A Figure 15. Depth contoured structure map of the *Bigenerina humblei*

Appendix B Isopach Maps

Biostrat Foram	Age (Ma)
Trimosina A	0.60
Angulogerina B	1.40
Lenticulina	2.25
Top Pliocene	3.37
Buliminella 1	4.38
Textularia X	5.40
Top Miocene	6.15
Bigenerina A	6.75
Discorbia 12	9.10
Textularia L	9.50
Bigenerina 2	10.80
BN 8	10.95
Uvigerina 3A	11.20
Uvigerina 3C	11.30
Uvigerina 3D	11.46
Uvigerina 3E	11.82
Textularia W1	12.00
Textularia W2	12.14
Textulaira W3	12.17
Textularia W3A	12.31
Textularia W4	12.38
Textularia W5	12.65
Bigenerina humblei	12.85

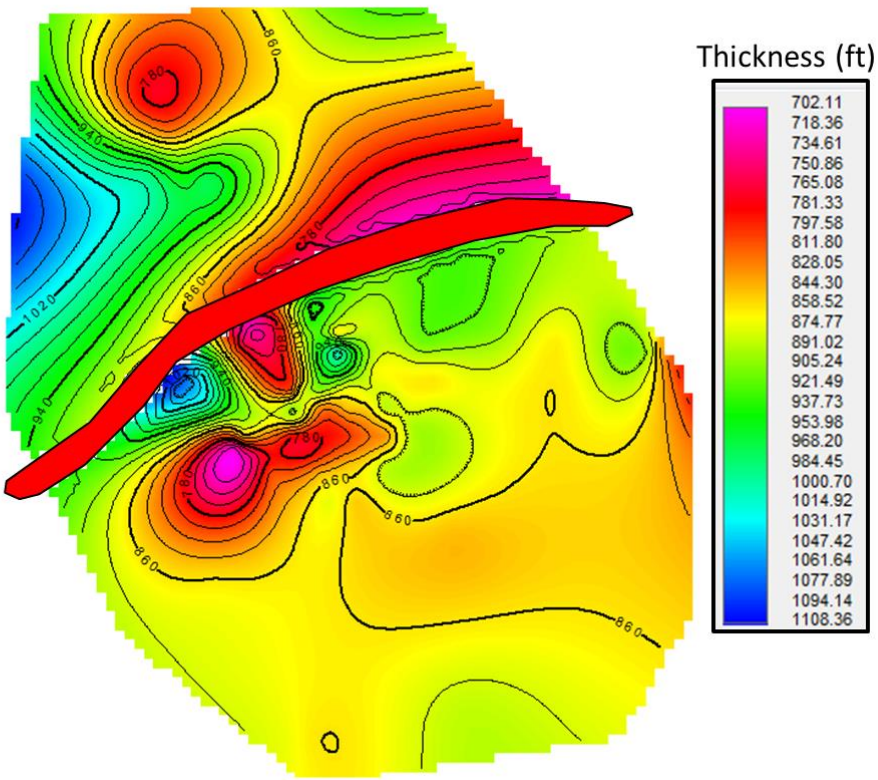

Appendix B Figure 1. Contoured Isopach map of the *Discorbia 12* to *Textularia L* biostratigraphic package.

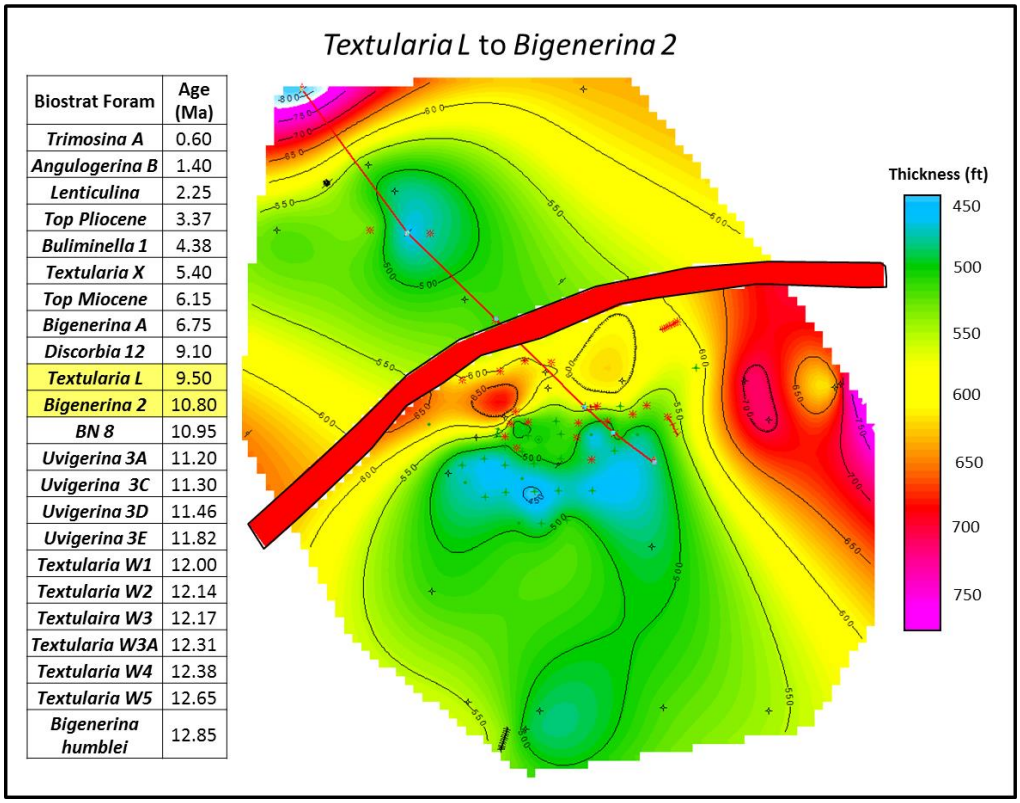

Biostrat Foram	Age (Ma)
Trimosina A	0.60
Angulogerina B	1.40
Lenticulina	2.25
Top Pliocene	3.37
Buliminella 1	4.38
Textularia X	5.40
Top Miocene	6.15
Bigenerina A	6.75
Discorbia 12	9.10
Textularia L	9.50
Bigenerina 2	10.80
BN 8	10.95
Uvigerina 3A	11.20
Uvigerina 3C	11.30
Uvigerina 3D	11.46
Uvigerina 3E	11.82
Textularia W1	12.00
Textularia W2	12.14
Textulaira W3	12.17
Textularia W3A	12.31
Textularia W4	12.38
Textularia W5	12.65
Bigenerina humblei	12.85

Appendix B Figure 2. Contoured Isopach map of the *Textularia L* to *Bigenerina 2* biostratigraphic

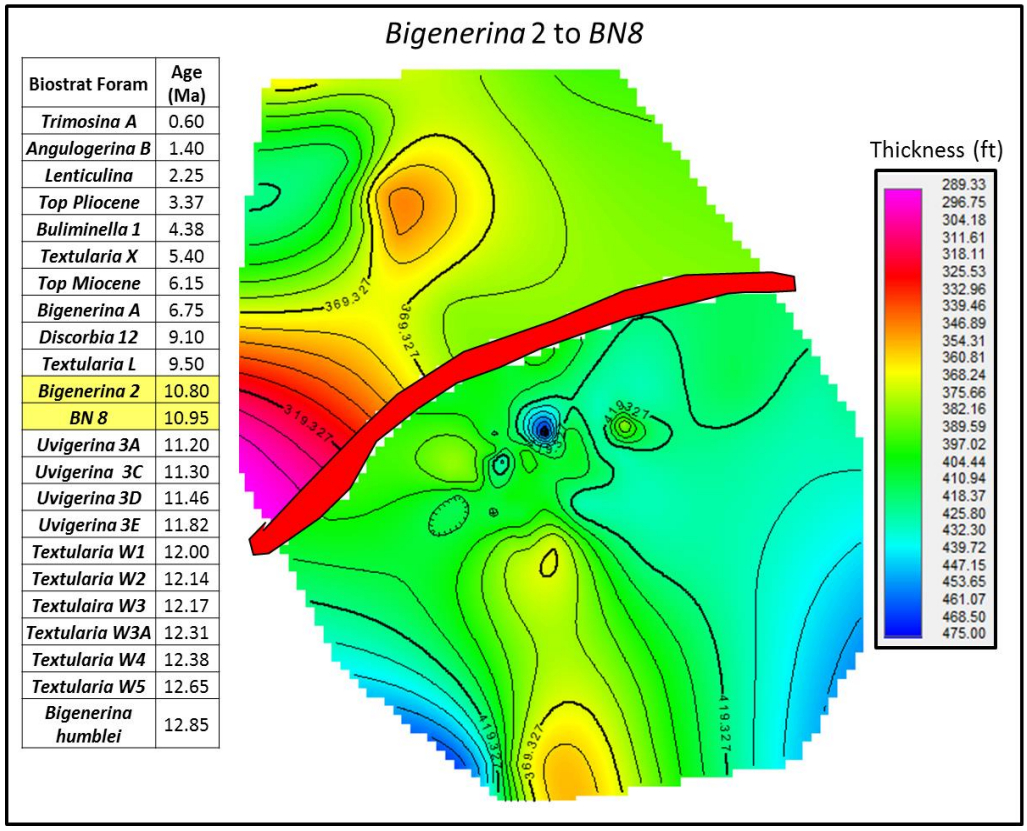

Biostrat Foram	Age (Ma)
Trimosina A	0.60
Angulogerina B	1.40
Lenticulina	2.25
Top Pliocene	3.37
Buliminella 1	4.38
Textularia X	5.40
Top Miocene	6.15
Bigenerina A	6.75
Discorbia 12	9.10
Textularia L	9.50
Bigenerina 2	10.80
BN 8	10.95
Uvigerina 3A	11.20
Uvigerina 3C	11.30
Uvigerina 3D	11.46
Uvigerina 3E	11.82
Textularia W1	12.00
Textularia W2	12.14
Textulaira W3	12.17
Textularia W3A	12.31
Textularia W4	12.38
Textularia W5	12.65
Bigenerina humblei	12.85

Appendix B Figure 3. Contoured Isopach map of the *Bigenerina 2* to *BN8* biostratigraphic package.

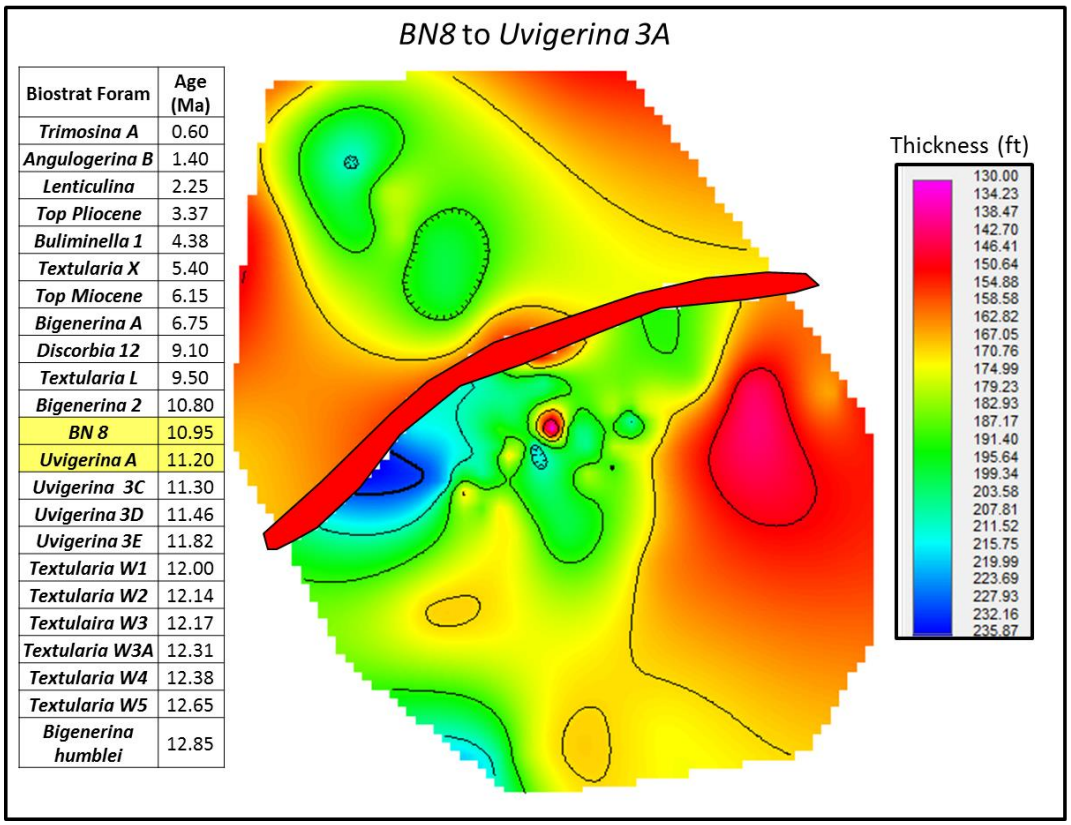

Appendix B Figure 4. Contoured Isopach map of the *BN8* to *Uvigerina 3A* biostratigraphic package.

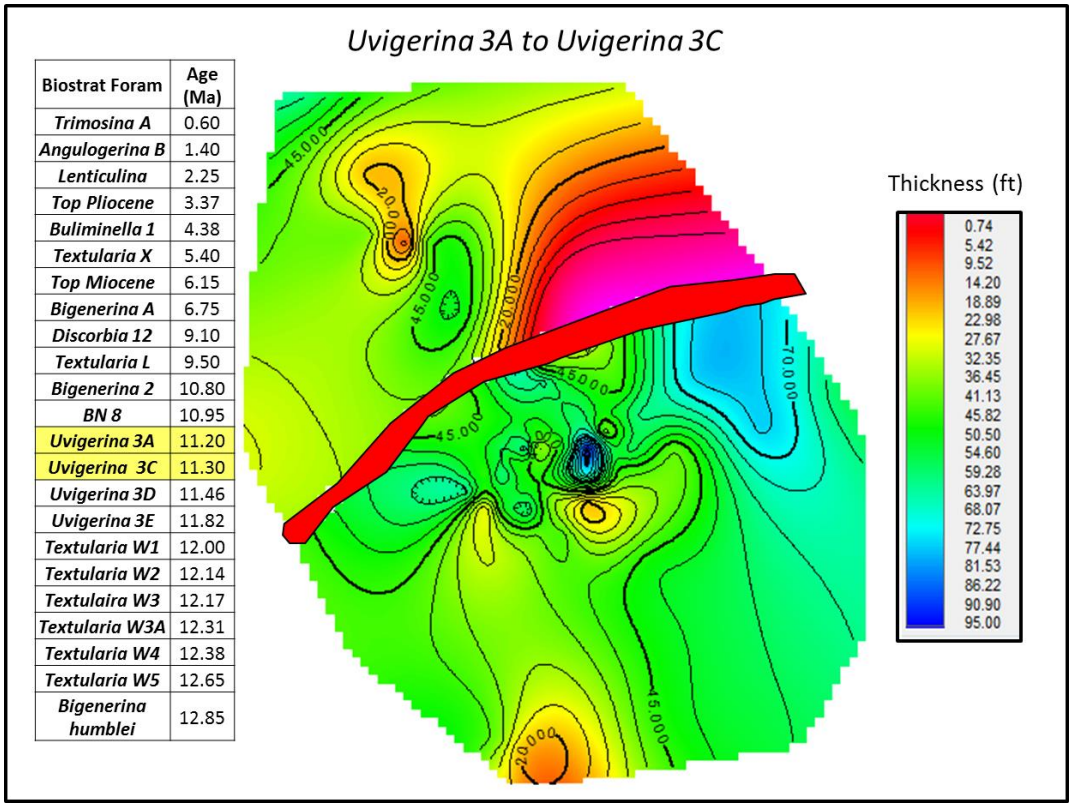

Appendix B Figure 5. Contoured Isopach map of the *Uvigerina 3A* to *Uvigerina 3C* biostratigraphic package.

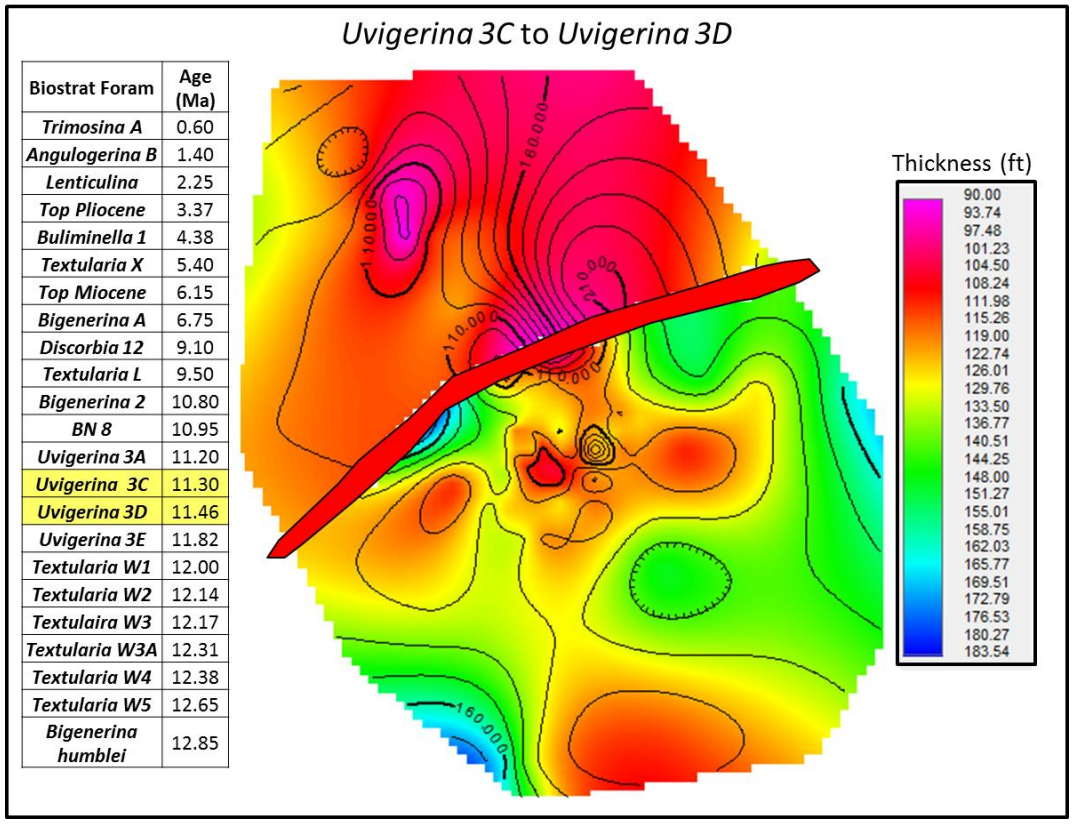

Appendix B Figure 6. Contoured Isopach map of the *Uvigerina 3C* to *Uvigerina 3D* biostratigraphic package.

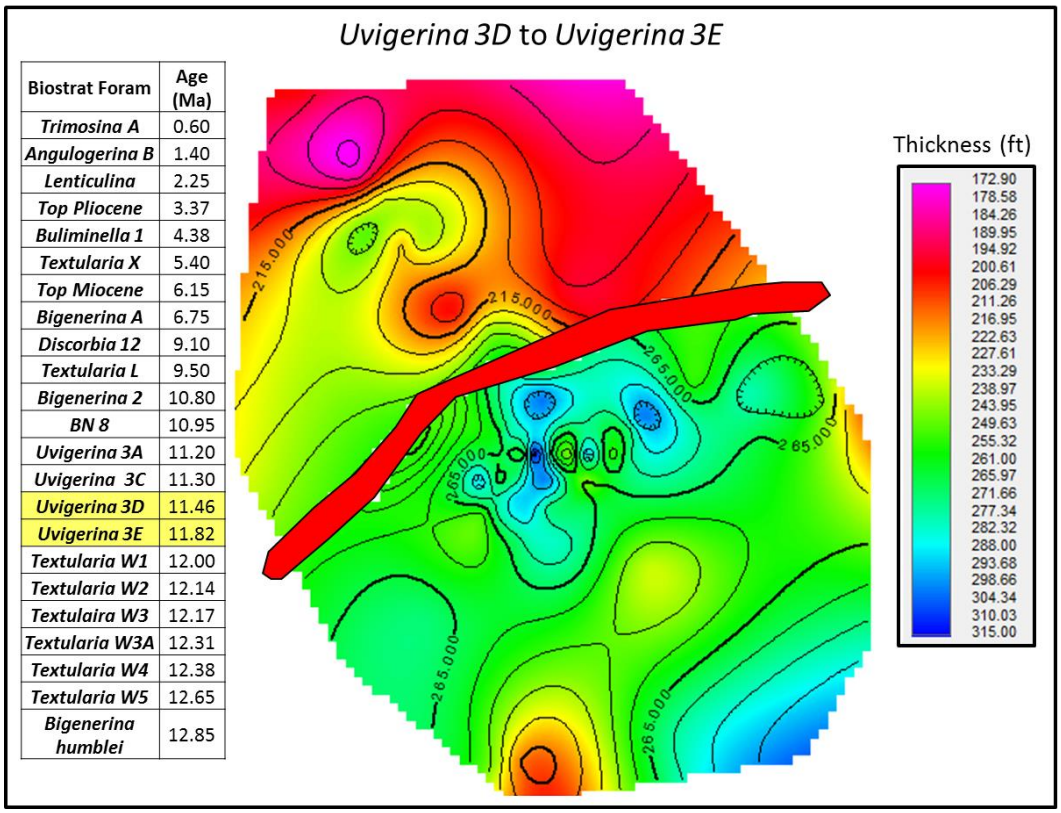

Appendix B Figure 7. Contoured Isopach map of the *Uvigerina 3D* to *Uvigerina 3E* biostratigraphic package.

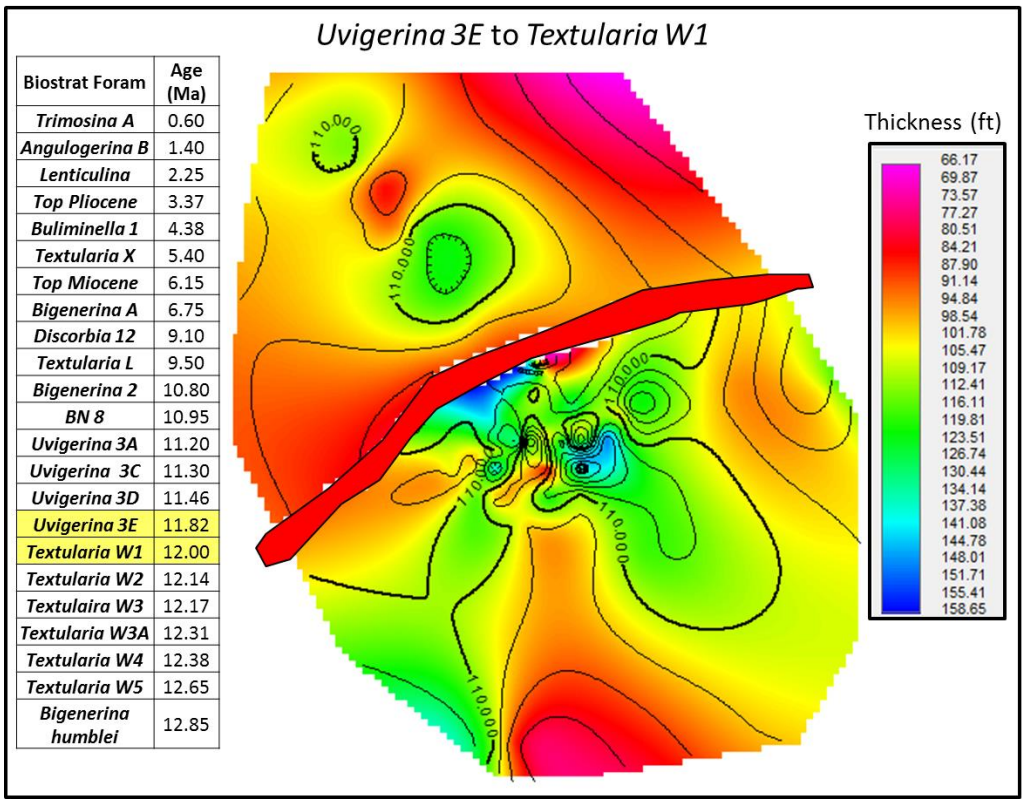

Appendix B Figure 8. Contoured Isopach map of the *Uvigerina 3E* to *Textularia W1* biostratigraphic package.

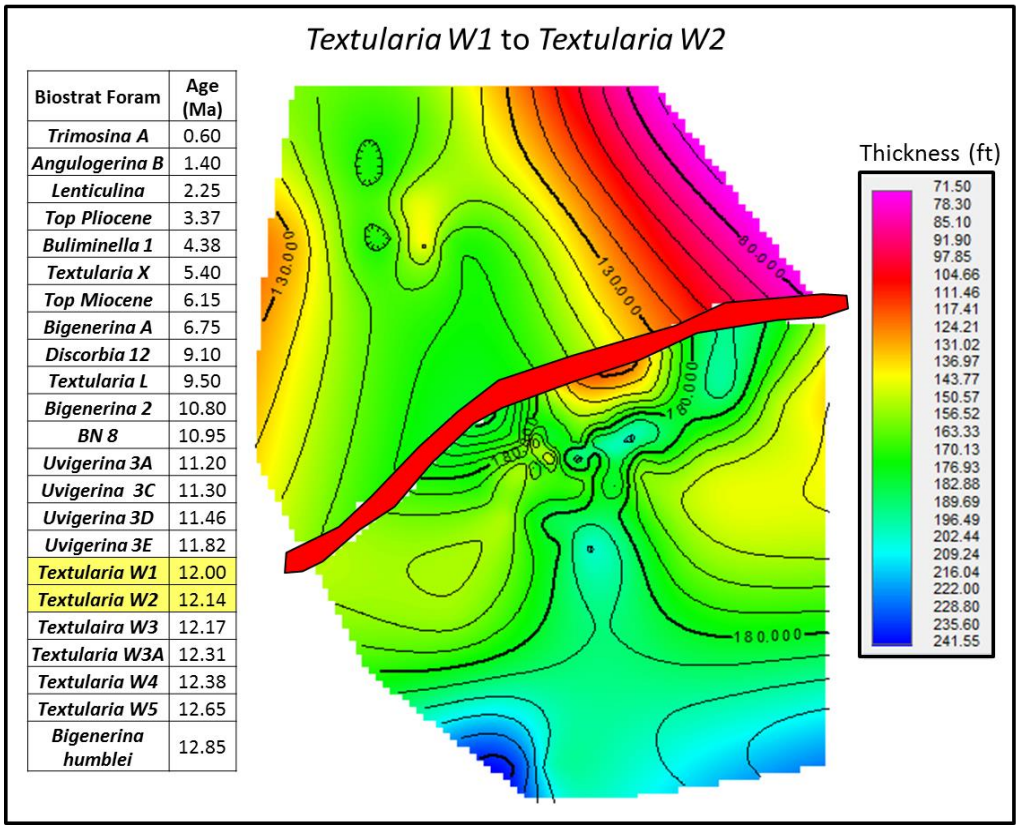

Appendix B Figure 9. Contoured Isopach map of the *Textularia W1* to *Textularia W2* biostratigraphic package.

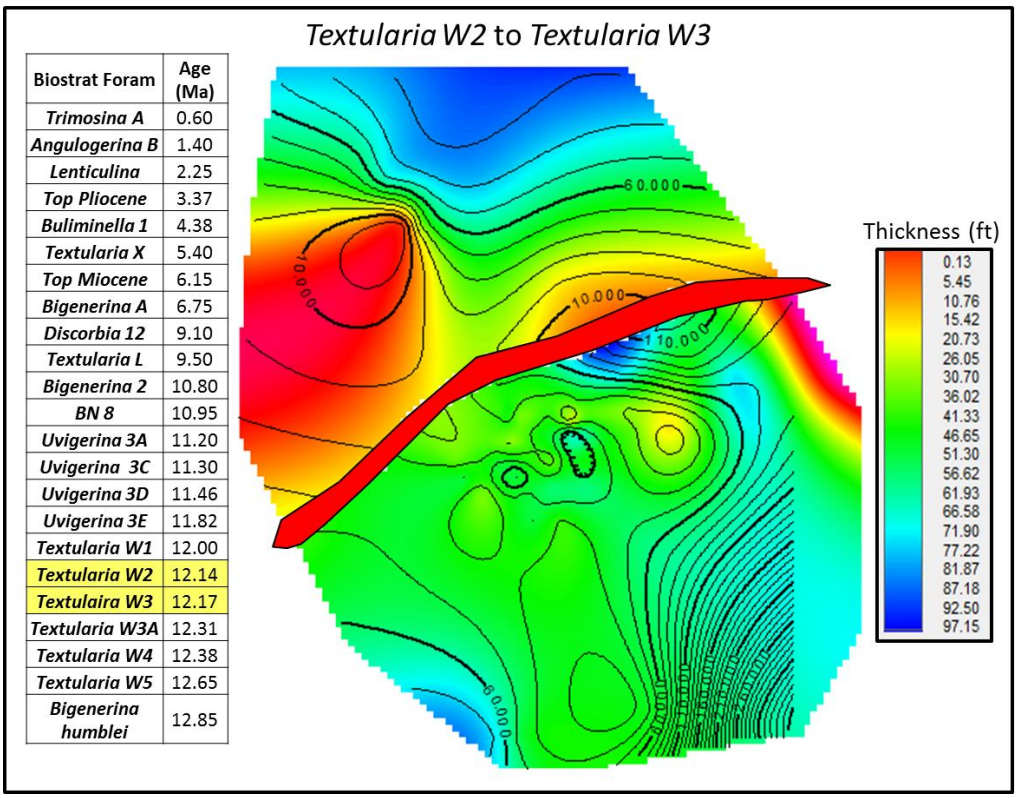

Appendix B Figure 10. Contoured Isopach map of the *Textularia W2* to *Textularia W3* biostratigraphic package.

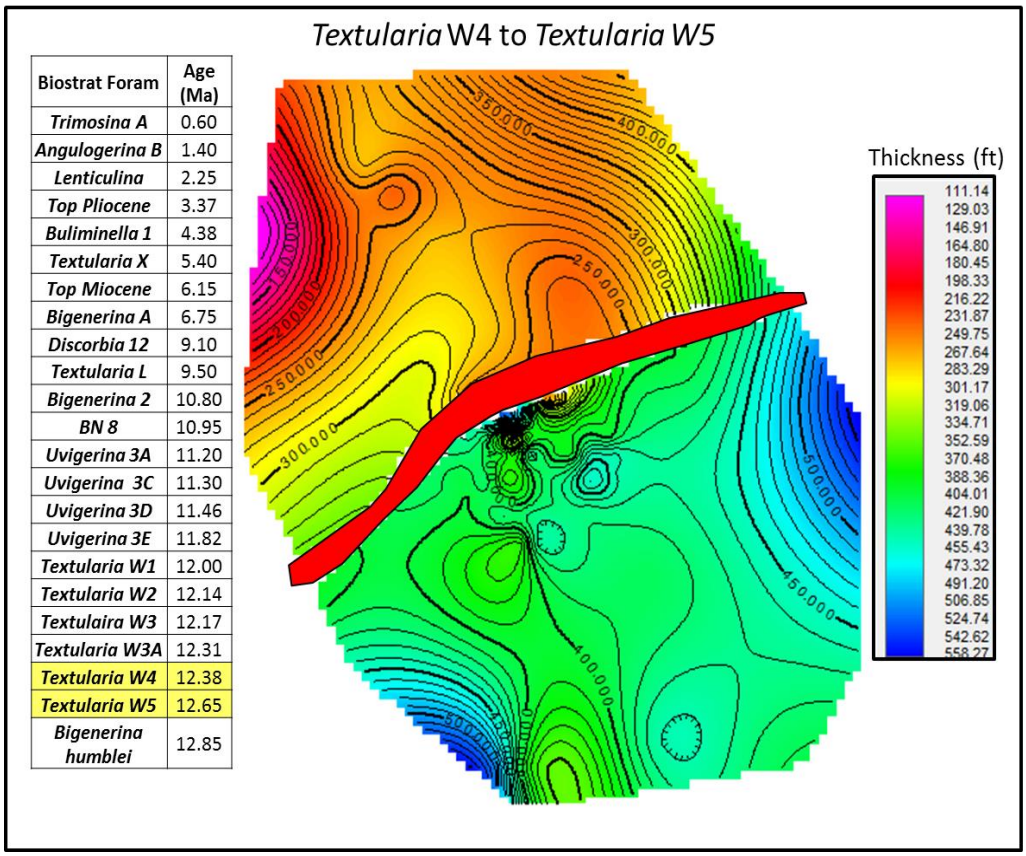

Appendix B Figure 11. Contoured Isopach map of the *Textularia W4* to *Textularia W5* biostratigraphic package.

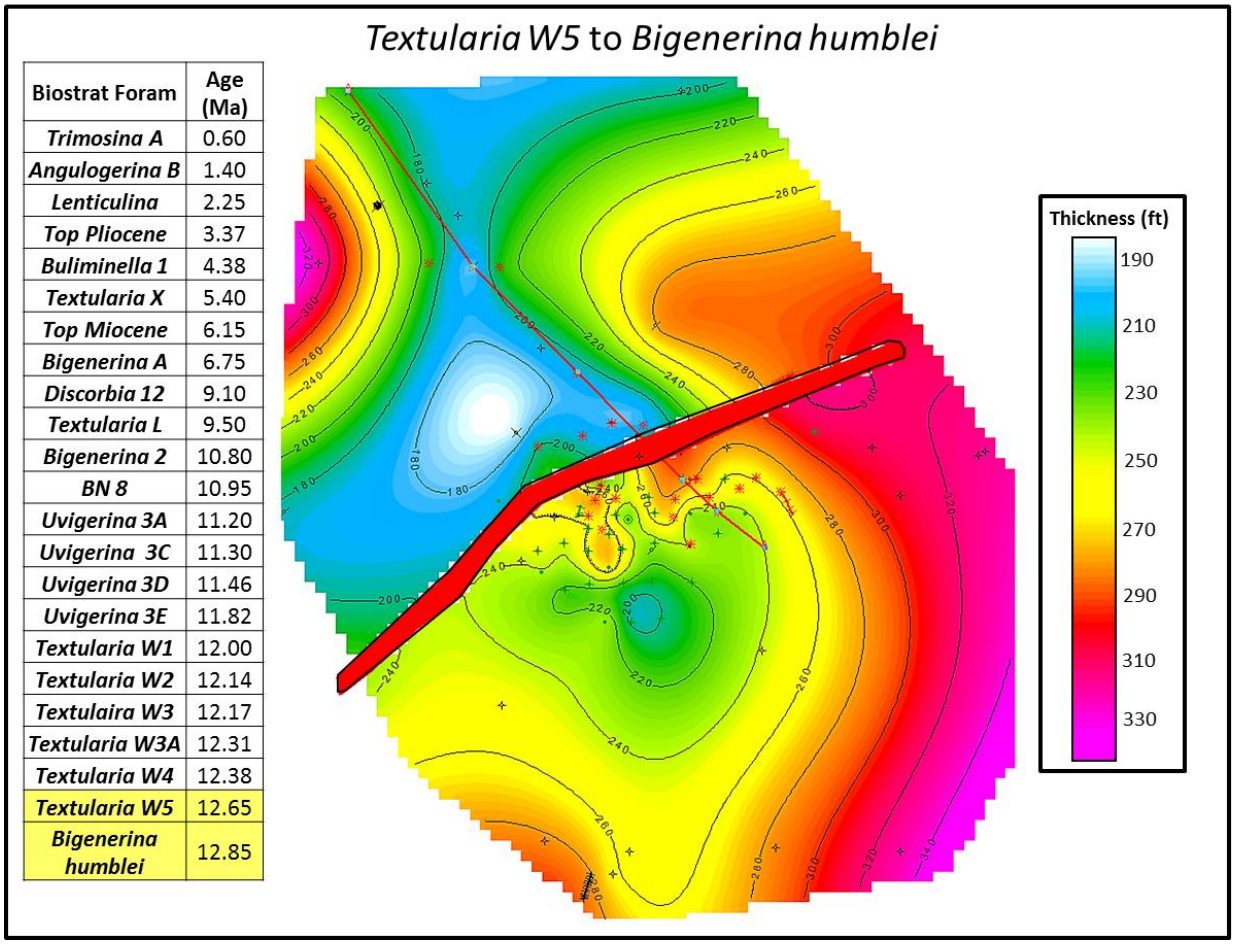

Appendix B Figure 12. Contoured Isopach map of the *Textularia W5* to *Bigenerina humblei* biostratigraphic

VITA

The author originally hails from Branford, Connecticut. He earned his B.S. in geology from Juniata College in Huntingdon, Pennsylvania, graduating in the spring of 2016. The following fall he joined the University of New Orleans Earth and Environmental Sciences graduate program to pursue his M.S. and became a member of Dr. Mark Kulps research group, focusing on whether deep-seated faults of southeastern Louisiana are still active and affecting near-surface stratigraphy and Holocene geomorphology.